PAUL SCHERRER INSTITUT

PSI

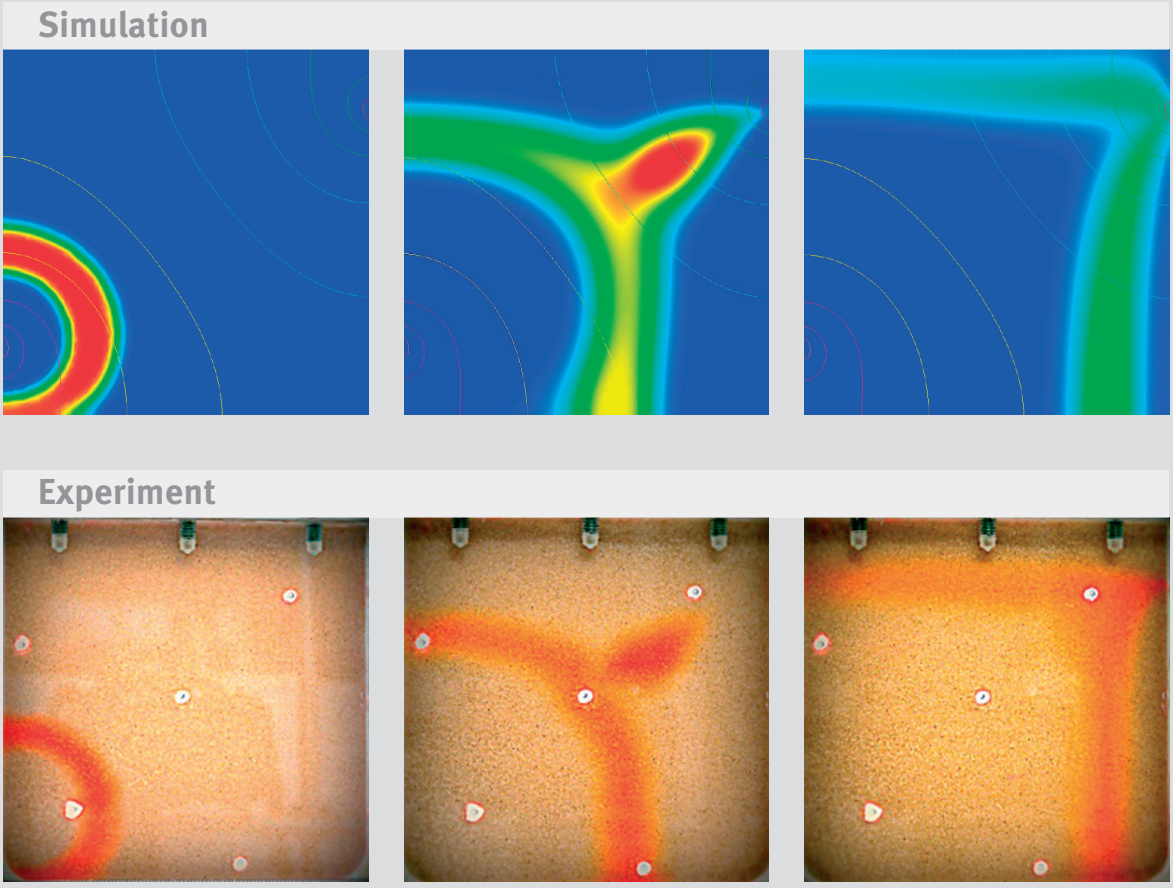

Progress Report 2013

Laboratory for Waste Management :: Nuclear Energy and Safety Department

Cover
Temporal evolution of a conservative tracer in a granular porous media: experiment versus simulation.

PAUL SCHERRER INSTITUT

PSI

Progress Report 2013

Laboratory for Waste Management
Nuclear Energy and Safety Department

See also our web-page
http://www.psi.ch/les/

Preface

The main task of the Laboratory for Waste Management is to carry out an R&D programme to strengthen the scientific basis for radioactive waste management.

The Laboratory serves an important national role by supporting the Swiss Federal Government and Nagra in their tasks to safely dispose of radioactive wastes from medical, industrial and research applications as well as from nuclear power plants. The activities are in fundamental repository geochemistry, chemistry and physics of radionuclides at geological interfaces and radionuclide transport and retardation in geological media and man-made repository barriers. The work performed is a balanced combination of experimental activities in dedicated laboratories for handling radioactive elements, field experiments and modelling. The work is directed towards repository projects and the results find their application in comprehensive performance assessments carried out by Nagra. In particular, a major priority for LES over the next decade or so will be to contribute to the Sachplan Geologische Tiefenlagerung ("Sectoral Plan").

This report summarises the activities and results achieved in the reporting period. It is organised as an overview followed by individual reports on the six waste management group/sub-programme activities.

We gratefully acknowledge the help of the institute's management and of Nagra in our work.

Table of Contents

1 OVERVIEW

M.H. Bradbury

1.1 Introduction

The progress made in the Laboratory for Waste Management (LES) over the period from January 1, 2013 to December 31, 2013 is summarised in the first part of the report. The activities carried out in the individual groups are then described in chapters 2 to 7 and are either predominantly "experimental" or predominantly "modelling" in their nature. However, there are strong interactions between groups, and between experimentalists and modellers.

1.2 General

The next major milestone in Stage 2 of the Sectoral Plan for Deep Geological Disposal (SGT) will be the selection of at least two sites each for high-level (SF/HLW) and low- and intermediate-level (L/ILW) radioactive waste repositories which is planned to take place at the end of 2016.

During 2013 the Lab has continued its strong involvement in the preparation of the numerous data bases and scientific reports required in Stage 2 for the Provisional Safety Analyses (PSAs) to be performed in 2014. As stated in the last annual report, the breadth and content of this work has continued to evolve and increase over time resulting in requirements for more comprehensive and detailed documentation.

The Lab is currently participating in three projects in the 7th EU Framework Programme: "Processes of Cation Diffusion in Clay Rocks", (CatClay); "Carbon-14 Source Term", (CAST); and, since November 2013, in the "FIRST-Nuclides" project.

LES's contribution to "Slow Processes in Close-to-Equilibrium Conditions for Radionuclides in Water/Solid Systems of Relevance to Nuclear Waste Management" (SKIN), was completed at the end of 2013.

The joint programme of work with the Hungarian Academy of Science, Centre of Energy Research, in connection with the Schweizer Erweiterungs-beitrag DEZA/SECO has been extended by 6 months and will now finish in April 2014.

The main multi- and bi-lateral co-operations with external institutions and universities are summarized in Table 1.1.

Table 1.1: *National and international co-operations.*

Co-operations
Nagra Major financial contribution Various technical working groups
Multinational 7th EU FP (CatClay, CAST, FIRST-Nuclides) Mont Terri Project (Diffusion Retardation, Clay Cement Interaction) Grimsel Test Site (Colloid Formation Migration)
Universities Bern, Switzerland (mineralogy, petrography, water chemistry, C-14 AMS) Surrey, United Kingdom; EPFL, Switzerland (cement systems, molecular modelling) Mainz, Germany (cement, montmorillonite) Strasbourg, France (glass) Tübingen, Germany (geosphere transport) ETH, Zürich, Switzerland (GEMS) FHNW Muttenz, Switzerland (gas phase analytics)
Research Centres CEA*, France (near- and far-field) CIEMAT, Spain (colloids) EMPA*, Switzerland (cement) IFR, HZDR*, Germany (XAS, TRLFS) INE, KIT*, Germany (near- and far-field; TRLFS) SCK/CEN, Belgium (clays) UFZ*, Germany (reactive transport) *formal co-operation agreements

Current PhD and postdoc projects being carried out in LES are listed below:

M. Bestel (PhD): "Water dynamics in compacted clay systems." Start date: September 2009. (Funding: SNF) LES participation.

Y. Chen (PhD): "Retardation of low-molecular weight organic compounds in clays". Start date: March 2013. (Funding: Nagra/PSI).

J. Poonoosamy (PhD): “Experimental benchmarks for verification and validation of reactive transport codes.” Start date: October 2012. (Funding: Nagra/PSI).

A. Shafizadeh (PhD): “Porosity and structural changes at clay-cement interfaces and their relations to transport properties.” Start date: March 2012: (Funding: Nagra/PSI Cross proposal, in collaboration with the Neutron Activation and Imaging Group (NUM)).

D. Soltermann (PhD): “The influence of Fe(II) on clay properties, the sorption of Fe(II) on clays and competitive sorption investigations: a combined macroscopic and microscopic study.” Start date: August 2010. (Funding: SNF).

Dr. B. Thien (postdoc): “COmbined hydrological, geochemical and geophysical modelling of geotTHERMal systems.” Start date: 1 February 2013. (SNF Sinergia project COTHERM).

Dr. B. Cvetković (postdoc) “Development of C-14 AMS-based analytical methods for the identification and quantification of C-14 labeled dissolved and volatile organic compounds.” Start date: November 2013. (Funding: Swissnuclear) Replacement for Dr. J. Schenzel (see below).

Within an international project on “Water transport in cements: A bottom – up approach based on NMR relaxation and imaging analysis and numerical modelling”, 1 PhD and 1 postdoc are jointly supervised by Dr. Faux (Physics Dep., Uni. Surrey, UK) and Dr. S. Churakov (LES). The co-ordinator is Prof. P. McDonald, Uni. Surrey, UK.

Dr. M. del Henar Rojo-Sanz (Guest Scientist): “The fate of selenium and technetium in a cementitious repository near-field under reducing conditions.” Start date: November 2012. (Funding: Verbundprojekt “Immorad”: Grundlegende Untersuchungen zur Immobilisierung langlebiger Radionuklide durch die Wechselwirkung mit endlagerrelevanten Sekundärphasen. Bundes-ministerium für Bildung und Forschung)

Dr. L. Pegado (Guest Scientist): On 31 October 2013 the SNF-Sinergia project finished. However as part of a follow up ICB-Dijon-PSI project "A thermodynamic model for C-S-H/C-A-S-H from a bottom up approach", Dr Pegado will be at LES approximately one day per week until June 2015.

Dr. Ph. Schaub (postdoc) left LES on April 30, 2013, to accept a position at the Swiss Federal Office of Energy. For financial reasons it was not possible to replace Dr. Schaub and hence the interesting work on a micro diffraction synchrotron-based approach for the characterization of complex materials in radioactive waste management has ceased.

Dr. J. Schenzel (postdoc) left LES on October 31, 2013, to accept a postdoc position at Eawag, Switzerland.

Dr. T. Kupcik (Guest Scientist) returned to INE/KIT Karlsruhe at the beginning of November 2013.

During 2013 members of LES participated in a number of international technical review groups: (i) “SARG (SFR extension, Application Review Group)”, SKB, Sweden (ii) “Expert Panel on Radionuclide Migration in Plastic Clay”, Ondraf/Niras and SCK-CEN, Belgium (iii) “Review panel of the Belgian programme on the behaviour of spent fuel in a cementitious environment”, Ondraf/Niras, Belgium (iv) “Advisory Group for the BIGRAD Consortium: Biogeochemical gradients and radionuclide transport”, Research Center for Radwaste and Decommissioning, University of Manchester, UK.

On February 26/27, 2013, the Waste Management Program Committee met for their annual meeting. The work performed within LES and the future plans were discussed, as usual. The valuable help and advice received from the members of the committee, both at the meeting and throughout the year, are appreciated by the whole Laboratory.

1.3 Sectoral Plan for Deep Geological Disposal (SGT)

Work associated with Phase 2 of the Sectoral Plan and the Provisional Safety Analyses (PSAs) planned by Nagra continued to be major activities in 2013. The extensive and comprehensive SDBs for the potential host rocks Opalinus Clay, “Brauner Dogger”, Effinger Member, Helvetic Marl, for the underlying confining units, and for MX-80 bentonite, were finalised after taking into account the comments from numerous reviews. Also, sorption isotherm measurements were extended to include Helvetic Marl. The experimental results were compared with blind predictions made using the “SDB derivation methodology” in a similar manner to that previously done for the other host rocks. The results of the comparisons were again very satisfactory.

The updated cement SDB, which took into account such “disturbance factors” as cement degradation, complexation of radionuclides with organic

degradation products, carbonisation etc., was completed and is in review.

In PA it is currently assumed that all materials (waste, backfill, container etc.) inside the caverns of L/ILW and ILW cement-based deep geological repositories are homogeneously distributed, and the whole can be treated in a "mixing-tank" approach. The consequence of this is that all radionuclides are distributed homogeneously in the cementitious near field after about 50 years. A report is currently being prepared whose aim is to assess the barrier function of the waste drums by considering the heterogeneity of the waste matrices and describing what effects this approach may have on PA.

After a series of intensive internal discussions (LES/Nagra), the reports on maximum radionuclide solubilities for the reference compacted MX-80 and concrete porewaters defined for Stage 2 of the Sectoral Plan using the modelling TDB 07/12 are nearing completion.

In many fields, including radioactive waste disposal, it is commonly assumed that the solubility of heavy metals such as Cu, Hg, Ag, etc. is essentially zero under strongly reducing conditions. From an extensive literature review and critical assessment of the solubilities of heavy metals in redox-state zero it was concluded that this is a serious misconception, and is the reason why dissolved metal atoms are not included in geochemical considerations. This "blind spot" in chemical equilibrium thermodynamics has lead to false interpretations of experimental data. In fact zero-valent metal species have significant solubilities e.g. $Ag_{(aq)}$ ~10^{-7} mol·L^{-1}. However, it must be acknowledged that the experimental data base is sparse.

Since one option being considered in the disposal of SF/HLW is a copper coated carbon steel canister, the chemotoxic properties of copper may become an issue. For this reason, maximum Cu concentrations in the concrete and bentonite reference porewaters were calculated and yielded values of $1 \cdot 10^{-6}$ mol·kg^{-1} (solubility limiting solid $Cu_2O_{(s)}$) and $7.5 \cdot 10^{-6}$ mol·kg^{-1} (solubility limiting solid $CuS_{(s)}$). If other controlling solid phase are assumed then the Cu concentrations are much lower: $7 \cdot 10^{-10}$ mol·kg^{-1} ($Cu_{(s)}$ or $CuS_{(s))}$) for bentonite and $3 \cdot 10^{-11}$ mol·kg^{-1} ($Cu_2O_{(s)}$) for cement.

The chemical stability of low molecular weight organic compounds under the conditions existing in a cementitious near-field is an important issue. Calculations revealed that the predominant dissolved species in the case of complete thermodynamic equilibrium are $CO_{2(aq)}$, HCO_3^-, CO_3^{2-} and, CH_4. However, at least at moderate temperatures, partial thermodynamic equilibria might prevail. In the case of partial thermodynamic equilibrium where methane is not formed, the predominant dissolved species were calculated to be, C_2H_6, in addition to $CO_{2(aq)}$, HCO_3^- and CO_3^{2-}. Furthermore, carboxylic acids were predominant when it was assumed that the formation of dissolved alkanes, i.e. methane, ethane, propane, butane and pentane, was kinetically inhibited. Thus, it is presently unclear whether or not complete equilibrium in the C-H-O system can be assumed under the conditions existing in a cement-based repository. In order to try to improve the situation the chemical stability of formic and acetic acids in laboratory experiments simulating the conditions in a cementitious near field were studied.

Reactive transport simulations, conducted with the coupled code OpenGeoSys-GEM, were again focused on the evolution of the in situ condition in the repository near fields for SF/HLW and L/ILW. The simulations included various layouts of the engineered barriers and transport scenarios in order to provide a scientific basis for the performance assessment of different repository design options. The evolution of mineralogy and porosity in the Engineered Gas Transport System (EGTS) was investigated at the interfaces of concrete (cavern backfill) with gravel and gravel with sand/bentonite (tunnel backfill). The influence of the degree of saturation on the mineralogical evolution in the EGTS system was also studied

1.4 Repository Chemistry

For the documentation of the PSI/Nagra TDB 12/07 it was decided to look in more detail at the specific ion interaction (SIT) parameters recommended by the NEA in their reviews of Ni, Se, Zr, Tc, Sn, Th, U, Np, Pu, and Am. This was done because the SIT has now been implemented both in GEMS, in MCOTAC and in PHREEQC, and some of the Swiss porewaters have ionic strengths up to about 0.8 mol·kg^{-1} H_2O which is outside the validity range of the Davies equation ($I <$ ~0.3 mol·kg^{-1} H_2O) currently used in speciation calculations. It was found that out of 149 cations considered, only 13% of the values for ε(cation, Cl^-) were measured, for the 88 anions considered, only 28% of the values for ε(anion, Na^+) were measured. From these numbers it is clear that the SIT cannot be routinely used in geochemical modelling calculations. Since the

large gaps in the knowledge of the interaction coefficients cannot be expected to be filled anytime soon by experimental means, estimation methods have to be developed.

^{79}Se is an important dose determining radionuclide, and three studies on this element are described in the current annual report. LES is participating in the European collaborative project "FIRST-Nuclides" which aims at understanding and quantifying the early release of radionuclides from spent fuel (SF) subject to aqueous corrosion in a geological repository (the so-called instant release fraction, IRF.) The first task foresees leaching experiments to be carried out in the PSI hot cells on high-burn up SF and cladding samples. This work started in September 2013 and will last for one year. A second activity concerns the spectroscopic characterisation of Se in spent fuel. The aim is to determine the primary oxidation state of Se in a non-leached SF sample in order to understand the behaviour of Se in the short-term aqueous leaching tests i.e. does Se contribute to the IRF. Currently the XANES results are inconclusive. Either the Se is present in the SF as a mixture of Se(0) and Se(IV), or it occurs almost exclusively as Se(-II).

The third study concerns the uptake of SeO_3^{2-} in calcite being studied in the framework of the EU project SKIN. The irreversible trace element uptake in growing minerals maybe a potentially important retardation mechanism for certain radionuclides, but cannot be accurately predicted using an equilibrium aqueous solid-solution thermodynamic model alone. The reason is that the experimentally measured trace element partitioning usually depends on precipitation rates and related kinetic effects. Measured fractionation coefficients in calcite overgrows are substantially higher than those predicted by the atomistic calculations for the solid solution - aqueous solution equilibrium. In the LES model this apparent contradiction can be explained by considering a very high Se surface enrichment factor, $1.5 \cdot 10^7$ versus 0.1-50 for cations, and a very low sub-surface diffusivity, 10^{-10} $nm^2 \cdot s^{-1}$ versus 10^{-2} $nm^2 \cdot s^{-1}$ for cations. This extreme case of entrapment is consistent with the fact that oxoanions are more difficult to move than cations in the calcite structure. Additional data measured under different calcite growth rate conditions are required to confirm this kinetic uptake mechanism.

Also within the EU SKIN project, LES is modelling the uptake of Ra by barite in terms of kinetics and binary solid solution formation between the $RaSO_4$ and $BaSO_4$ end-members. Experimental data were modelled assuming two kinetic stages with widely different growth rates. The first stage fell within the range observed in earlier recrystallization experiments whereas the rate observed in the second stage was very fast and was interpreted as being a non-equilibrium precipitation (entrapment) process.

Within the COTHERM project the mineralogical and porosity evolution of an Icelandic hydro-thermal systems are being modelled. In a first attempt the OpenGeoSys-GEM was used to model a single fluid path with a 1D porous media approach. This was not entirely successful, because the applied kinetic model was not appropiate. In the next phase the work will concentrate on properly accounting for the secondary mineral precipitation kinetics in the reactive transport modelling.

The development work on GEMS has continued. At room temperature *T* and pressure *P*, aquatic chemical systems rarely achieve a truly reversible equilibrium state. Phase metastability and solid-aqueous reaction kinetics must be accounted for when chemical models are embedded in reactive transport simulations performed using coupled codes. *Partial equilibrium* occurs if some components in some phases are subject to additional metastability restrictions (AMR). The GEMS3K chemical speciation solver can handle AMRs and can be directly employed for simulating the kinetics of a time-dependent chemical process. An illustrative example is given in a simulation of the seeded precipitation of portlandite $Ca(OH)_2$ from aqueous solution.

1.5 Repository near field

1.5.1 Clay systems

Inorganic carbon is ubiquitous in almost all porewaters of interest in the Swiss radioactive waste disposal programme and many radionuclides readily form complexes with it. An experimental study was undertaken to measure and model the uptake of U(VI) on montmorillonite in the absence and presence of carbonate. Sorption edges and isotherms were measured in this study, and the carbonate conditions ranged from equilibrium with atmospheric pCO_2, to 1, 3 and 5 mM $NaHCO_3$ in solution. All of the data could be successfully modelled with the 2SPNE SC/CE sorption model. Ternary surface complexes were required in the case of the carbonate containing systems ($\equiv S^S OUO_2CO_3^-$ and $\equiv S^S OUO_2(CO_3)_2^{3-}$ on the

strong sites and $\equiv S^{W1}OUO_2CO_3^-$ on the weak sites).

Iron, in some form or another, is an element that is present everywhere in radioactive waste disposal systems. Under reducing conditions iron will be present as Fe(II) in solution. As part of a broad-based PhD study on the behaviour of Fe(II), competitive sorption effects with other transition metals on a synthetic iron-free montmorillonite (IFM) were investigated. The sorption of one element was measured at "trace metal" concentration in the presence of a "competing metal" whose concentration was varied from trace to relatively high concentrations (10^{-7} to 10^{-3} M). The combinations chosen were (1) trace Zn(II) and Fe(II) as competing metal and (2) trace Fe(II) and Zn(II) as competing metal. In case 1 competition between the two metals occurred, and could be modelled with the 2SPNE SC/CE sorption model, whereas in case 2 no competition effects were measured. This somewhat surprising effect was tentatively explained as being the result of electron transfer effects to Fe(III) in the lattice oxidising the Fe(II) on the surface to Fe(III) which then occupies a different sorption sites and is not influenced by the presence of Zn(II). (This interpretation implies that the synthetic "iron-free" montmorillonite must have some residual Fe(III) in the lattice.)

During 2013, the progress made on the investigations into the influence of aqueous phase speciation on diffusion was slow. No results from experiments involving both radio-labelled ligand and cationic radionuclide species were obtained. However, the pre-treatment of montmorillonite with EDTA and the investigation of the transport behaviour of the bicarbonate ion were completed and the first experiments using radiolabelled ligands are currently underway.

Additional experiments intending to demonstrate that the concentration of surface species is the dominant driving force for diffusion in Na-montmorillonite of cation tracers such as $^{22}Na^+$ and $^{85}Sr^{2+}$ were carried out. The set up in such experiments consists of using electrolyte solutions of different concentration on the two sides of the diffusion cell, but with equal tracer concentrations, and then monitoring the activities in the two half cells. The dynamics in the experiments with $^{85}Sr^{2+}$ are much faster than in the previous experiments with $^{22}Na^+$ owing to the stronger sorption of $^{85}Sr^{2+}$ and the lower bulk dry density of the montmorillonite used. The large tracer fluxes involved required the use of diffusion cells with flushed filters. The complex behaviour of the system could be modelled with a single-porosity model incorporated in Comsol Multiphysics, in which the diffusive tracer fluxes were linked to the concentrations of the background electrolyte via a cation exchange mechanism.

A generic study was undertaken to estimate the influence of the "inactive inventory", i.e. stable isotopes, on the migration of radionuclides from waste canisters into the surrounding bentonite (or Opalinus Clay). The model radionuclide chosen was the bivalent $^{59}Ni(II)$ cation; the stable isotopes Ni(II), Fe(II), Mn(II), Zn(II) and Cu(II) were considered as possible bivalent cations competing with $^{59}Ni(II)$ for the same sorption sites in bentonite (or Opalinus Clay). A simplified 1-D modelling approach was used for reactive transport calculations using MCOTAC including the 2SPNE SC/CE sorption model. Sorption competition causes a reduction in the sorption of $^{59}Ni(II)$ and results in a faster migration by up to two orders of magnitude in the arrival time at specified locations in the bentonite (or Opalinus Clay). The sorption competition effects obtained for a two-component system (e.g. one competing metal and the $^{59}Ni(II)$ tracer) do not sum up linearly in a multi-component system i.e. several competing metals plus a $^{59}Ni(II)$ tracer. Fe, Zn and Mn have about the same effect on the migration of $^{59}Ni(II)$, depending on their respective concentrations in the porewater, but Cu has the potential to have a much stronger effect.

1.5.2 Cement

The anaerobic corrosion of steel in a cementitious near field can potentially produce ^{14}C containing low molecular weight (LMW) organic compounds which could be major contributors to the dose released from an L/ILW repository. A number of activities are on going whose aim is to quantify the situation.

The first question is whether such LMW organic molecules are stable under the hyper-alkaline, reducing conditions of a cement-based repository. A custom-made gas-tight overpressure reactor was manufactured, and sampling and analytical methods were tested using an oxygen-free, portlandite-saturated solution (pH = 12.5) containing $3 \cdot 10^{-3}$ M Na-acetate spiked with ^{14}C acetic acid. This solution was aged under strict anoxic conditions for up to 60 days under a N_2 atmosphere at a pressure of 4 bar. The ^{14}C activity in the aqueous phase did not change over a period of 60 days. Gas chromatographic coupled to mass spectrometry revealed LMW organic compounds

in the gaseous phase, which is being investigated further.

Five irradiated stainless steel nuts (Brennelement-Führungsrohrmuttern) were received from the Kernkraftwerk Gösgen (KKG) and transported to the PSI Hot Laboratory. Before beginning the corrosion experiments it was important to know the ^{14}C inventory. This was done in a stepwise dissolution process of samples cut from the original nuts using a mixture of concentrated HCl and HNO_3 heated to boiling point in a first step, and a mixture of boiling concentrated sulfuric, perchloric and nitric acid in a second dissolution step. The carbon contained in the activated steel was released as CO_2 and collected in two traps containing 1 M NaOH solution. Aliquots were taken from the NaOH solutions and the ^{14}C activities were determined by liquid scintillation counting (LSC). The total ^{14}C inventory from three replicates was determined to be 17841 ± 2524 $Bq \cdot g^{-1}$, showing that the ^{14}C inventory in the activated steel is very low.

An analytical approach had been developed which allows volatile and dissolved LMW organics (number of carbon atoms $C \leq 5$) to be identified and quantified using gas chromatography (GC) coupled with mass spectrometry (MS) for the volatile LMW organics, and high performance ion exclusion chromatography (HPIEC) coupled with mass spectrometry (MS) and conductivity detection (CD) for the dissolved LMW organics. In 2013 a series of test corrosion experiments with inactive iron powders in alkaline solution was carried out. The formation of dissolved and volatile small organic molecules was determined as a function of time. The iron powders from two different manufacturers, i.e. Sigma Aldrich and BASF, were used. Prior to use, the powders, produced by reducing $Fe(CO)_5$ with hydrogen, were pre-treated according to a procedure reported by Deng et al. (1997). For the batch-type corrosion experiments, the iron powders (1 g) were immersed in 20 mL of three different artificial cement pore fluids with different pH values (pH = 13.3, pH = 12.5, pH = 11.5) in zero-headspace, gas-tight vials and shaken end-over-end in a N_2 atmosphere glove box for a maximum of 35 days. Dissolved and volatile organics were determined in the supernatant solution. For HPIEC, aliquots of the solution were filtered using special cartridges to remove components which interfered with the analysis (e.g. Fe, Cl). Samples for subsequent headspace GC-MS analysis were generated using a method developed at the Institute of Chemistry and Bioanalytics Fachhochschule Nordwestschweiz for extracting volatile organics from the supernatant solution. The results seem to indicate that the pre-treatment process applied to the iron powder was responsible for the analytical results concerning the detection of low and constant levels of formate, acetate, malonate and oxalate. In contrast, the methane, ethane/ethene, propane and butane concentrations increased with time, suggesting that these molecules were formed as a consequence of the corrosion process.

^{14}C, in the form of low molecular weight organic compounds such as acetic and formic acids, has been used in diffusion studies on hardened cement pastes (HCP). The data from these experiments were analysed with the aid of Comsol Multiphysics to calculate diffusion coefficients and sorption values. The tracer/HCP interaction was considered in the model in terms of a simple K_d formalism. The experimental measurements included both a through-diffusion and a subsequent out-diffusion phase. The best-fit K_d values for sorption were $\sim 10^{-4} \cdot m^3\ kg^{-1}$ and, hence, the anion/HCP interaction is very weak. However, for anion de-sorption, a four times larger K_d value had to be used in order to be able to reasonably reproduce the measurements. The reason for this observed discrepancy is not understood. The investigations are continuing.

As part of the investigations on the geochemical interactions at cement – clay interfaces, a cell has been designed and made which allows the in situ measurement of water content across the sample using neutron tomography and radiography, through-diffusion tracer experiments and X-ray tomography measurements. The first experiments started in May 2013 and neutron radiography images of a sample after several months of interaction showed that there was a noticeable increase in water content in the cement domain next to the interface, and also an increase in the water content in the clay away from the interface These changes in the porosity can be explained either by the swelling of the clay and/or changes in the water composition due to the intermixing of cement and clay porewater with precipitation and dissolution reactions.

Extended X-ray absorption fine structure (EXAFS) spectroscopy studies and batch sorption experiments on the Np(IV) and Np(V) uptake by calcium silicate hydrates (C-S-H phases) and HCP have shown that these cations are incorporated into the interlayer of C-S-H phases rather than bound to the surface. Desorption tests further showed that ^{237}Np sorption on C-S-H phases and HCP is a fast

and reversible process. (Desorption equilibrium was reached within a maximum of five days.)

During solidification of the waste, and during the operational phase of the repository, i.e. under oxidizing conditions, Se is expected to exist predominantly as SeO_3^{2-} and to sorb on the different cement phases (C-S-H, AFm, AFt,…) of HCP. After the closure of the repository, however, conditions will slowly become reducing, which might eventually result in a transformation of SeO_3^{2-} into Se(-II). In 2013, kinetic studies of Se(IV) uptake by different cement phases were carried out. The experiments showed that the R_d values for C-S-H phases were high. This is, at least in part, due to their very high specific surface area. It is expected that C-S-H phases are the uptake-controlling phase for Se(IV) in HCP due to the large portion of C-S-H phases in HCP.

The electrochemical reduction of Se(IV) to Se(-II) in solution is a challenging task. An experimental procedure to reduce Se(IV) to Se(-II) under alkaline conditions was tested in the glove box ($[O_2]< 0.1$ ppm) using an electrochemical cell with three electrodes. The reduction procedure was successful and was complete after 250 h. The Se(-II) solution will be used in future sorption experiments on cement phases.

In order to understand the ion sorption by a C(-A)-S-H phase at an atomistic scale, an accurate description of the acid-base properties at solid-liquid interfaces is essential. Intrinsic pK_a constants of five distinct groups on the C-S-H surface were calculated for 11 Å tobermorite as a model phase using thermodynamic integration based on ab initio molecular dynamics simulations at the density functional theory (DFT) level. The goal is to include the calculated constants into the current mesoscopic models for C-S-H phases and to apply this revised model to the description of ion sorption by cement.

1.6 Repository far field

Within 7th EU Framework Programme project CatClay the results of ^{60}Co(II) and ^{65}Zn(II) diffusion as a function of ionic strength into Opalinus Clay samples from the Mont Terri Rock Laboratory using K_d approach were modelled using PHREEQC. The modelling indicated that the sorption of ^{60}Co(II) and ^{65}Zn(II) on intact samples was lower than the sorption measured on crushed material.

However, using the in-house reactive transport code MCOTAC incorporating the 2SPNE SC/CE sorption model and the SIT ionic strength correction, the ^{60}Co and ^{65}Zn diffusion results in Opalinus Clay at all ionic strengths (1, 0.3 and 0.19 M) could be modelled successfully with one consistent data set in which the sorption values were in accord with those from dispersed systems. It should also be mentioned that "competitive sorption" from Fe(II) was included in the modelling with MCOTAC.

It is extremely important that such discrepancies as those indicated above are cleared up. For this reason a task force will be set up within LES to specifically address the question whether the sorption values and sorption models developed from dispersed system measurements are valid in intact samples.

Also within CatClay work was carried out to assess whether strongly sorbing radionuclide species bound to the compacted illite surfaces contribute to the overall diffusive fluxes i.e. whether they are mobile or not. In the original planning it was foreseen to carry out tracer diffusion experiments in a Na-illite with Sr^{2+}, Zn^{2+}, and Eu^{3+}. Because of experimental difficulties it was decided to focus on the bivalent metals and to include Co^{2+}. First experiments were carried out using special membrane confined diffusion cells. The layout of the cells required that the modelling be carried out in 3D and a suitable 3D model was set up using Comsol Multiphysics. Because of the low concentrations used, most of the results could be described using a constant K_d value which tended to be lower than those measured in dispersed clay suspensions in batch tests. Also, there were tentative indications that a sorption-enhanced diffusion mechanism may be operating.

In this context, further in-diffusion experiments on Opalinus Clay performed at different aqueous caesium concentrations could be interpreted in terms of an increase in the effective diffusion coefficient with decreasing caesium concentration i.e. sorption-enhanced diffusion.

In order to understand the molecular mechanism of Cs migration in partially saturated clays, and to explain the results of laboratory measurements, Grand Canonical Monte Carlo and Molecular Dynamics simulations were applied to model the adsorption of water films onto external surfaces of Cs and Na montmorillonites as a function of partial water pressure, and to derive the surface diffusivity of Cs and Na at different partial water pressures using molecular dynamics simulations. The results suggest that ion mobility in adsorbed water films on external basal surfaces of clay is similar to that

in the near-surface water of a saturated pore as long as the thickness of the adsorbed water film is more than two water layers. At lower partial water pressures (i.e. thinner water films) the ion mobility dramatically decreases. In contrast, the average water mobility in thin water films is higher than in the water-saturated system due to the enhanced mobility of water molecules close to the vapor−film interface.

In preparation for the over coring in the DR-A chemical perturbation experiment at Mont Terri preparatory activities (November 2013), scoping calculations have been performed to estimate the extent of the perturbations in the porewater and rock and to optimize the sampling strategy. In particular, the effect of a filter on the concentrations in the reservoir has been investigated and the data of the first (pre-perturbation) phase of the experiment have been modelled.

The sorption of Cs has been modelled in terms of a three-site cation exchange model. From comparisons between simulations and experimental Cs data in the pre-perturbation phase, it appears that the diffusive resistance of the filter is much smaller than predicted. This is possibly indicative of advective flow across the filter and within the external water-filled gap between the filter and the rock. The filter and gap parameters derived from the Cs data were used for the simulations with all other tracers or ions. A good agreement with the HTO, I^- and Br^- data of the pre-perturbation phase was obtained using very similar parameters to those found in earlier experiments.

The first preparatory experimental results from a PhD project on the structure-transport relationships for small molecular weight organic compounds in Opalinus Clay and clay minerals using acetate lactate and gluconate as test compounds revealed that these are rapidly degraded, most probably by microbial processes. K_2CrO_4 added to the porewater solutions is being tested as a microbial inhibitor in infiltration experiments using compacted clay minerals or clay rocks. Some preliminary batch sorption measurements on pure illite were also carried out. The experimental equipment for the high-pressure infiltration experiments using intact cores of Opalinus Clay are currently being set up.

One of the aims of the joint research project between the Hungarian Academy of Sciences (Centre for Energy Research) and the Paul Scherrer Institut (LES) was to test the capabilities of the 2SPNE SC/CE and Cs sorption models to make blind predictions of the sorption isotherms on the Hungarian Boda Claystone Formation (BCF) using parameters already obtained from illite i.e. applying the “bottom-up” modelling approach. Sorption isotherms for Cs(I), Ni(II), Co(II), Eu(III), Th(IV) and U(VI) were measured and modelled. Generally, a good agreement between the measured data and the predicted values was found for most of the metals except for Ni(II) and Co(II) where the blind predictions under predicted the sorption at higher equilibrium concentrations.

EXAFS spectroscopy was used to provide additional information on the sorption processes occurring. Zn (II) was chosen as a chemical analogue for Ni(II) and Co(II) because of the lower detection limits and the better signal to its noise ratio in the Fe rich rock matrix. The EXAFS results clearly showed precipitation to be an additional process taking place in the isotherm region where prediction and measurements deviated. Precipitation is the most probably reason for the mismatch. These findings suggest that there could be solubility limiting phases in the argillaceous rock-groundwater systems which are not currently included in the thermodynamic data bases, possibly layered double hydroxides (LDH) and/or phyllosilicate phases.

The benchmarking of (reactive) transport codes, especially against experimental measurements, is an important activity required to support the credibility of numerical simulations. In this context, the evolution of porosity in natural and artificial media, and the associated change in transport parameters, is of major interest for many natural and engineered systems. In the framework of a PhD project 1D and 2D reactive transport experiments have been set up. In a first experiment to characterise the flow field, a dye tracer was injected into a 2D apparatus containing a granular porous medium. The experimental results were compared with a numerical model prediction and a good match was found. A second experiment, which includes dissolution and precipitation processes, is currently being developed. This experiment will be modelled with the reactive transport code OpenGeoSys-GEM.

LES Organigram 2013

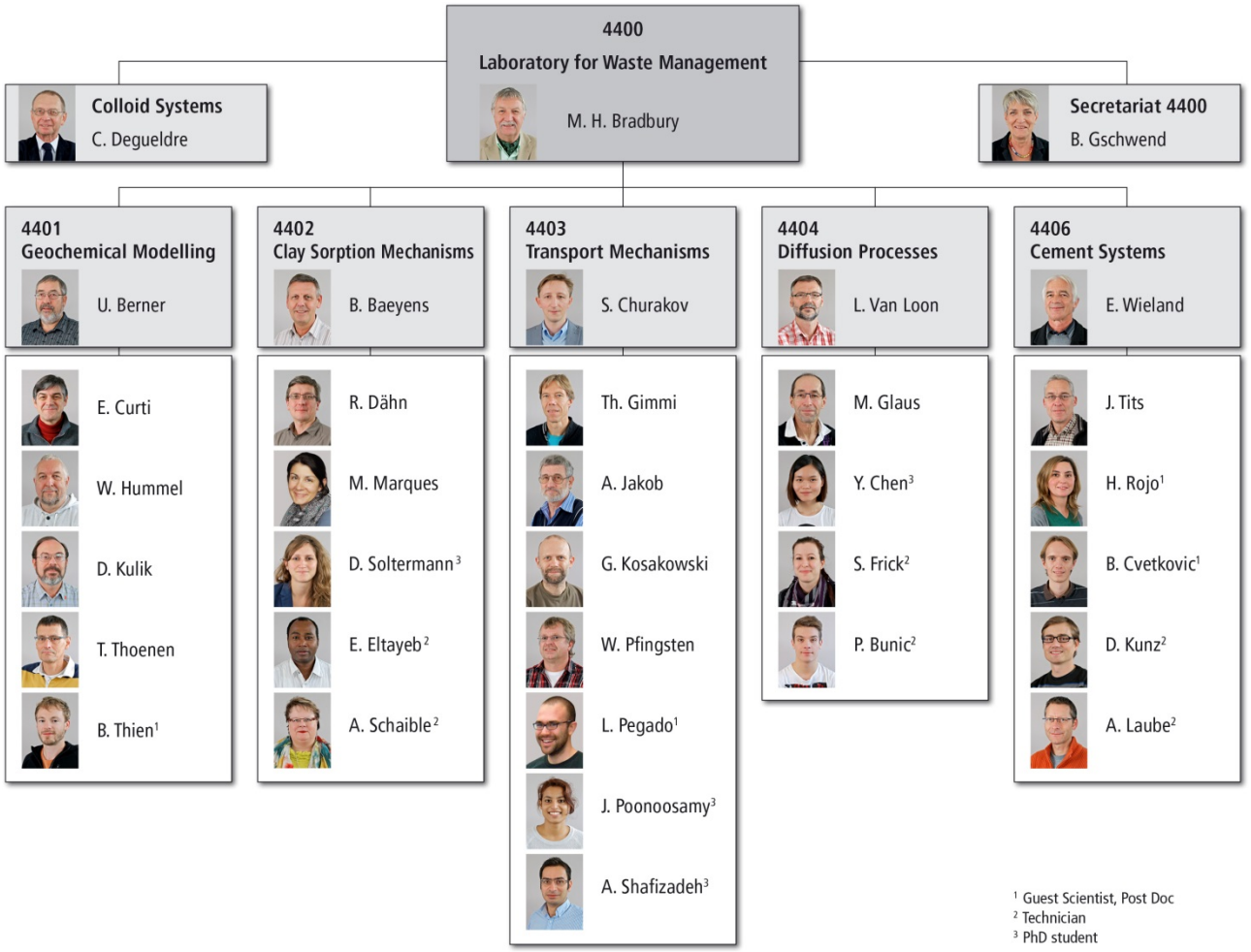

A few words of farewell from Mike Bradbury.

After over eight and a half years as Head of the Laboratory for Waste Management, it is now time to exit stage left. As can be read in this LES Annual Report for 2013, the last for which I will be responsible, the Lab is in a good scientific shape, continues to carry out high quality research in the chosen areas of activity, and applies the results successfully in Nagra's safety analyses. There will undoubtedly be changes necessary in the coming years (called "living in interesting times"), but I am convinced that the Lab is good enough, and strong enough, to weather these changes and even benefit from them.

The 26+ years which I have spent at PSI have been interesting, rewarding and happy years, not least of all because I was fortunate enough to have worked in a constructive, positive and supportive environment. I would like to express my heartfelt thanks to all my friends and colleagues at PSI, in LES, at Nagra and internationally who helped to make my work a pleasure over the years. I leave LES in good hands.

2 GEOCHEMICAL MODELLING

U. Berner, W. Hummel, E. Curti, D. Kulik, T. Thoenen, B. Thien (post doc)

2.1 Overview

As in 2012, a substantial part of the Geochemical modelling Group's work in 2013 was related to the Swiss Sectoral Plan for Deep Geological Disposal. This work comprised of finalizing contributions to two Nagra Technical Reports on the geochemical evolution of the near-field of planned geological repositories for spent fuel/high level waste and intermediate level waste. It also included writing/contributing to reports in the open literature, describing the basics of the afore-mentioned Nagra Technical Reports. Further topics related to the Swiss Sectoral Plan explicitly mentioned in this annual report are:

- Estimating maximum concentrations for chemotoxic elements
- Dissolved metals in redox state zero
- Review of the quality of SIT coefficients for aqueous radionuclide species
- Radium uptake by barite
- Spectroscopic characterization of Se fission products in spent fuel

Particularly good progress was made in modelling the kinetics of precipitation on surfaces (trace element uptake in host minerals). A substantial part of this annual report is therefore dedicated to the description of basic modelling concepts in this field in sub-section 2.5.

2.2 Work for the Sectoral Plan

2.2.1 Estimation of maximum concentrations of copper in concrete- and bentonite reference waters

Copper is not a critical element from the point of view of radiotoxicity, but it's chemotoxic properties may be an issue. Hence, maximum concentrations in the above mentioned reference waters were estimated. Thermodynamic data on copper are not included in the updated PSI/Nagra TDB 12/07 (THOENEN, 2012). Therefore, the necessary thermodynamic data were collected from the literature (PUIGDOMENECH, 2000; RICKARD & LUTHER III, 2006; POWELL et al., 2007; GRIVÉ et al., 2009).

The operational procedure was as follows: For the reference concrete and bentonite porewaters the activities of relevant species (H^+, OH^-, e^- (Eh), HS^-, S^{2-}, HCO_3^-, CO_3^{2-}, SO_4^{2-}, Cl^-) were taken from BERNER & KOSAKOWSKI (2011a, 2011b). A simplified speciation calculation was then performed by using these activities and the previously collected Cu data (BERNER, 2013).

Results for the concrete reference porewater: For a pH of 12.5 and an Eh of -498 mV, a maximum concentration of $7.5 \cdot 10^{-6}$ mol·kg^{-1} of dissolved Cu(I) was evaluated for $Cu(II)S_{(s)}$ as the limiting solid. The speciation in solution is determined by $Cu(I)Cl_2^-$ (86 %) and $Cu(I)Cl_{(aq)}$ (11 %). Under the given pH/Eh conditions elemental $Cu^0_{(s)}$, as well as $Cu(I)_2S_{(s)}$, are slightly oversaturated and could lead to lower maximum dissolved Cu concentrations. Based on the available thermodynamic data, and $Cu(I)_2O_{(s)}$ as the limiting solid phase, a much lower concentration of dissolved Cu would result i.e. $3 \cdot 10^{-11}$ mol·kg^{-1}.

Results for the bentonite reference porewater: For a pH of 7.8 and an Eh of -204 mV, elemental $Cu^0_{(s)}$ limits the dissolved Cu concentration to $7 \cdot 10^{-10}$ mol·kg^{-1} and a similar concentration is found when the limiting solid is $Cu(II)S_{(s)}$. Relevant species in solution are $Cu(I)Cl_{(aq)}$ (72 %) and $Cu(I)HS_{(aq)}$ (28 %). Hydroxide- and carbonate complexes are not relevant. The potential limiting solid $Cu(I)_2O(s)$ would produce a maximum Cu concentration of $1 \cdot 10^{-6}$ mol·kg^{-1}.

Both reference porewaters have the predominance of Cu(I) in common. A key issue is the nature of the limiting solid and, subsequently, its thermodynamic and kinetic properties. An interesting observation is the potential importance of elemental copper as a solubility limiting solid (see the following section).

2.2.2 Dissolved metals in redox-state zero: A blind spot in chemical thermodynamics

The dissolution of metals such as silver in aqueous solutions is usually considered solely as an oxidative dissolution according to the electrochemical half-cell reaction

$$Ag_{(s)} \Leftrightarrow Ag^+ + e^-$$

Whereas the solubility of zero-valent mercury is well known (CLEVER et al., 1985), experimental data on the solubility of other metals such as silver

is scarce (KOZLOV & KHODAKOVSKIY, 1983; DOBROWOLSKI & OGLAZA, 1963). The explicit equilibrium

$$Ag_{(s)} \Leftrightarrow Ag_{(aq)},$$

although published and discussed by KOZLOV & KHODAKOVSKIY (1983), is not included in any thermodynamic data base. The same is true for $Hg_{(aq)}$. The misconception that heavy metals are "insoluble" seems to be so powerful that dissolved metal atoms are not included in geochemical considerations. This blind spot in chemical equilibrium thermodynamics has consequences.

(1) The calculated "solubility abyss" for heavy metals under reducing conditions does not exist.

In the field of radioactive waste disposal, solubility limits of contaminants are important safety issues. In the case of metals such as silver, conventional model calculations lead to a "solubility abyss" under strongly reducing conditions. There, silver metal is the thermodynamically stable phase and the calculated concentration of dissolved silver is virtually zero (dashed line in Fig. 2.1). This is an artefact due to the omission of $Ag_{(aq)}$. If we include the experimental data of DOBROWOLSKI & OGLAZA (1963) in our model, then the total dissolved silver concentration stays above 10^{-7} $mol \cdot L^{-1}$ (solid line in Fig. 2.1).

(2) "Unclear differences" in experimental data sets, and strange model parameters are due to the ignorance of zero-valent metal species. In some very careful experimental determinations of the solubility of silver sulphide, $Ag_2S_{(s)}$, there are large differences between the data sets in acidic solutions (SCHWARZENBACH & WIDMER 1966; STEFÁNSSON & SEWARD, 2003a). "The reason for this is unclear" (STEFÁNSSON & SEWARD, 2003a). However, these differences can be explained by considering $Ag_{(aq)}$ in the speciation model, and assuming that the data sets have been measured under slightly different redox conditions. Measurements of the solubility of gold in water resulted in pH independent values and have been interpreted in terms of oxidative dissolution leading to extremely strong $AuOH_{(aq)}$ complex formation (STEFÁNSSON & SEWARD, 2003b). At 25°C the authors derive log K = 20.6 for the equilibrium $Au^+ + OH^- \Leftrightarrow AuOH_{(aq)}$. Thus, the complex $AuOH_{(aq)}$ would be about six orders of magnitude more stable than $ZrOH_3^+$, $NpOH_3^+$ and $PuOH_3^+$, the strongest mono-hydroxo complexes in our data base.

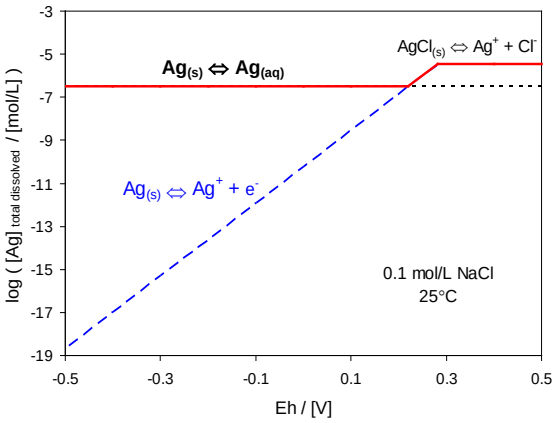

Fig. 2.1: *Solubility of silver in water as a function of the redox potential. Solid line: total dissolved silver; dashed and dotted lines: minor dissolved silver species. Data for* $Ag_{(aq)}$ *taken from DOBROWOLSKI & OGLAZA (1963).*

However, assuming a solubility of zero-valent gold similar to $Ag_{(aq)}$, the experiments can be interpreted as being governed by the formation of $Au_{(aq)}$.

Fig. 2.2 depicts the current status of data base gaps concerning zero-valent dissolved metal species, and the chances of filling these gaps.

Fe	Co	Ni	Cu	Zn
Ru	Rh	Pd	Ag	Cd
Os	Ir	Pt	Au	Hg

Fig.2.2: *Part of the periodic table of the elements. Red rectangles: elements whose zero-valent dissolved species could be important in aqueous solutions. Black symbols: zero-valent species well established (Hg), few publications available (Ag), or re-interpretation of experiments possible (Au, Pt, Pd). White symbols: No data found so far.*

2.2.3 Review of the quality of SIT coefficents for aqueous radionuclide species

The Specific Ion Interaction Theory (SIT) is the NEA method of choice for the determination of activity coefficients of aqueous species, and was used for all NEA reviews on the chemical thermodynamics of radionuclides as well as for the PSI/Nagra Chemical Thermodynamic Data base 12/07. The SIT expresses activity coefficients with a Debye-Hückel-derived term accounting for

long-range electrostatic interactions which are dominant at low concentrations, and specific cation-anion interaction coefficients (ε) describing short-range non-electrostatic interactions which are dominant at higher concentrations.

For the documentation of the PSI/Nagra TDB 12/07 (THOENEN, 2012) we decided to take a closer look at the specific ion interaction parameters recommended by the NEA in their reviews of Ni, Se, Zr, Tc, Sn, Th, U, Np, Pu, and Am. This was done for the following reasons: (1) In the documentation of the previous version of our data base, Nagra/PSI TDB 01/01, the ion interaction parameters were not discussed in a consistent and complete manner, and many of them were not even mentioned. This had little consequences for the application of the data base, since, at that time, no geochemical modelling codes were able to deal with the SIT approach. In the meantime, the SIT has been implemented both in GEMS, MCOTAC and in PHREEQC. (2) Some of the porewaters in potential host rocks for the disposal of radioactive waste in Switzerland have elevated salinities, with ionic strengths up to about 0.8 mol · kg^{-1} H_2O. This is clearly outside the validity range of the Davies equation (valid for I < ~0.3 mol · kg^{-1} H_2O), which has so far been used in speciation calculations related to solubility limits and sorption data bases. As the ionic strength of the porewaters with elevated salinites is mainly due to dissolved NaCl, it may be feasible to use the SIT. Various solubility experiments in NaCl background electrolytes have shown that the SIT is applicable at NaCl concentrations up to saturation with rock salt.

Close scrutiny of the specific ion interaction coefficients of cations with Cl^- , ε(cation, Cl^-), and of anions with Na^+, ε(anion, Na^+), yielded somewhat surprising results (see Fig. 2.3). For a total of 149 cations considered, only 13% of the values for ε(cation, Cl^-) were measured, 7% were estimated and 80% are undetermined. For a total of 88 anions considered, 28% of the values for ε(anion, Na^+) were measured, 30% were estimated and 42% are undetermined.

It is obvious from these numbers that, at present, the SIT cannot be routinely used in geochemical modelling calculations. Since the large gaps in the knowledge of interaction coefficients cannot be expected to be filled anytime soon by experimental means, estimation methods have to be considered that are based on the few measured interaction coefficients.

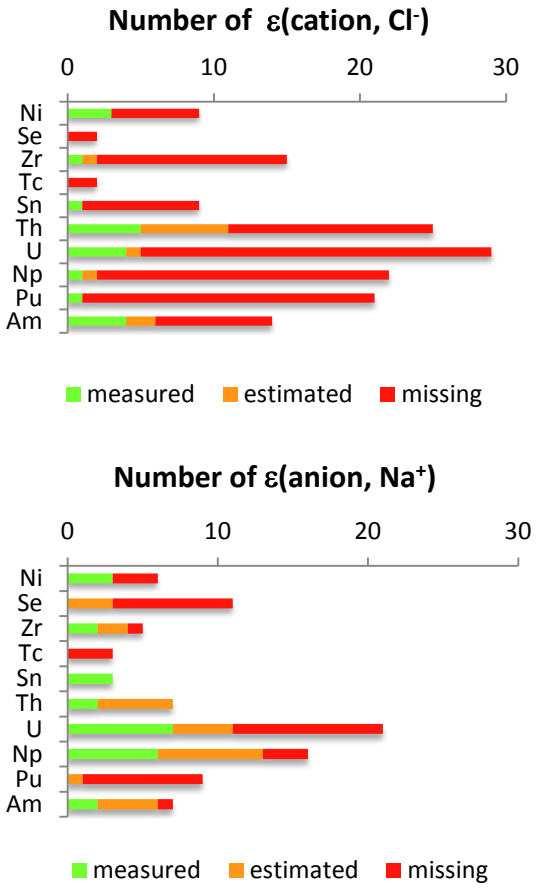

Fig. 2.3: *Quality of SIT coefficients for cations with Cl^- (above) and anions with Na^+ (below).*

2.2.4 Radium uptake by barite

In the framework of the European collaborative project SKIN, LES is in charge of modelling experimental data on the uptake of Ra by barite produced by the project partners (Forschungszentrum Jülich (FZJ), Karlsruhe Institute of Technology (KIT) and Studsvik). The objective of these experiments is to determine the kinetic mechanisms and thermodynamic properties of (Ba,Ra)SO_4 solid solutions formed during recrystallization of initially pure barite in saturated solutions. During the past year, the data supplied by FZJ were modelled assuming a simple kinetic model as well as binary solid solution formation between the $RaSO_4$ and $BaSO_4$ end-members. Fig. 2.4 shows the results of tests carried out with synthetic barite powder (Sachtleben®) at low solid/liquid ratio. The radium concentration was found to decrease slowly during the first 3-4 months. Subsequently, a sudden decrease by two orders of magnitude was observed between 120 and 180 days. After that time an equilibrium state was apparently reached.

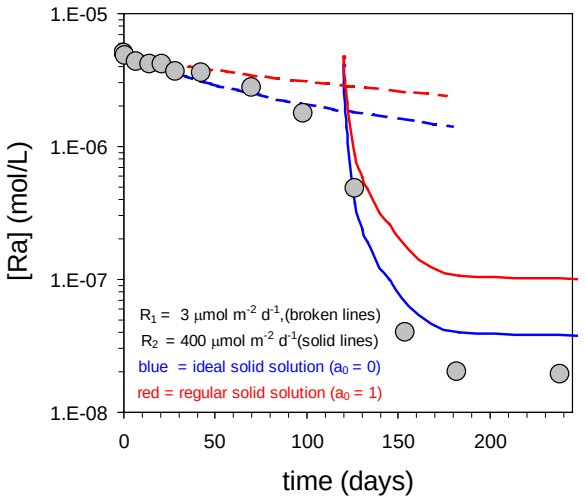

Fig. 2.4: *Experimentally determined Ra concentrations and model results for barite recrystallization tests conducted at FZJ at room temperature and 0.5 g · L^{-1}.*

This pattern can be modelled assuming two kinetic stages with widely different growth rates (3 µmol $m^{-2}·d^{-1}$ and 400 µmol $m^{-2}·d^{-1}$, normalized to the initial mineral surface area). Whereas the first stage falls well within the range of growth rates observed in earlier recrystallization experiments (CURTI et al., 2010), the rate observed in the second stage cannot be reconciled with typical slow recrystallization processes such as Ostwald ripening. Rather, it is indicative of the sudden precipitation of a new, more stable $(Ba,Ra)SO_4$ phase. Because the Ra concentrations measured after 150 days lie below the ideal solid solution equilibrium line, a negative interaction parameter (a_0 = -0.8) would be required to explain such data. This contradicts the results of the earlier mentioned experiments, and recent atomistic simulations predicting a positive interaction parameter of 1.0 ± 0.4 (VINOGRAD et al., 2013). These data therefore suggest non-equilibrium precipitation (entrapment) during the second (fast) kinetic stage. The evolution of Ra concentrations in this experiment will be monitored further.

The modelling of the experimental data from the other two partners is still in progress and will be presented in the next LES annual report.

2.3 FIRST-Nuclides Project

2.3.1 Spent fuel leaching experiments

The European collaborative project "FIRST-Nuclides" aims at understanding and quantifying the early release of radionuclides from spent fuel (SF) subjected to aqueous corrosion in a geological repository (the so-called instant release fraction, IRF). Three different PSI laboratories are involved in this project with two major tasks. The first task foresees leaching experiments to be carried out in the PSI hot cells on high-burnup SF and cladding samples from the Gösgen and Leibstadt nuclear power plants using a 19 mM NaCl - 1 mM $NaHCO_3$ (pH ~ 7.4) leaching solution, as agreed by all the project partners. The leaching experiments were started in September 2013 and will last for one year.

2.3.2 Spectroscopic characterization of Se fission products in spent fuel

The second task, in which LES is directly involved, deals with the spectroscopic characterization of Se fission products in SF, particularly ^{79}Se, a dose-determining nuclide in the safety analyses of radioactive waste disposal sites. Under oxidizing conditions, selenium forms soluble and poorly sorbing oxo-anionic species ($Se(IV)O_3^{2-}$ and $Se(VI)O_4^{2-}$). These species are expected to be readily mobilized in contact with water. In contrast, Se(0) and Se(-II) are sparingly soluble, and should not contribute significantly to the IRF. Earlier leaching experiments on Leibstadt SF failed to reveal the presence of Se in the aqueous phase, in spite of several months leaching time and sensitive analytical techniques (JOHNSON et al., 2012). The main objective of the present XAS measurements was to determine the primary oxidation state of Se in the non-leached SF sample in order to understand the behaviour of Se nuclides in short-term aqueous leaching tests.

First results have been obtained in three measuring campaigns conducted between November 2012 and May 2013. In the first campaign (INE-beamline, ANKA), the feasibility of X-ray absorption measurements on spent fuel samples at the Se K edge was tested using non-irradiated UO_2 powder pellets doped with 10, 100 and 2000 ppm SeO_2. This test was successful and usable XANES spectra could be collected even from the UO_2 sample with only 10 ppm SeO_2. An acceptable EXAFS spectrum was recorded on the 100 ppm sample, which is the most representative of the Se concentrations expected in SF (50-150 ppm, depending on burnup).

The other two campaigns were conducted at the MicroXAS beamline (SLS, PSI). A micro-dispersed UO_2 spent fuel sample (burnup 79 GWd/tU) from the Leibstadt light water reactor was prepared by gently grinding the pellet surface and then imprinting the abraded surface on Kapton tape. The adhering particles (10-15 µm max.) were

then covered by a second Kapton tape layer and mounted onto a dedicated sample holder for active XAS measurements. This preparation technique was necessary to comply with the strict radiation protection limits enforced at the microXAS beamline. Sample preparation was carried out in such a way as to preserve the radial distance of the SF particles from the pellet centre. This allowed both the porous rim of the pellet, supposed to be enriched in segregated nuclides, and the central zone of the pellet to be examined.

Fig. 2.5 shows the mean and envelope of the 16 Se XANES spectra obtained from the SF sample (grey lines) along with the spectra of three reference compounds measured during the same campaigns. Smoothing of the SF spectra was necessary for determining the exact edge position, due to the high noise/signal ratio (see Fig. 2.6) arising from the very low Se concentrations (~100 ppm), the heavy matrix (UO_2) and the small thickness (2-3 μm) of the SF particles.

Our data suggest that the Se present in the SF could be a mixture of Se(0) and Se(IV). Indeed, a linear combination fit (LCF) analysis showed that the SF spectra can be explained by considering an approximate 50%:50% mixture of Se(0) and $Se(IV)O_2$ (on an atomic basis). On the other hand, including ZnSe(-II) in the LCFs showed that this component is always dominant (> 80%, in some cases 100%, see Fig. 2.6) suggesting that selenium may occur almost exclusively as Se(-II) in the SF.

The current work focuses on theoretical XANES spectra calculations with *Feff* and *FitIt*, in order to test the latter assumption. Furthermore, efforts are being made to improve the sample preparation by using the focused ion beam technique.

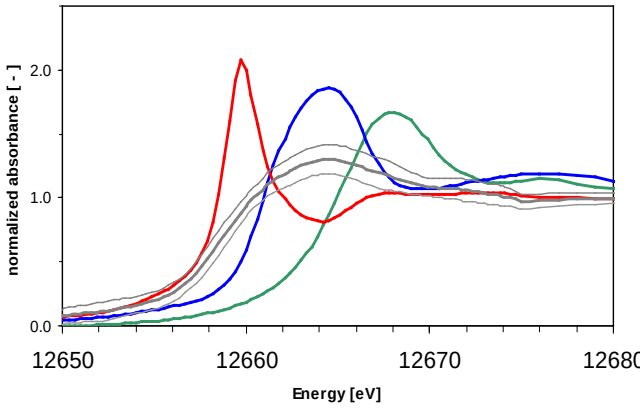

Fig. 2.5: *Average smoothed Se XANES from the spent fuel sample (thick grey line) and envelope of all individual spectra (thin grey lines) compared with the reference spectra (red = Se(0), blue= Se(IV)O, green = $Na_2Se(VI)O_4$).*

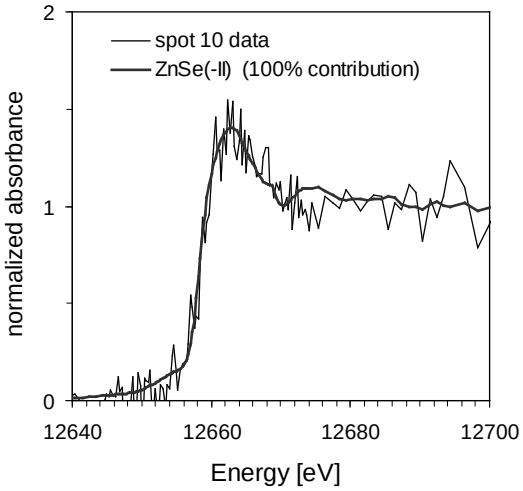

Fig. 2.6: *Some individual spectra from the spent fuel sample (here "spot 10") can be reproduced with a 100% contribution of the ZnSe(-II) reference spectrum.*

2.4 Metastability and kinetics

2.4.1 Modelling kinetics of trace element uptake in host minerals

Irreversible trace element uptake in growing minerals cannot be accurately predicted using an equilibrium aqueous solid-solution thermodynamic model alone because the experimentally measured trace element partitioning usually depends on precipitation rates and related kinetic effects. In the framework of the SKIN project, we developed a new approach suitable for complex geochemical systems. Details were given in the LES annual report 2012.

We recently investigated the uptake of anions in calcite (e.g. $Se(IV)O_3^{2-}$ which substitutes for CO_3^{2-}). Measured fractionation coefficients in calcite overgrowths are substantially higher than those predicted by the atomistic calculations for the solid solution- aqueous solution equilibrium (HEBERLING et al. 2013). This apparent contradiction can be explained in our modelling approach (Fig. 2.7) by considering a very high Se surface enrichment factor ($1.5 \cdot 10^7$ versus 0.1-50 for cations) and a very low sub-surface diffusivity (10^{-10} $nm^2 \cdot s^{-1}$ versus 10^{-2} $nm^2 \cdot s^{-1}$ for cations). This extreme case of entrapment is consistent with the fact that oxoanions are more difficult to move than cations in the calcite structure. Actually, the unit cell volume of calcite increases with the $Se(IV)O_3^{2-}$ content in the structure (AURELIO et al., 2010). Other experimental data involving different calcite growth rates are required to confirm this kinetic uptake mechanism of $Se(IV)O_3^{2-}$ by calcite.

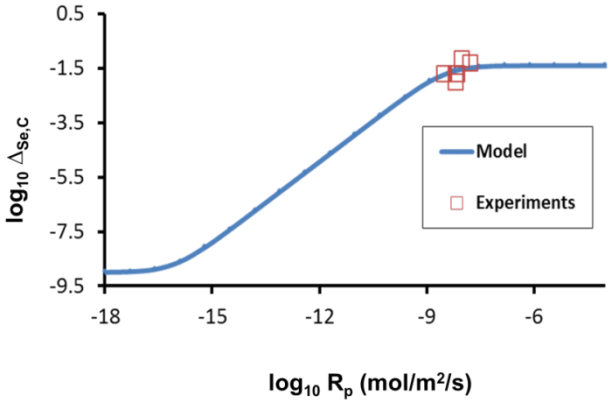

Fig. 2.7: *Fractionation coefficient as a function of growth rate for Se in calcite.*

2.4.2 Modelling water-rock interactions in Icelandic hydrothermal systems

This modelling study on the mineralogical and porosity evolution of Icelandic hydrothermal systems is part of the COTHERM project. The geothermal systems of interest are typically high enthalpy systems where a magmatic pluton located at a few km depth increases the geothermal gradient and triggers a hydrothermal circulation. The bedrock is expected to interact and equilibrate with circulating fluids. The spatial and temporal variable mineralogical evolution typically depends on the composition, temperature (and pressure) of the circulating fluid, the composition of the rock, and the character of fluid pathways (fractured or porous medium). In a first attempt, we modelled only one fluid path with a 1D porous media approach using the OpenGeoSys-GEM code. We included basalt mineral dissolution kinetics according to PALANDRI & KHARAKA (2004). For secondary minerals, we considered that they reach equilibrium with the aqueous fluid. Our first modelling results showed that such a concept is not able to satisfactorily describe the mineralogical assemblages as observed in the field by GUDMUNDSSON & ARNORSSON (2005) and by other Icelandic partners of the COTHERM project.

Therefore, we are working on properly accounting for the secondary mineral precipitation kinetics in reactive transport modelling. Currently the kinetic data are collected from the literature and implemented in an OpenGeoSys-GEM compatible data base. A typical precipitation kinetic equation is (PHAM et al., 2011):

$$\frac{dn}{dt} = S \cdot K_{298.15} \cdot e^{\frac{E}{R}\left(\frac{1}{T}-\frac{1}{298.15}\right)} \cdot (\Omega - 1)^2 + k_N \cdot Vol \cdot e^{-\Gamma \cdot \left(\frac{1}{T^{3/2} \cdot ln(\Omega)}\right)^2}$$

were *dn/dt* is the mineral mole amount variation (mol·s^{-1}), *S* is the reactive surface area of the mineral (m^2·g^{-1}), $K_{298.15}$ is the mineral precipitation constant (mol·m^2 s^{-1}) at 298.15 K, *E* is the activation energy of the reaction (J·mol^{-1}), *R* is the ideal gas constant (8.314 J mol^{-1}K), *T* is the temperature of the system (K), Ω is the saturation index of the solution for the considered mineral, k_N is the nucleation rate (mol s^{-1}L^{-1}), *Vol* is the volume of aqueous solution in the system (L), and Γ is the nucleation parameter (dimensionless). The first part of the equation is related to growth, and the second to nucleation. This approach allows secondary mineral precipitation kinetics to be considered more rigorously than the common approach of setting up arbitrary initial surfaces to start precipitation.

This task remains a challenge because available experimental kinetic parameters are relatively sparse in the literature. Where they exist, they are often inconsistent. The experimentally determined mineral surface area is not necessarily the same as the reactive surface area. Kinetic rates are always normalized to mineral surfaces, and usually the BET surface area is considered or it is estimated from the granulometry. However, the reactive surface area which needs to be considered in the calculations is the surface which is actually participating in the precipitation processes. Work on this topic is ongoing.

2.4.3 Fundamental concepts to model metastability and kinetics

Fundamental concepts developed over the years and underlying our recent R&D work on the TKinMet library implementation in the GEM software, were presented in an invited talk at the 3rd Waste-Cement Interaction Workshop, Gent, Belgium, May 6-8, 2013. Here, a short overview is given, illustrated with an example of the seeded growth of portlandite $Ca(OH)_2$.

At room temperature *T* and pressure *P*, aquatic chemical systems rarely achieve a truly reversible equilibrium state. No mineral solid precipitates or dissolves instantly; some (e.g. clays) dissolve relatively fast, but do not precipitate. Particulate solid nanophases with large specific surface areas are metastable with respect to their bulk counterparts due to the positive surface free energy contribution (WU & NANCOLLAS, 1999; NAVROTSKY, 2011). Hence, phase metastability and solid-aqueous reaction kinetics must be accounted for in any realistic chemical thermodynamic model of a complex aquatic

system. This becomes crucial when chemical models are embedded in reactive transport simulations performed using coupled codes such as PHAST (PARKHURST et al., 2010) or OpenGeoSys-GEM (SHAO et al., 2009) which combine a fluid transport model with a chemical speciation solver using a discretization of the system in space and time. Such simulations are based on the principles of local and partial equilibria.

Local equilibrium is assumed to take place in each control volume according to the assigned composition and the thermodynamic parameters of state (*P,T,* surface areas of phases *A*). *Partial equilibrium* occurs if some components in some phases are subject to additional metastability restrictions (AMR). All phases and components without AMR take part in the achievement of the partial equilibrium state under the mass balance common to the whole system.

Thus, a chemical speciation solver that can handle AMRs, such as the GEMS3K code (KARPOV et al., 2001; KULIK et al., 2013), can be directly employed for simulating the kinetics of a time-dependent chemical process by setting each AMR as a function of time *t*, the time step duration Δt, the surface area $A_{k,t}$ of *k*-th solid phase, and the net kinetic rate $R_{n,k,t}$ (details below). In principle, AMRs may also depend on a linkage of the surface of one phase (e.g. overgrowth, surface precipitate, adsorbed layer) to the volume or surface area of another phase (seed, substrate, adsorbent), which may have its own kinetics. This makes it possible to follow changes in the composition of the former separately from the composition and properties of the latter.

In a simulation, the mole amount $n_{k,t+\Delta t}$ of the solid at time $t+\Delta t$ is set for precipitation by the upper AMR $\overline{n}_{k,t+\Delta t}$ or for dissolution by the lower AMR $\underline{n}_{k,t+\Delta t}$:

$$\begin{aligned} \overline{n}_{k,t+\Delta t} &= n_{k,t} + A_{k,t} R_k \Delta t \quad \text{if} \quad \log_{10} \Omega_k > \varepsilon \\ \underline{n}_{k,t+\Delta t} &= n_{k,t} - A_{k,t} R_k \Delta t \quad \text{if} \quad \log_{10} \Omega_k < -\varepsilon \end{aligned} \tag{2.1}$$

where $0 < \varepsilon < 10^{-5}$ is a numerical tolerance. The direction depends on the sign of the phase stability index $log_{10}\Omega_k$, explained below. n_k is the amount (mol) of the *k*-th phase.

The GEM IPM algorithm [KULIK et al., 2013], as implemented in the in-house GEM software, has a great potential for thermodynamic modelling of mineral-water reaction kinetics because it can directly handle the AMRs. The chemical system is defined by the bulk composition vector, $n^{(b)}$, specifying the input amounts of chemical elements and charge; the standard molar Gibbs energies of all dependent components (species), go, at T, P of interest; the parameters of (non)ideal models of mixing in solution phases (Wagner et al., 2012), needed to calculate activity coefficients λj of species indexed with j; and the optional AMRs. After each GEM run, the primal (speciation vector $\hat{n}^{(x)}$) and dual (vector $\hat{u}^{(b)}$of chemical potentials of elements and charge) results provide concentrations and activities of all of the components in all of the phases. The stability index Ωk of any phase, even if it is absent from the mass balance, is found as a dual-thermodynamic estimate of the sum of anticipated mole fractions $\hat{x}_j$ of all phase components:

$$\Omega_k = \sum_j \hat{x}_j \sum_j \exp\left(\hat{n}_j - {g_j^\circ}/{RT} - ln\lambda_j - \Xi_k \right) \tag{2.2}$$

where the index *j* runs over all components in the phase; *R* is the universal gas constant; Ξ_k is a term for converting species concentration into the common mole fraction scale (e.g. ln *P* for gases; ln 55.5085 for aqueous species); and $\hat{\eta}_j$ stands for the *dual-solution chemical potential*

$$\hat{n}_j = \sum_i a_{ij} \hat{u}_i^{(b)} \tag{2.3}$$

where the index *i* runs over all elements and charge, and a_{ij} is the formula stoichiometry coefficient of *i*-th element in *j*-th species (e.g. 2 for O in SiO_2).

In the GEM IPM algorithm, the Ω_k index (Eq. 2.2) is considered in the *stability criterion* for any phase. Usage of this index together with the set input lower- $\underline{n}_j$ or upper $\overline{n}_j$ AMRs as function of time, according to the chosen kinetic rate law, allows GEMS to simulate the kinetics of mineral-aqueous reactions and trace element uptake. Some rate equations have been implemented in the new TKinMet class library of GEMS codes. Eventually, TKinMet will become a flexible software tool, extending and superseding existing models and codes capable of kinetic simulations (PARKHURST & APPELO, 1999; MADE et al., 1994; FRITZ et al., 2009; MIRONENKO & ZOLOTOV, 2012).

In the TKinMet library, mineral-water interaction kinetic rate laws are considered in the traditional form derived from (LASAGA, 1998; PALANDRI & KHARAKA, 2004; SCHOTT et al., 2012):

$$R_{n,k,t} = -\sum_r^{N(r)_k} \left\{ \theta_{k,r,t} f(\kappa, E)_{k,r} f(\Pi a)_{k,r,t} f(\Omega)_{k,r,t} \right\} \tag{2.4}$$

$R_{n,k,t}$ is the total precipitation or dissolution rate (in mol·m^{2}·s^{-1}); $N(r)_k$ is the number of parallel reactions that affect the amount of *k*-th solid phase; *r* is the index of reaction; $\theta_{k,r}$ is the effective fraction of *k*-th phase surface area assigned to the *r*-th reaction. Time-dependent parameters A_k and $\theta_{k,r}$ may either depend on a built-in model of particle size/area/shape evolution (see below) or be externally controlled from the mass transport code. In Eq (2.4), which can accommodate various literature rate laws, $f(\kappa,E)_{k,r}$ is the *reaction rate constant term* including the temperature correction; $f(\Pi a)_{k,r,t}$ is the *activity product term* and $f(\Omega)_{k,r,t}$ is the affinity term for the *r*-th reaction, which can take different forms, all using the current *k*-th phase stability index Ω_k (Eq 2.2).

In Eq. (2.4), the net rate $R_{n,k,t}$ has units of mol·m^{2}·s^{-1}. However, in modern kinetic models, the mean orthogonal *velocity of surface propagation* $R_{L,k,t}$ in m s^{-1} is considered. $R_{L,k,t}$ is related to $R_{n,k,t}$ by:

$$R_{L,k,t} = V_{M,k} R_{n,k,t} = \frac{M_{M,k}}{\rho_k} R_{n,k,t} \qquad (2.5)$$

where $V_{M,k}$ is the mineral molar volume in m^{3}· mol^{-1}; $M_{M,k}$ is the molar mass of the phase in kg·mol^{-1} and ρ_k is the phase density in kg·m^{-3}.

The specific surface area of the mineral is defined as $A_{S,k} = A_k / m_k$ (in m^{2}·kg^{-1}) or $A_{V,k} = A_k / V_k$ (in m^{-1}). Upon growth or dissolution, both $A_{S,k}$ and $A_{V,k}$ values vary with time because of changing particle size, shape, and surface roughness. Hence, in kinetic simulations reactive surface areas must be corrected after each time step, either externally by the reactive transport model or internally in a TKinMet library function, currently implemented as:

$$A_{V,k,t} = A_{V,k,t-\Delta t} \frac{\psi_{k,t-\Delta t}}{\psi_{k,t}} \frac{d_{p,k,t-\Delta t}}{d_{p,k,t} + 2R_{L,k,t}\Delta t} \qquad (2.6)$$

where $A_{V,k,t}$ is the initial specific surface area; $d_{p,k}$ is the mean particle diameter; $R_{L,k}$ is the linear rate (Eq. 2.5); $0 < \psi_k \le 1$ is the shape factor $\psi_k = 6V_p / (d_p A_p)$ called *sphericity*; $d_p = 6/(\psi_k A_{V,k})$; $V_p = \frac{1}{6}\pi d_p^3$ is the *mean particle volume*; and $A_p = A_k V_p / V_k$ is the *mean particle surface area*. The initial $\psi_{k,0}$ value must be set at the beginning of the simulations. Perfect mineral crystals must have a sphericity about 0.8 ± 0.1; values below 0.7 apply to thin platelets or to rough surfaces of aggregate particles.

In Eq. (2.6), the evolution in time of $\psi_{k,t}$ describes the impact of changing morphology and surface roughness on the specific surface area, and thus on dissolution or precipitation. This can be imposed by the mass transport code, or by a TKinMet function

$$\psi_k(t) = \psi_{0,k} + \psi_{1,k} u + \psi_{2,k} u^2 + \ldots \qquad (2.7)$$

where $\psi_{0,k}$, $\psi_{1,k}$, $\psi_{2,k}$, … are the empirical coefficients, and the *u* variable is the stability index, $u = \log_{10} \Omega_{k,t}$, or another function of time.

For a solid solution, the TKinMet code allows the splitting of the phase amount $n_{k,t+\Delta t}$ to the upper or lower AMRs of phase components in the partial equilibrium state at time $t+\Delta t$. Some parameters, e.g. the dissolution rate constant, the activation energy, reaction type and order constants, are considered as chemical properties of the solid, and kept in the respective phase definition. Specific surface area $A_{S,k}$ and the reactive fraction $\theta_{k,r}$, are set externally, depending on the particular reactive-transport or crystallization pathway model. For the uptake of trace elements in a solid solution, the rate equation for the host mineral is used as the basis for the uptake kinetics modelling (THIEN et al., 2013).

To illustrate the new capabilities of TKinMet, let us consider a simulation of the seeded precipitation of portlandite $Ca(OH)_2$ from aqueous solution. The kinetic rate constant and shape factor were adjusted to the experimental data of TADROS et al. (1976) who prepared supersaturated solutions by mixing equal volumes of 0.07 M $CaCl_2$ and 0.14 M NaOH stock solutions under CO_2-free conditions. In one series of experiments the crystallization of portlandite was initiated by adding 10 mg of seed portlandite crystals of A_S = 2.1 m^{2}·g^{-1} to 300 ml of the supersaturated solution. The time variation of the conductance was followed until constant conductance was achieved. It was assumed that plots of log(conductance at *t* – conductance at equilibrium) are proportional to log($[Ca]aq,_t$ – $[Ca]_{aq,eq}$), provided that the Cl^- and Na^+ concentrations remain constant during growth. With this assumption, the initial $[Ca]_{aq}$ = 0.0351 *m*, and the equilibrium $[Ca]_{aq,eq}$ = 0.0231 *m* in this system (Table 2.1) and the conductance data from Figure 2 in TADROS et al., 1976) were converted into total dissolved $[Ca]_{aq}$ values using a spreadsheet, with an estimated uncertainty < 0.3·10^{-3} *m*.

Model calculations were performed using the GEM-Selektor v.3.3 code prototype in the "Kinetics" test modelling project, at *P*=1 bar, *T*=25°C. The initial system recipe was set as given in Table 2.2 and the Davies equation was used for

computing aqueous activity coefficients. The input thermodynamic data were taken from the GEMS version of the PSI-Nagra database 12/07 (THOENEN, 2012). The initial saturation index of portlandite was 2.836, the total dissolved $[Ca]_{aq}$ = 0.0351 *m*. In a separate GEM calculation of equilibrium in the same system, but without the upper AMR for portlandite, $[Ca]_{aq,eq}$ was found to be equal to 0.0231 *m*.

Kinetic parameters for portlandite were set according to a rate equation $R_{Port} = \kappa^{-}_{Port}(1-\Omega_{Port})$. The rate constant κ^{-}_{Port}, together with the parameters of in the equation $\psi_{Port}(t) = \psi_0 + \psi_1 u$, $u = \log_{10}\Omega_{Port,t}$, were adjusted in trial-and-error simulations using the GEM-Selektor process module with graphics dialog.

Table 2.1: *Recipe of the initial chemical system.*

Property	Name	Quantity	Units
xa_	Aqua	299.26	g
xa_	CaCl2	0.0105	mol
xa_	NaOH	0.021	mol
xd_	Portlandite	0.01	g
bi_	Nit	0.0016	mol
bi_	O	0.0004	mol
dul_*	Portlandite	0.000135	mol

*Upper AMR for portlandite

Table 2.2: *Parameters of the kinetic rate model.*

Comment	Value	Reference
Net rate constant at 25°C $\kappa^{-}_{k,r}$ (mol·m^2·s^{-1})	-3.23·10^{-5}	Fit to data
Sphericity $\psi_0 + \psi_1 u$:		Geometry fit to data
ψ_0	0.83	
ψ_1	-1.6	
Reactive surface fraction $\theta_{k,r}$	1.0	Assumed
Initial specific surface area $A_{S,0}$ (m^2·g^{-1})	2.1	experiment
Initial "seed" mass (g)	0.01	experiment

This fit shows that a significant change in morphology of portlandite particles must take place during the early stages of growth. Some model sensitivity cases are given in Fig. 2.9. The upper plot shows the "best" fit for constant ψ_{Port} = 1.0 and κ^{-}_{Port} = -2.1 mol·m^{-2}·s^{-1} values which shows that the absence of a correction for morphology change leads to an incorrect shape of the model curve that cannot be fixed by adjusting the rate constant alone. The right-hand side shows the impact of too large time step duration.

Even the above, relatively simple example of portlandite seeded growth, shows that mineral kinetic models can be quite sensitive to changes in the particle/pore morphology, initial size distributions, and surface roughness. Being able to account for such factors is perhaps the most important gap in out current knowledge (MARINI et al., 2000; MIRONENKO & ZOLOTOV, 2012; SCISLEWSKI & ZUDDAS, 2010), in reactive transport modelling related to the impact of porosity changes on transport parameters and on reactive surface areas of minerals. An efficient approach to model various classical and non-classical nucleation and crystallization pathways is another challenge. These issues will be addressed in further work on the TKinMet library with applications in Sinergia COTHERM, PSI CROSS, and other on-going or applied-for projects.

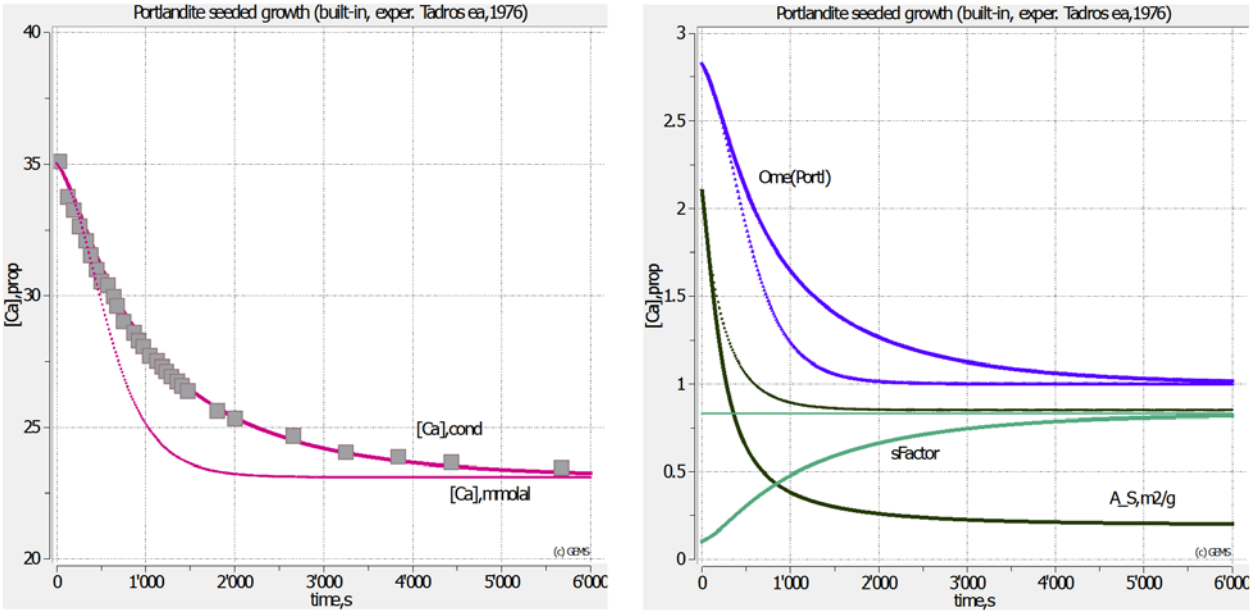

Fig. 2.8: *Simulation of the seeded growth of portlandite (full curves) in comparison with the experimental dataof* TADROS ET AL. *(1976) (squares), compared to another simulation with constant shape facto* ψ_{Port} = *0.83 (thin dotted curves). Ome(Portl) denotes* $\Omega_{Port,t}$.

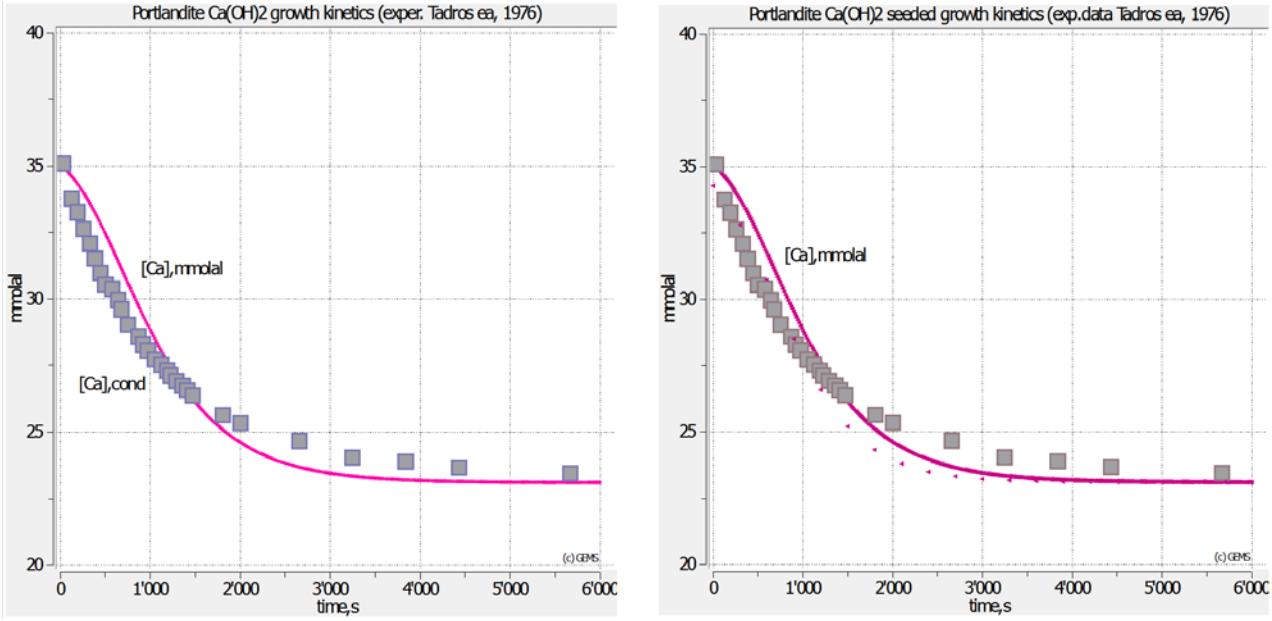

Fig. 2.9: *Sensitivity of kinetic simulations of seeded growth of portlandite. Upper plot: "best fit" with* ψ_{Port} *= 1.0,* κ^{-}_{Port} *= -2.1 mol·m*$^{-2}$*·s*$^{-1}$*, and* Δt *= 15 or 30 s. Lower plot: the same model run compared with one for a time stepping of* Δt *= 300 s (dots).*

2.5 References

AURELIO G., FERNANDEZ-MARTINEZ A., CUELLO G.J., ROMAN-ROSS G., ALLIOT I., CHARLET L. (2010)
Structural study of selenium(IV) substitutions in calcite. Chemical Geology 270, 249-256.

BERNER U., KOSAKOWSKI G. (2011a)
Freigabe Bentonitporenwässer. PSI Internal Report AN-44-11-12.

BERNER U., KOSAKOWSKI G. (2011b)
Freigabe Betonporenwasser. PSI Internal Report AN-44-11-21.

BERNER U. (2013)
Abschätzung der Löslichkeit von Kupfer in Zement – und Bentonitreferenzwässern. PSI Internal Report AN-44-12-10, Villigen.

CLEVER H.L., JOHNSON S.A., DERRICK M.E. (1985)
The solubility of mercury and some sparingly soluble mercury salts in water and aqueous electrolyte solutions. J. Phys. Chem. Ref. Data 14, 631-680.

CURTI E., FUJIWARA K., IIJIMA K., TITS J., CUESTA C., KITAMURA A., GLAUS M.A., MÜLLER W. (2010)
Radium uptake during barite recrystallization as a function of solution composition at 23 ± ^{o}C: An experimental ^{133}Ba and ^{226}Ra tracer study. Geochim. Cosmochim. Acta 74, 3553-3570.

DE PAOLO D.J. (2011)
Surface kinetic model for isotopic and trace element fractionation during precipitation of calcite from aqueous solutions. Geochim. Cosmochim. Acta 75, 1039-1056.

DOBROWOLSKI J., OGLAZA J. (1963)
Zastosowanie izotopu ^{110}Ag do badania rozpuszczalnosci srebra metalicznego i chlorku srebra w roztworach wodnych siarczanu cynku. Nucleonika 8, 79-81 (in Polish).

FRITZ B., CLEMENT A., AMAL Y., NOGUERA C. (2009)
Simulation of the nucleation and growth of simple clay minerals in weathering processes: The NANOKIN code. Geochim. Cosmochim. Acta 73, 1340-1358.

GRIVÉ M., RIBA O., MONTOYA V., DURO L. (2009)
Update of the ThermoChimie data base: Reporting of new data selection 2009. November 2009 Project ANDRA-TDB6-Task1 (Amphos21).

GUDMUNDSSON B.T., ARNORSSON S. (2005)
Secondary mineral-fluid equilibria in the Krafla and Namafjall geothermal systems, Iceland. Appl. Geochem. 20, 1607-1625.

HEBERLING F., VINOGRAD V.L., POLLY R., HECK S., ROTHE J., GALE J.D., BOSBACH D., GECKEIS H., WINKLER B. (2013)
A thermodynamic entrapment model for the quantitative description of Selenium (IV) incorporation into calcite. Geochim. et Cosmochim. Acta (submitted).

JOHNSON L., GÜNTHER-LEOPOLD I., KOBLER WALDIS J.B., LINDER H.P., LOW J., CUI D., EKEROTH E., SPAHIU K., EVINS L.Z. (2012)
Rapid aqueous release of fission products from high burn-up LWR fuel: Experimental results and correlations with fission gas release, J. Nucl. Mat. 420, 54–62.

KARPOV I.K., CHUDNENKO K.V., KULIK D.A., AVCHENKO O.V., BYCHINSKII V.A. (2001)
Minimization of Gibbs free energy in geochemical systems by convex programming. Geochem. Internat. 39, 1108-1119.

KOZLOV V.K., KHODAKOVSKIY I.L. (1983)
The thermodynamic parameters of atomic silver in aqueous solution at 25-280°C. Geochem. Inter. 20, 118-131 (translated from Geokhimiya 6 (1983) 836-848).

KULIK D.A., WAGNER T., DMYTRIEVA S.V., KOSAKOWSKI G., HINGERL F.F., CHUDNENKO K.V., BERNER U. (2013)
GEM-Selektor geochemical modelling package: revised algorithm and GEMS3K numerical kernel for coupled simulation codes. Comput. Geosci. 17, 1-24.

LASAGA A.C. (1998)
Kinetic theory in the Earth sciences. Princeton University Press, Princeton NJ.

MADÉ B., CLEMENT A., FRITZ B. (1994)
Modelling mineral/solution interactions: The thermodynamic and kinetic code KINDISP. Comput. Geosci. 20, 1347-1363.

MARINI L., OTTONELLO G., CANEPA M., CIPOLLI F. (2000)
Water-rock interaction in the Bisagno valley (Genoa, Italy): Application of an inverse approach to model spring water chemistry. Geochim. Cosmochim. Acta 64, 2617-2635.

MIRONENKO M.V., ZOLOTOV M. Y. (2012)
Equilibrium–kinetic model of water–rock interaction. Geochem. Internat. 50, 1-7.

NAVROSTKY A. (2011)
Nanoscale effects on thermodynamics and phase equilibria in oxide systems. Chem. Phys. Chem. 12, 2207 – 2215.

PARKHURST D.L., APPELO C.A.J. (1999)
User's guide to PHREEQC (Version 2). U.S. Geol. Survey WRIR 99–4259, 312 p.

PARKHURST D.L., KIPP K.L., CHARLTON S.R. (2010)
PHAST Version 2. U.S. Geol. Survey Techn. Methods 6–A35, 235 p.

PHAM V.T.H., LU P., AAGAARD P., ZHU C., HELLEVANG H. (2011)
On the potential of CO_2-water-rock interactions for CO_2 storage using a modified kinetic model. J. Greenhouse Gas Control 5, 1002-1015.

POWELL K.J., BROWN P.L., BYRNE R.H., GAJDA T., HEFTER G., SJÖBERG S., WANNER H. (2007)
Chemical speciation of environmentally significant metals with inorganic ligands (IUPAC Technical Report). Pure Appl. Chem. Vol. 79/5, 895-950.

PUIGDOMENECH I. (2000)
Thermodynamic data on copper. SKB Technical Report TR-00-13, SKB, Stockholm. Sweden.

RICKARD D., LUTHER III G.W. (2006)
Metal sulfides and clusters. In: Reviews in Mineralogy & Geochemistry 61, 421-504, Vaughan D.J., (Ed.).

SCHOTT J., OELKERS E.H., BENEZETH P., GODDERIS Y., FRANCOIS L. (2012)
Can accurate kinetic laws be created to describe chemical weathering? C. R. Geoscience 344, 568–585.

SCHWARZENBACH G., WIDMER M. (1966)
Die Löslichkeit von Metallsulfiden II. Silbersulfid. Helv. Chim. Acta 49, 111-123.

SCISLEWSKI A., ZUDDAS P. (2010)
Estimation of reactive mineral surface area during water-rock interaction using fluid chemical data. Geochim. Cosmochim. Acta 74, 6996–7007.

SHAO H., DMYTRIEVA S.V., KOLDITZ O., KULIK D.A., PFINGSTEN W., KOSAKOWSKI G. (2009)
Modelling reactive transport in non-ideal aqueous–solid solution system. Applied Geochem. 24, 1287-1300.

STEFÁNSSON A., SEWARD T.M. (2003a)
Experimental determination of the stability and stoichiometry of sulphide complexes of silver(I) in hydrothermal solutions to 400°C. Geochim. Cosmochim. Acta 67, 1395-1413.

STEFÁNSSON A., SEWARD T.M. (2003b)
The hydrolysis of gold(I) in aqueous solutions to 600°C and 1500 bar. Geochim. Cosmochim. Acta 67, 1677-1688.

TADROS M.E., SKALNY J., KALYONCU R.S. (1976)
Kinetics of calcium hydroxide crystal growth from solution. J. Colloid Interf. Sci. 55, 20-24.

THIEN B.M.J., KULIK D.A., CURTI E. (2013)
Modelling trace element uptake kinetics in secondary minerals. Procedia Earth and Planetary Science 7, 838-841. Water – Rock Interaction 14 Conference, Avignon, France, June 9-14, 2013.

THOENEN T. (2012)
The PSI/Nagra Chemical Thermodynamic Data base 12/07: Compilation of updated and new data with respect to the Nagra/PSI Chemical Thermodynamic Data Base 01/01. PSI Internal Report TM-44-12-06.

VINOGRAD V.L., BRANDT F., ROZOV K., KLINKENBERG M., REFSON K., WINKLER B., BOSBACH D. (2013)
Solid–aqueous equilibrium in the $BaSO_4$–$RaSO_4$–H_2O system: First-principles calculations and a thermodynamic assessment. Geochim. Cosmochim. Acta 122, 398–417.

WAGNER T., KULIK D.A., HINGERL F.F., DMYTRIEVA S.V. (2012)
GEM-Selektor geochemical modelling package: TSolMod C++ class library and data interface for multicomponent phase models. Can. Mineral. 50, 1173-1195.

WATSON E.B. (2004)
A conceptual model for near-surface kinetic controls on the trace-element and stable isotope composition of abiogenic calcite crystals. Geochim. Cosmochim. Acta 68, 1473-1488.

WU W., NANCOLLAS G.H. (1999)
Determination of interfacial tension from crystallization and dissolution data: a comparison with other methods. Adv. Colloid Interf. Sci. 79, 229-279.

3 TRANSPORT MECHANISMS

S.V. Churakov, Th. Gimmi, A. Jakob, G. Kosakowski, W. Pfingsten, L. Pegado (post doc), J. Poonoosamy (PhD), A. Shafizadeh (PhD)

3.1 Overview

In 2013, the main research activities of the Transport Mechanisms Group were focused on the simulations of the evolution of the in situ condition in the repository near fields for SF/HLW and L/ILW. The simulations included various layouts of the engineered barriers, and transport scenarios, in order to provide a scientific basis for the performance assessment of various repository design options (e.g. an optimal layout of backfill in the Engineered Gas Transport System, evolution of the porewater chemistry, and the integrity of the cementitious near field). The results of these simulations provided an important basis for a number of reports for Stage 2 of the Sectoral Plan for Deep Geological Disposal (SGT). The reactive transport simulations were conducted with the coupled code OpenGeoSys-GEM which has become the standard tool in LES for modelling in situ conditions in the near field of SF/HLW and L/ILW repositories and their evolution in time and space. The coupled code is maintained at a "state-of-the-art" level due to the continual development of GEMs by the Geochemical Modelling Group, international collaboration within the OpenGeoSys-GEM developer consortium and participation in international benchmarking exercises.

A further important project in the group was the coordination of the modelling activities and sampling in the DR-A experiment at the Mont Terri Rock Laboratory. Unlike previous experiments, the DR-A is investigating the effects of chemical perturbations in the porewater on ion transport in the Opalinus Clay. The data measured in the field experiments are used as inputs for the models and concepts applied in transport simulations.

A step forward in understanding sorption and transport in compacted clay systems was achieved through the inclusion of sorption models based on data from dispersed systems in the successful reactive transport simulation of ion transport in Opalinus Clay and compacted bentonite taking into account sorption competition effects.

The simulations carried out in performance assessment studies span time frames of a million years and therefore have to be conceptually simple and numerically robust. To maintain "state-of-the-art" capabilities numerical codes are benchmarked and modelling competences are continuously expanded. In this context, small-scale laboratory transport experiments are being conducted in the framework of PhD projects to provide important data, and a basis for checking the transport model calculations. On the other hand, atomistic simulations provide insights into the molecular mechanisms of transport and sorption processes at the nano scale and help to justify the assumptions made in the macroscopic models.

3.2 Sectoral Plan for Deep Geological Disposal

3.2.1 Geochemical evolution of in situ conditions in the Engineered Gas Transport System

The evolution of mineralogy and porosity at material interfaces in the Engineered Gas Transport System (EGTS) was investigated through reactive transport calculations. The systems studied included the interfaces of concrete (cavern backfill) with gravel, and gravel with sand/bentonite (tunnel backfill) as shown in Fig. 3.1.

With the aid of 1D reactive transport models, the effect of different layouts and backfill material distributions in the EGTS were examined under fully water saturated conditions. The dimensions of the buffering layer (e.g. gravel, sand-bentonite mix, etc.) between the clay and concrete materials mainly affect the diffusive transport in the water phase. SiO_2 rich materials (e.g. amorphous SiO_2) are not in thermodynamic equilibrium with the cement porewater. The so-called alkali silica reaction (ASR) occurring in concrete between cement paste and SiO_2 rich-reactive aggregates might lead to a long term degradation of concrete and suppress mineral precipitation near interfaces.

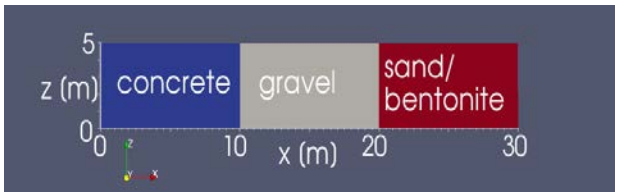

Fig. 3.1: *Conceptual layout for the two-dimensional simulations of the in situ conditions in EGTS with spatially varying fluid saturation.*

The influence of the degree of saturation on the mineralogical evolution in the EGTS system was calculated using a simplified 2D model (KOSAKOWSKI & WATANABE, 2013). Fig. 3.1 shows a cavern entrance filled with a concrete/mortar backfill on the left and an access tunnel backfilled with a sand/bentonite mixture on the right. A 10 m long section filled with gravel separates the cement and clay materials. The flow rates used in the reactive transport simulations were extracted from local scale multi-phase flow calculations on the re-saturation of the repository (SENGER & EWING, 2009). A scenario in which a steady state flow regime from the access tunnels (right) towards the emplacement cavern (left) is established after about 1000 years was applied. In the initial setup, only the lower part of the model domain was saturated and the upper part of the model domain was partially saturated (Fig. 3.2).

The gravel layer has a very low residual saturation and a very narrow capillary fringe. Mass transport is strongly hindered by the low hydraulic and diffusive conductivities of the partially saturated domains. The transport of Cl^-, which was used as a model conservative tracer, is strongest in the fully saturated domain and significantly delayed in the (upper) partially saturated zone (Fig. 3.3). The concentration distribution of dissolved Na shows a more complicated pattern because Na is consumed by the formation of clay and zeolite minerals and participates in cation exchange reactions.

The mineralogical evolution under fully saturated conditions using the 2D model is very similar to the results obtained in the 1D model, whereas a decrease in water saturation very much reduces transport in the fluid phase and also reduces the associated mineralogical changes. In the scenario considered, the clogging of the concrete/gravel interface does not take place because the precipitation of calcium-silicate-hydrates at the interface is suppressed by the fast consumption of alkali ions by ASR reactions.

In evaluating the results it is important to keep in mind that the data obtained in reactive transport simulations are influenced by the model assumptions on the reactivity of minerals (kinetics), the transport properties of materials at the interfaces, and also the numerical model parameters such as mesh size. These model dependencies lead to large uncertainties in the predictions and require the concepts and parameters to be checked by experiments.

3.2.2 DR-A experiment in the Mont Terri rock laboratory

The DR-A experiment at the Mont Terri Rock Laboratory is being carried out to investigate the effects of chemical perturbations in the porewater (high ionic strength pulse) on the transport of tracers and major ions in the Opalinus Clay. In these experiments, the tracer concentrations in the reservoir are continuously monitored on-line. Over-coring is planned towards the end of 2013. Preparatory activities for the over-coring include scoping calculations to estimate the extent of the perturbations in the porewater and the exchanger; and to optimize the sampling strategy. In particular, the effect of a filter on the evolution of concentrations in the reservoir has been investigated and the data of the first (pre-perturbation) phase of the experiment have been modelled. Modelling of the data from the post-perturbation phase has been started.

Fig. 3.4 shows the effect of the presence of a filter and the water-filled gap between filter and rock for a mobile tracer and a sorbing tracer. For the mobile tracer, the dilution by mixing with the fluid in the filter and gap is important and leads to a notable initial concentration drop within the first ~1-2 days. The filter has only a small effect on the reservoir concentrations of mobile tracers, as can be seen when comparing simulations with or without filter and gap when the effect of dilution for the former is eliminated (by assuming an initial concentration C_i=1 in the filter and the gap). In contrast, the diffusive filter resistance is very important for sorbing tracers (e.g. Cs). Thus, Cs data are most sensitive to the filter properties.

The sorption of Cs has been modelled in terms of a three-site cation exchange model (BRADBURY & BAEYENS, 2000) with the site capacities derived from the illite content of Opalinus Clay. From the comparisons between simulations and experimental Cs data in the pre-perturbation phase, it appears that the diffusive resistance of the filter is much smaller than predicted. This is possibly indicative of advective flow across the filter and within the external water-filled gap between the filter and the rock. It was thus necessary to use a

very large diffusion coefficient for the filter, and an increased value for the external gap, in order to account for the advective mixing. A good match with the experimental Cs data of the pre-perturbation phase could then be obtained using ion exchange parameters from JAKOB et al. (2009) and a slightly smaller pore diffusion coefficient compared to earlier experiments (Figure 2b). The filter and gap parameters derived from the Cs data were than used for the simulations with all other ions. A good agreement with the HTO (Fig. 3.5a) and the I^- and Br^- data (not shown) of the pre-perturbation phase was obtained by using very similar parameters to those in earlier experiments.

Based on the fits obtained in the first phase, predictions for the post-perturbation phase after increasing the Na, K, and Cl concentrations approximately match the measurements for Cs (Fig. 3.5b). However, they are only roughly approximate for other ions (Fig. 3.6) when using the same diffusion coefficient for all ions. A better match is obtained when species-specific diffusion coefficients are used (Fig. 3.6). Finally, a Donnan approach has been introduced in the model to take anion exclusion into account. Simulations with the Donnan model are on-going.

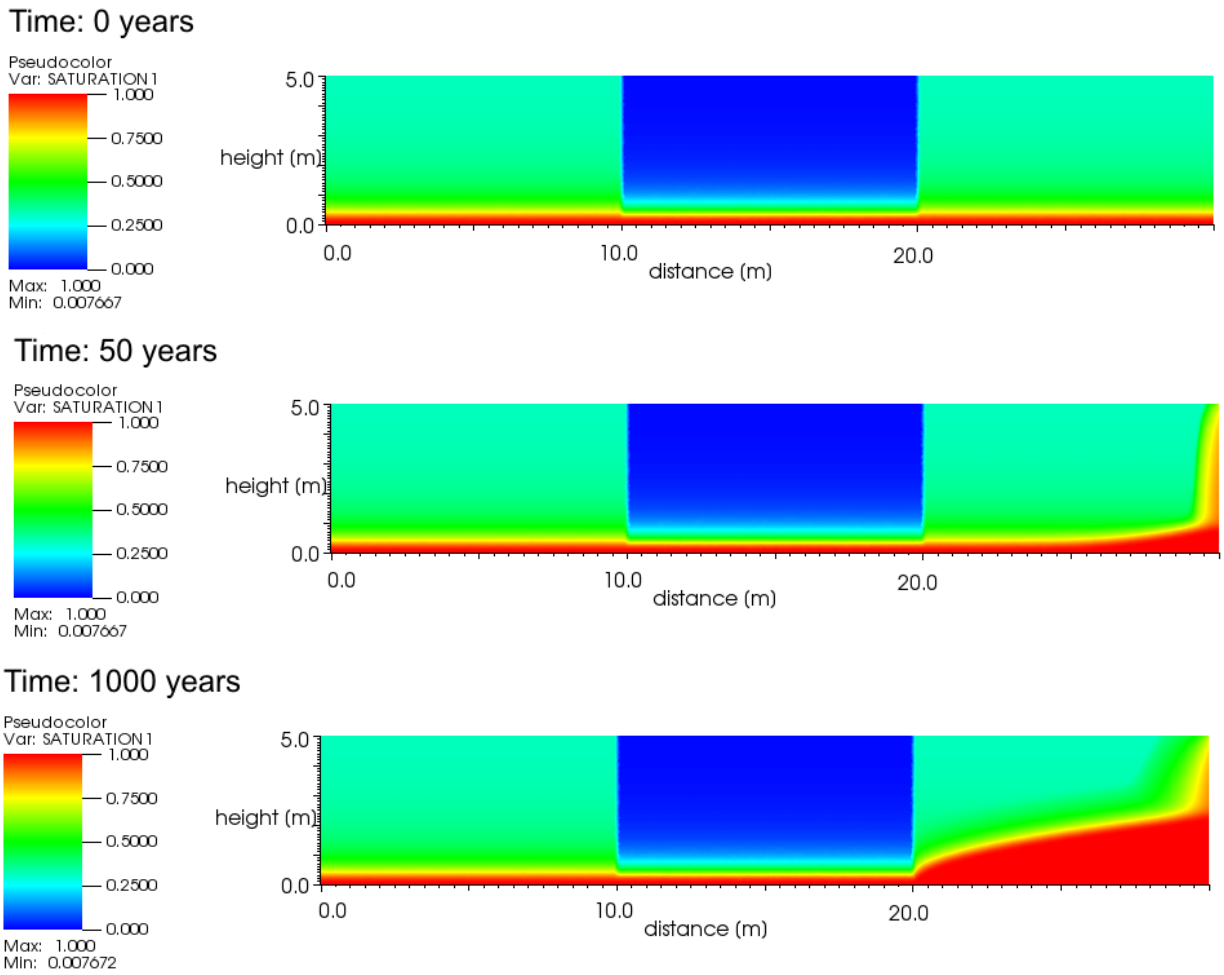

Fig. 3.2: *Evolution of the degree of saturation (from top to bottom): initially, after 50 years, and after 1 000 years. The bottom picture is close to steady state if no changes in the boundary conditions or porosity occur.*

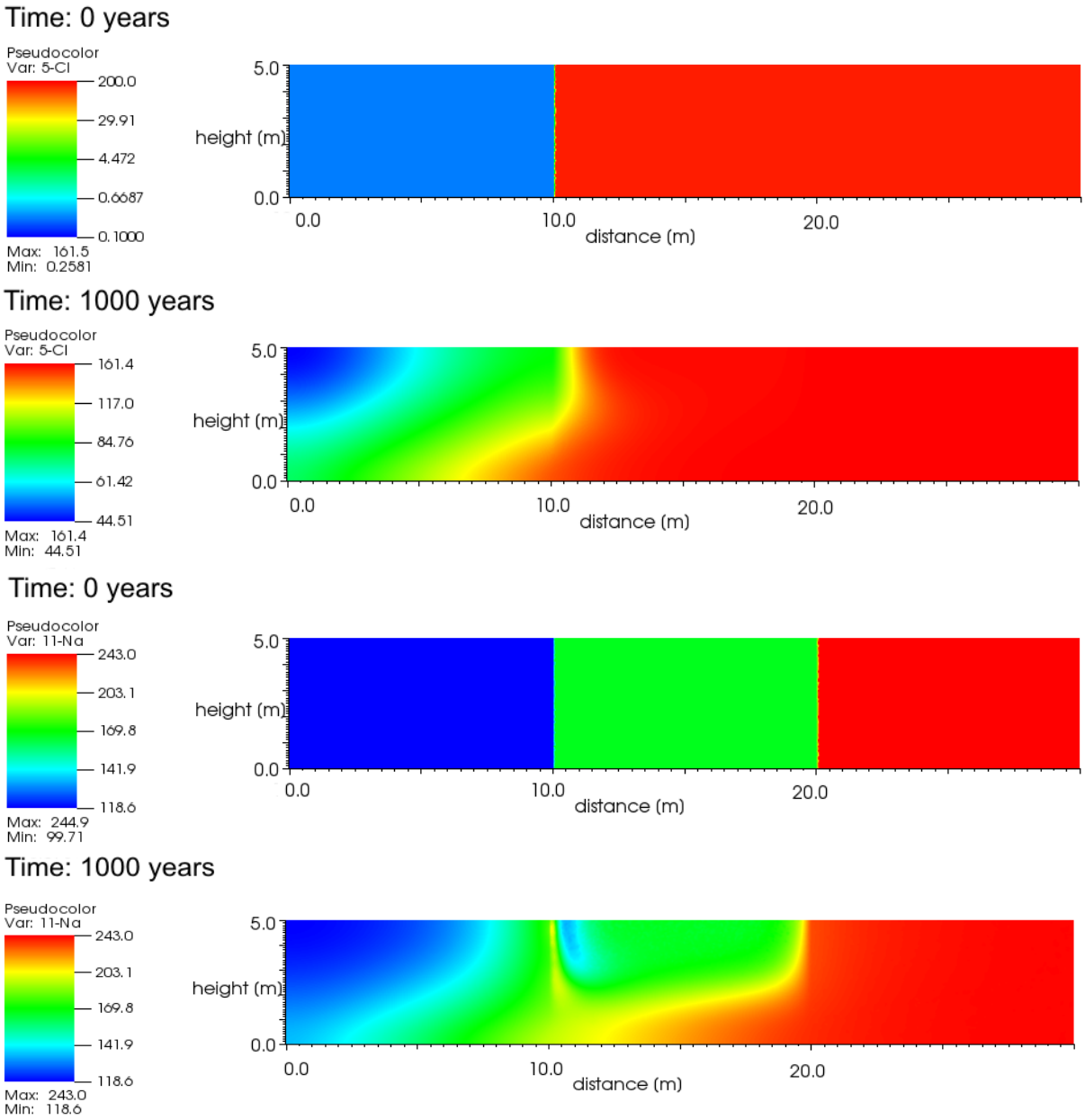

Fig. 3.3: *Concentrations (mol·m^{-3}) of total dissolved Na^+ (bottom) and Cl^- (top) in the porewater initially, and after 1 000 years.*

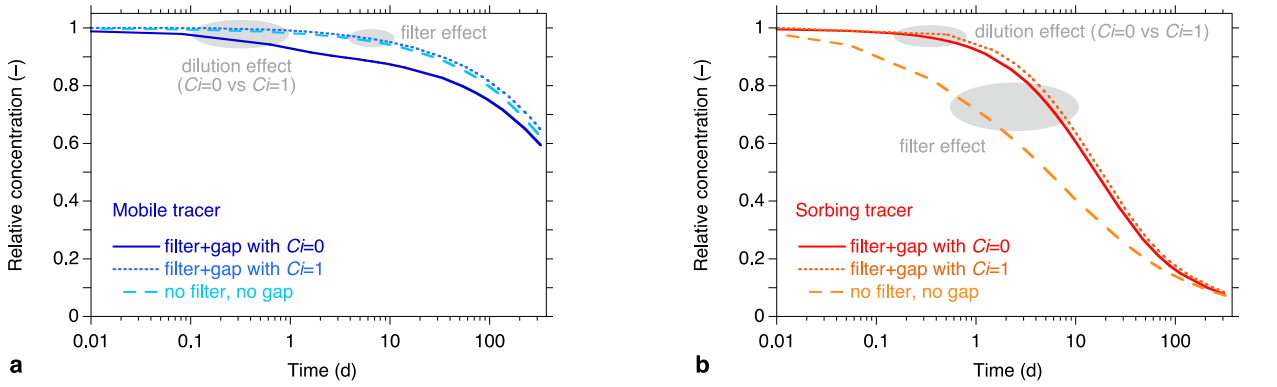

Fig. 3.4: *Effect of filter and gap in the experimental setup on the tracer concentrations in the reservoir for (a) a conservative tracer such as HTO, and (b) a sorbing tracer such as Cs. For the conservative tracer, dilution in the fluid in the filter and gap having initially zero concentration (C_i=0), has a significant effect. For the strongly sorbing tracer, the mixing is mitigated by the slow diffusion through the filter.*

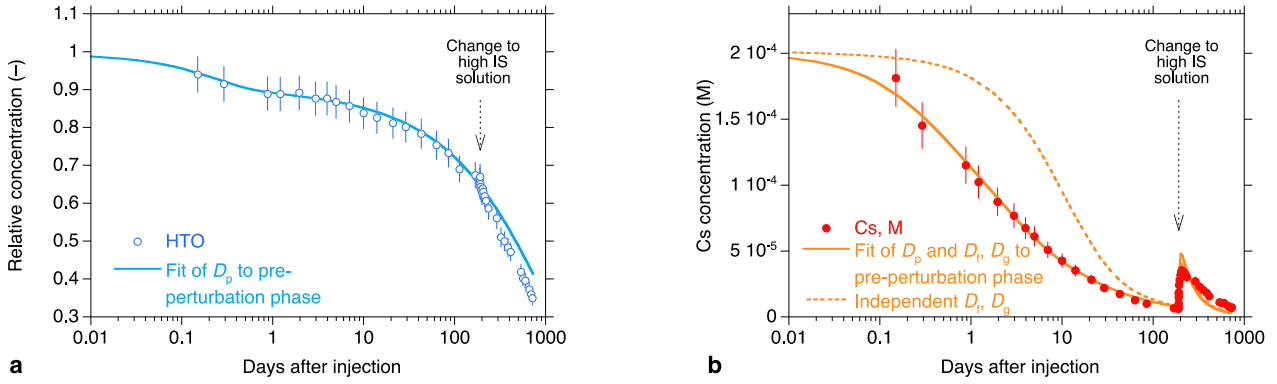

Fig. 3.5: *Measured data and simulation results for (a) HTO and (b) Cs, in the DR-A experiment.*

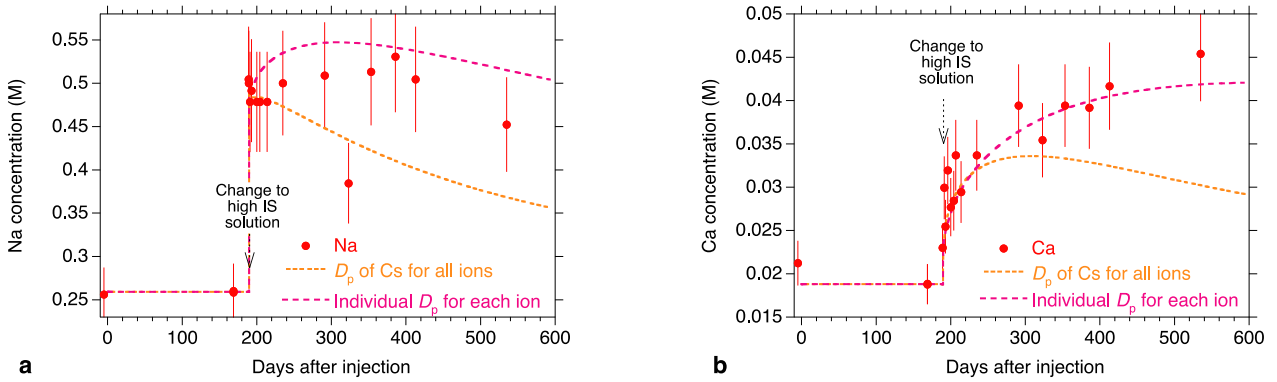

Fig. 3.6: *Measured data and simulation results for some of the major cations in the DR-A experiment.*

3.2.3 Modelling of Zn and Co in-diffusion experiments: Application of the 2SPNE SC/CE sorption model and SIT ionic strength corrections.

Several studies have been performed to assess the influence of ionic strength on the diffusion/ sorption of radionuclides. These have yielded empirical laws for the effective diffusion coefficient as a function of ionic strength when using a K_d approach. Here, an approach is presented in which the well-established 2SPNE SC/CE sorption model (BRADBURY & BAEYENS, 2005) has been included in the reactive transport code MCOTAC (PFINGSTEN, et al. 2011) and applied to interpret diffusion experiments in compacted system at higher ionic strength using the SIT ionic strength correction (HUMMEL, 2009, THOENEN, 2012). The results obtained with SIT and Davies corrections were compared with the data from recently performed laboratory experiments on the in-diffusion of the moderately sorbing radionuclides ^{60}Co and ^{65}Zn into Opalinus Clay at low and high ionic strengths.

The simulations with the SIT ion strength correction are in excellent agreement with the experimental results which indicate that the Co and Zn concentration profiles are almost independent of the ionic strength (Fig. 3.7). In contrast, the application of the Davies model predicts a strong variation of the diffusion profiles at high ionic contradicting the experimental observations. The failure of the Davies model at high ionic strengths should not be unexpected since it is well known that its validity is limited to ionic strengths < 0.5 M. For lower ionic strength both the Davies and SIT approaches yield consistent results. The simulations clearly demonstrate the importance of using the correct thermodynamic model (i.e. the SIT-ionic strength correction) for the interpretation of the diffusion experiments at higher ionic strengths.

An improved fit for the Co and Zn in-diffusion data was obtained with the model taking into account the sorption competition of Zn(II) and Fe(II) with Co(II) in the clay porewater. The Fe(II) concentration in Opalinus Clay porewater is buffered by the solubility of siderite. However, the reservoir solution used in the experiments contained no Fe(II). The equilibration of the sample with the artificial Fe(II)-free porewater resulted in the development of an Fe(II) gradient in the clay.

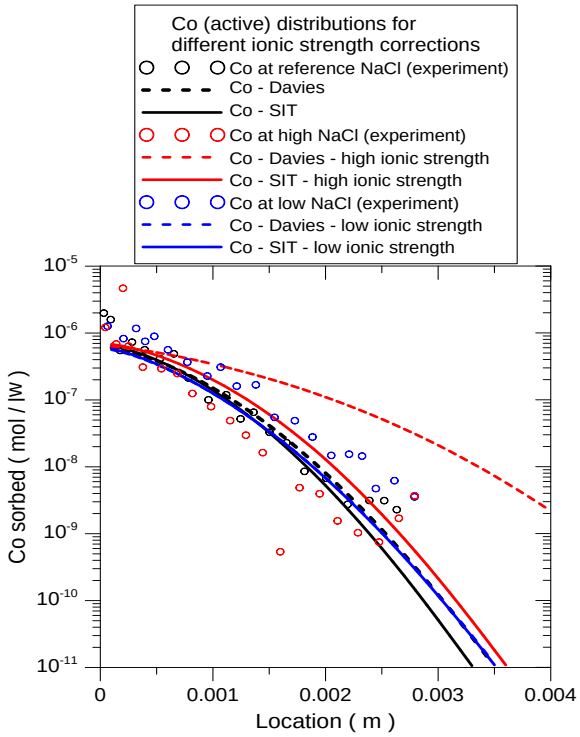

Fig. 3.7: *Measured and calculated Co profiles in the Opalinus Clay sample for porewaters with different ionic strengths (high refers to 1 M, low to 0.15 M whereas the reference ionic strength is about 0.3 M). The ionic strength of the porewater was varied by adjusting the NaCl concentration. The diffusion profiles were calculated using MCOTAC with either the Davies or the SIT ionic strength corrections and the diffusion coefficient fitted to the experimental data at the reference ionic strength. The profiles obtained with the Davies and SIT corrections are very similar at the reference and low ionic strength. The profiles obtained with the SIT at high ionic strength are in very good agreement with the experimental data. In contrast, the use of Davies significantly overestimates the experimentally measured penetration depth of the Co tracer into the Opalinus Clay sample.*

Fig. 3.8 shows the fits to the Co and Zn profiles for different pre-equilibration times. For the short pre-equilibration times a characteristic two-slope profile of Co-concentration develops due to the sorption competition with Fe(II).

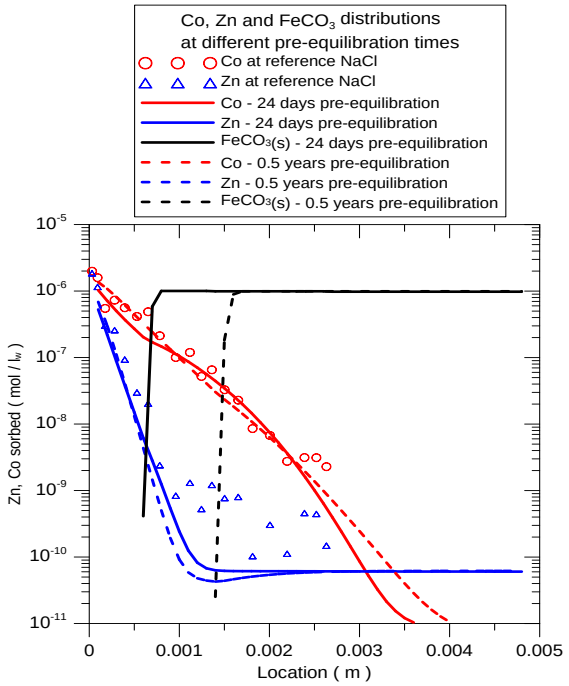

Fig. 3.8: *Measured and calculated Zn and Co profiles in the Opalinus Clay sample for the reference ionic strength of ~0.3 M. Calculations have been performed using MCOTAC for two different pre-equilibration times assuming Fe out-diffusion from the sample into the reservoir. Fe is initially buffered by siderite in the sample which becomes depleted with time.*

3.2.4 Influence of the "inactive inventory" on the migration of ^{59}Ni(II) in the vicinity of a high level waste repository

A generic model approach was used to estimate the influence of the "inactive inventory", i.e. stable isotopes, on the migration of radionuclides from waste canisters into the surrounding bentonite or Opalinus Clay. The model radionuclide chosen was the bivalent ^{59}Ni(II) cation; the stable isotopes Ni(II), Fe(II), Mn(II), Zn(II) and Cu(II) were considered as possible bivalent cations competing with ^{59}Ni(II) for the same sorption sites in bentonite or Opalinus Clay. A simplified 1D modelling approach was used for reactive transport calculations using the MCOTAC code including the 2SPNE SC/CE sorption model. The calculated ^{59}Ni(II) breakthrough curves in bentonite and Opalinus Clay are compared to illustrate the influence of the individual stable isotopes present in the porewater.

Sorption competition causes a reduction in the sorption of ^{59}Ni(II), and results in a faster migration of ^{59}Ni(II) by up to two orders of magnitude in the arrival time at specified locations in the bentonite or Opalinus Clay. This effect is strongest for the highest stable isotope concentrations. Fe, Zn and Mn have about the same effect on the migration of ^{59}Ni(II), depending on their respective concentrations in the porewater. Cu, however, has the potential to cause a much stronger effect (see Fig. 3.9). The sorption competition effects obtained for a two-component system (e.g. one competing metal and the ^{59}Ni(II) tracer) do not sum linearly in a multi-component system i.e. several competing metals plus a ^{59}Ni(II) tracer. In the various scenario calculations an upper limit for the reduction in the ^{59}Ni(II) retardation has been calculated by taking into account the sorption competition influence of all the stable metals.

Although the considered model calculations include several simplifications and assumptions, they cover a wide range of possible sorption competition scenarios in the near field of a high level waste repository. More specific scenario calculations would be possible if a detailed "geochemical inventory" of radionuclides and stable isotopes were to become available. Nevertheless, upper limits for the effects of sorption competition of bi-valent stable isotopes on the migration of ^{59}Ni migration in the vicinity of a high level nuclear waste repository were assessed.

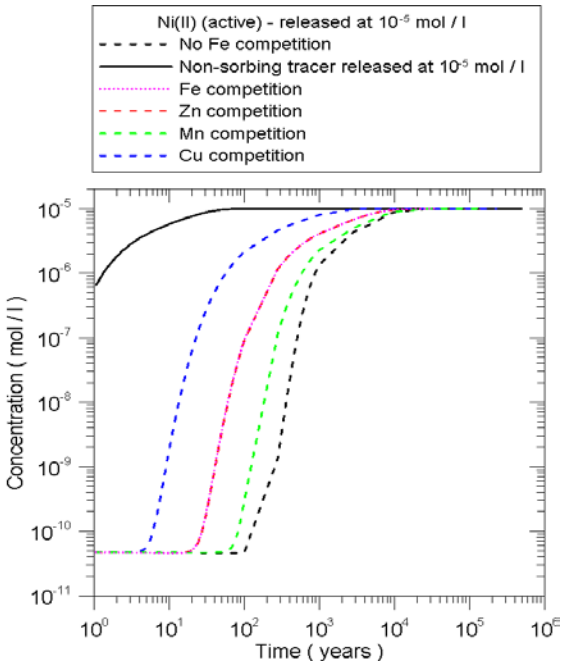

Fig. 3.9: *Calculated ^{59}Ni(II) breakthrough curves at 0.4 m within the bentonite for sorption competition with the individual stable metals; Fe(II) at $5.3 \cdot 10^{-5}$ (siderite solubility limit), Zn(II) at $1 \cdot 10^{-5}$M, Mn(II) at $3.4 \cdot 10^{-5}$ M and Cu(II) at $4.3 \cdot 10^{-7}$ M. (The breakthrough curve for a non-sorbing tracer is shown for comparison)*

3.2.5 Modelling diffusion of ^{14}C labelled organic tracers through hardened cement pastes

Activation products are radioactive isotopes formed by the absorption of neutrons by certain stable isotopes particularly in and surrounding the core of a nuclear reactor. Examples are ^{14}C and ^{60}Co. In nuclear reactors the radionuclide ^{14}C is formed due to absorption of neutrons by carbon, nitrogen, and oxygen. However, nuclear power plants are not the only source for ^{14}C containing radioactive waste. In Switzerland, ^{14}C effluents arise on-site at national research laboratories, universities, bio-tech labs and pharmaceutical companies. In nuclear power plants ^{14}C can be found mainly in the fuel, in the cladding or, to a lesser extent, in the coolant. The activated steel is the major contributor to the ^{14}C inventory in low-level waste repositories released during the course of anaerobic corrosion.

Although the half-life of ^{14}C (5730 years) is relatively short, it generally exists in forms which have a high mobility in groundwater which make it a dose-relevant nuclide (NAGRA, 2002; p. 261). Therefore, it is important to investigate the diffusion and sorption characteristics of the most important organic species so that the values can be used in safety assessment studies.

^{14}C in the form of low molecular weight organic compounds such as acetic and formic acid has been used in diffusion studies on hardened cement pastes (HCP). (See also the contribution in the Cement Systems group chapter). The data from these experiments were analysed with the aid of Comsol Multiphysics to extract diffusion coefficients and sorption values. Based on the assumptions of homogeneous and isotropic transport properties, a 1D transport model is sufficient. The tracer/HCP interaction was considered in the model in terms of a simple K_d isotherm formalism. The experiments included both a through-diffusion and a subsequent out-diffusion phase. The very good data regarding the diffusive flux [$mol \cdot m^{-2} \cdot s^{-1}$] of the ^{14}C labelled acetic acid anion across both boundaries, as well as the corresponding modelling results, are shown in Fig. 3.10.

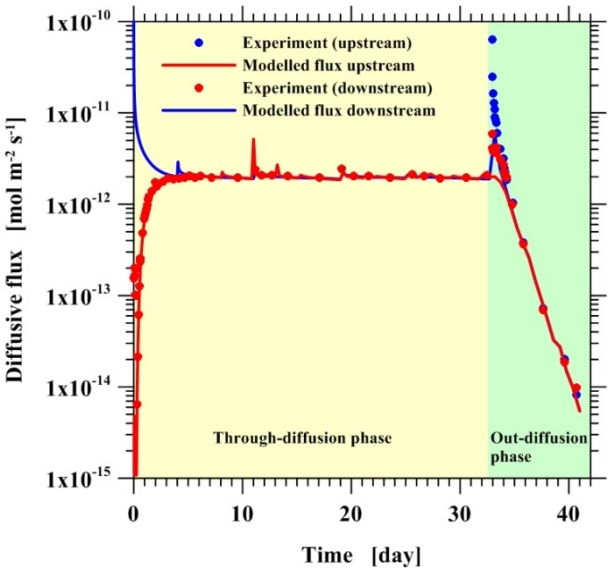

Fig. 3.10: *Experimental (points) and modelled (lines) tracer fluxes [$mol \cdot m^{-2} \cdot s^{-1}$] for ^{14}C labelled acetic acid anions through a HCP sample at the upstream (blue) and downstream boundary (red) versus time (days). For the through-diffusion phase (first 33 days), the flux was measured at the low concentration side only. For the out-diffusion phase the fluxes were measured at both low and high concentration sides.*

The best-fit K_d values for sorption are in the order of 10^{-4} $m^3 \cdot kg^{-1}$ and, hence, the anion/HCP interaction is very weak. However, for anion de-sorption, a four times larger K_d value had to be used in order to reasonably reproduce the measurements in the falling edge. The reason for the observed discrepancy between tracer uptake by the HCP and its subsequent release is presently not understood. The investigations are continuing.

3.2.6 Experimental study of cement-clay interactions

Within a PhD project (Amir Shafizadeh), a diffusion cell has been developed for in situ investigations of the geochemical interaction at cement – clay interfaces. The cell contains small cylindrical samples of clay and cement ~5 mm in diameter. The cell design allows the in situ measurement of water content across the sample using neuron tomography and radiography, through-diffusion tracer experiments and X-ray tomography measurements.

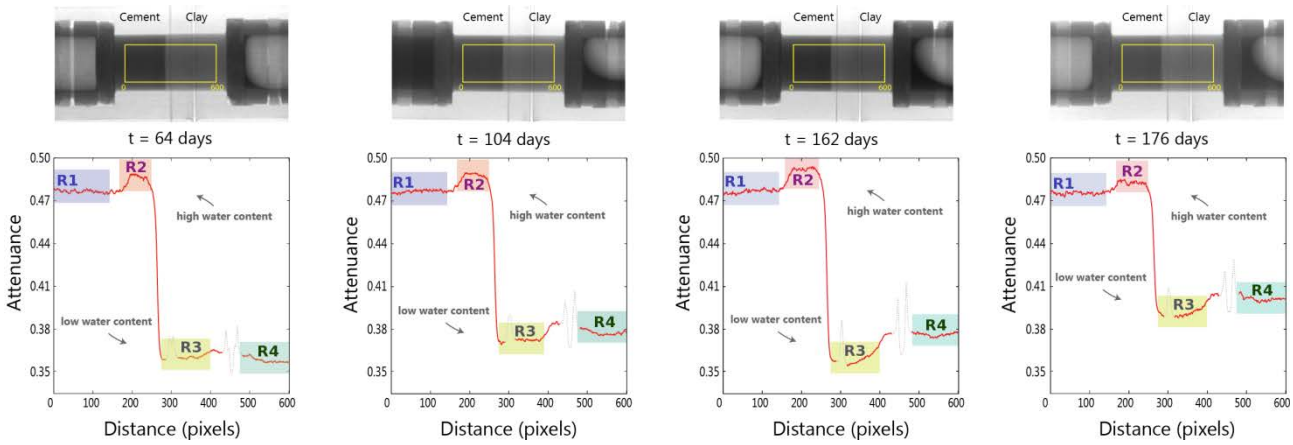

Fig. 3.11: *Neutron radiography images of a sample after 2, 3, 5 and 6 months interaction times. The cement and clay domains are on the left and right hand sides, respectively. The average intensity of the transmitted neutrons is normalized to the average value in domain R1 (at t=64 days). Larger values of I_0/I correspond to lower intensities of transmitted neutrons (i.e. higher water contents).*

The first experiments started in May 2013. Neutron radiography images of a sample after 3, 4, 5 and 6 month interaction times are shown in Fig. 3.11. The average intensity of the transmitted neutrons over the specified area has been derived for each image. It can be clearly observed in all of the images that the cement (left) has a higher water content than the clay (right). After several months of interaction there is a noticeable increase in the water content in the cement domain next to the interface (domain R2), and also an increase in the water content in the clay away from the interface (domain R4). These changes in the porosity can be explained either by the swelling of the clay and/or changes in the water composition due to intermixing of cement and clay porewater with precipitation and dissolution reactions. A detailed quantification of the changes in the chemical and mineralogical composition across the interface will be obtained by a postmortem analysis.

3.3 Fundamental understanding of transport and sorption mechanisms

3.3.1 Acid-base properties of C-S-H

Within the post-doc project "Thermodynamic equilibrium in C(-A)-S-H from molecular simulations" (L. Pegado), a subproject of the SNF-funded Sinergia project "Stable phase composition in novel cementitious materials: C(-A)-S-H (Calcium-(Aluminium)-Silicate-Hydrate)", ion sorption by a C-S-H phase is being investigated at an atomistic scale. The accurate description of acid-base properties at solid-liquid interfaces is a fundamental prerequisite to the understanding of ion sorption equilibrium. Intrinsic acidity constants (pKa's) of specific surface sites in C-S-H cannot be determined experimentally. Typically, such quantities are calculated from de-protonation enthalpies obtained from gas-phase ab initio calculations. Recently, however, the determination of pKa's from thermodynamic integration based on ab initio molecular dynamics simulations at the density functional theory (DFT) level has been established as a state-of-the-art method (SULPIZI et al., 2012). In this approach the calculations are done directly in the condensed phase and very important features such as solvent relaxation and polarization effects are taken into account.

Intrinsic pKa constants of five distinct groups on the C-S-H surface were calculated using 11 Å tobermorite as a model and focusing on two limiting cases: fully polymerised and fully de-polymerised silicate "dreierketten" chains. The former are used for the calculation of pKa's of the two -OH groups on bridging tetrahedra (Si^bO^1H and Si^bO^2H; see Fig. 3.12) and the latter for the two -OH groups in pairing tetrahedra (Si^pO^1H and Si^pO^2H) in the vicinity of a defect (removed bridging tetrahedron). The goal is to include the calculated constants into the current mesoscopic models for C-S-H (LABBEZ et. al., 2006) and to apply this revised model to the description of ion sorption by cement. Preliminary results from Titrating Grand Canonical Monte Carlo simulations in the framework of the primitive model of electrolytes, show a good agreement with experimental zeta potential values. In particular, the charge-reversal of C-S-H particles, occurring for high electrostatic coupling, is well reproduced.

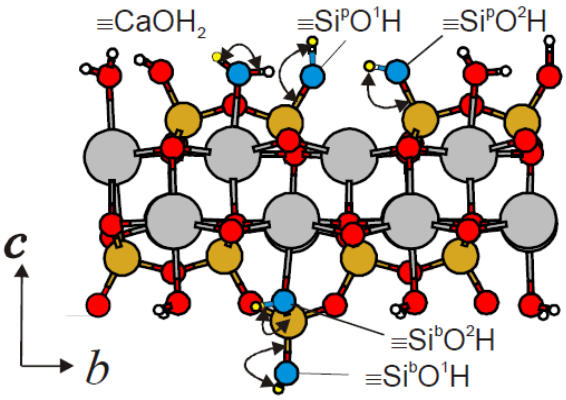

***Fig. 3.12**: Illustration of the different –OH groups on the surface of C-S-H (blue=oxygen and yellow=hydrogen). For the remaining atoms grey= Ca, orange=Si, red= O and white= H.*

3.3.2 Cation and water transport in clays under partially saturated conditions

Recently, ion and water transport in Calovo-Oxfordian clay rocks was investigated experimentally under partially saturated condition (SAVOYE et al., 2012). In order to understand the molecular mechanism of Cs migration in partially saturated clays, and to explain the results of laboratory measurements, Grand Canonical Monte Carlo and Molecular Dynamics simulations were applied to model the adsorption of water films onto external surfaces of Cs and Na montmorillonites as a function of partial water pressure. The diffusive mobility of Cs and Na at different partial water pressure was obtained by molecular dynamics simulations. The results suggest that ion mobility in adsorbed water films on external basal surfaces of clay is similar to that in the near-surface water of a saturated pore as long as the thickness of the adsorbed water film is more than two water layers. At lower partial water pressures (i.e. thinner water films) the ion mobility dramatically decreases. In contrast, the average water mobility in thin water films is higher than in the water-saturated system due to enhanced mobility of water molecules close to the vapor−film interface.

3.4 Benchmarking of coupled codes

Benchmarking of transport codes is an important activity which supports the credibility of the numerical simulations. It is essential for reactive transport codes describing complex geochemical interactions and/or radionuclide migration in the vicinity of a nuclear waste repository or in laboratory experiments.

3.4.1 SS-Bench

Within “SS-Bench”, initiated and launched by the Belgian Nuclear Research Centre, SCK·CEN, we performed simulations of the chemical degradation of a cracked concrete under near surface disposal conditions (PERKO et al., 2013) using a simplified 2D model. The objective was to gain an improved understanding of the rate of degradation of a cracked concrete structure, and ultimately to assess its impact on the transport of radionuclides and chemotoxic components. Chemical degradation of concrete affects physical and mechanical properties and consequently accelerates the migration of radionuclides through the cementitious engineered barriers. This benchmark was performed in several steps, beginning with the dissolution of only one mineral (portlandite) and constant physical properties (porosity, bulk density). The problem was then extended to evolving material properties and to more complex mineralogies.

One major finding obtained in the benchmark was that although the codes used by the participating teams relied on substantially different numerical approaches, the results obtained were all very similar and consistent. Differences in the details of the results could be traced back to differences in numerical methods and chemical setups. In terms of long-term predictions for concrete evolution, contaminant transport and risk assessment, the codes will yield results which are comparable. The benchmark considered an equilibrium chemistry approach in combination with slow transport (diffusion and advection) which results in a very slow progress of the dissolution fronts. During the course of the calculations we demonstrated that such a type of system requires the use of a flux corrected transport method (FCT) to avoid the physically unrealistic accumulation of precipitates at dissolution fronts (KOSAKOWSKI & WATANABE, 2013). This correction was recently implemented in the OpenGeoSys-GEM code.

3.4.2 Cooperation with Centre for Environmental Research, Leipzig

In 2013 co-operation with the Helmholtz Centre for Environmental Research (UFZ, Leipzig, Germany) in the field of reactive transport concentrated on further developing the coupled code OpenGeoSys-GEM in connection within the Grimsel LCS project and fostering the contacts between PhD students of both institutions.

In the summer of 2013 the OpenGeoSys Version 5.4.06 was published. The coupling between UFZ's OpenGeoSys general purpose transport code and the GEMS-PSI Gibbs Energy Minimization code for geochemical modelling was extended to work with the Richards flow module of OpenGeoSys. In addition, the new parallel OpenGeoSys implementation with PETSC and FCT libraries was extended to the coupled OpenGeoSys-GEM version. The release included two new benchmarks for OGS-GEM with PETSC library.

3.4.3 Experimental benchmarks for the verification and validation of reactive transport codes

The evolution of porosity in natural and artificial media, and the associated change in transport parameters, is of major interest for many natural and engineered systems. For instance, in the disposal of nuclear waste in a deep geological repository, concrete materials will be used to construct supports, as cavern backfill and for waste conditioning. The diffusion of the cement porewater into the surrounding clay host rock will lead to the precipitation and/or dissolution of mineral phases near the clay-cement interface and might subsequently lead to a reduction/increase in the porosity (DAUZERES et al., 2010). Such processes will have consequences for mass transport phenomena within the repository. Several modelling studies have been carried out to predict the effect of the alkaline plume on clay barriers (DE WINDT, 2004; TROTIGNON et al., 2005; DE WINDT et al., 2007; COCHEPIN et al., 2008). The numerical modelling demonstrated that for scenarios with porosity reduction, the simulation results were strongly influenced by the reaction kinetic parameters used in the model, and the numerical mesh refinement (MARTY et al., 2009). Thus, for reliable predictions of the long-term evolution of in situ conditions in the repository near field, the underlying numerical and conceptual models have to be calibrated by data from field and/or laboratory experiments

In the framework of a PhD project partially supported by Nagra (Jenna Poonoosamy), 1D and 2D reactive transport experiments in granular media have been set up in which the evolution with time can be easily assessed. In the first experiment a simple 2D benchmarking apparatus of dimensions 0.1 m by 0.1 m and containing a granular porous medium (silicon dioxide, SiO_2) was set up. A conservative dye tracer (Eosin) was injected at the inlet port. A second injection of the dye tracer took place at injection port 'a' five hours later. This allowed the flow field to be characterised. The experimental results were compared with a numerical model prediction and a good match between the two was achieved as can be seen in Fig. 3.13.

The second experiment, which includes dissolution and precipitation processes, is currently being developed. The principle is shown in Fig. 3.14. The injection of barium chloride accelerates the dissolution of strontium sulfate and barium sulfate precipitates. The dissolution of strontium sulfate (molar volume $4.26 \cdot 10^{-5}$ $m^3 \cdot mol^{-1}$) followed by the precipitation of a mineral with bigger molar volume, barium sulfate (molar volume $5.21 \cdot 10^{-5}$ $m^3 \cdot mol^{-1}$), leads to a decrease in porosity and consequently to a change in the permeability and diffusivity in the reactive layer.

During the course of the experiment the pressure at the upper and lower boundary of the reactive layer was monitored; this allows changes in the permeability to be assessed. The status of the reaction is controlled by sampling the effluent. In addition, the precipitate and the pore space changes will be investigated with high-resolution X-ray tomographic methods. 1D experiments are also being planned to parameterize the kinetic law which governs strontium dissolution in the presence of barium chloride. This experiment will be modelled with the reactive transport code OpenGeoSys-GEM.

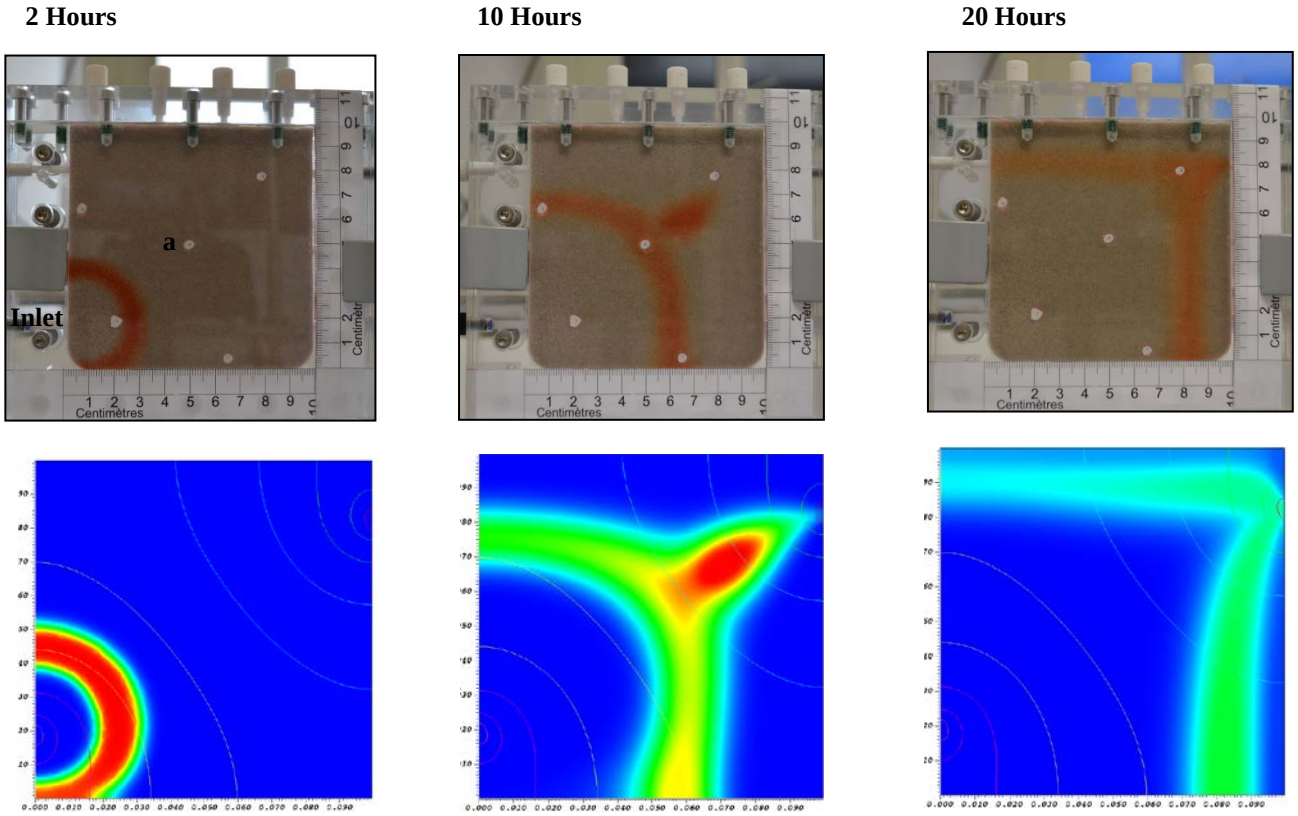

Fig. 3.13: *Comparing experimental results (top) and simulation results from the OpenGeoSys code (bottom) at different times after Eosin injection at the inlet.*

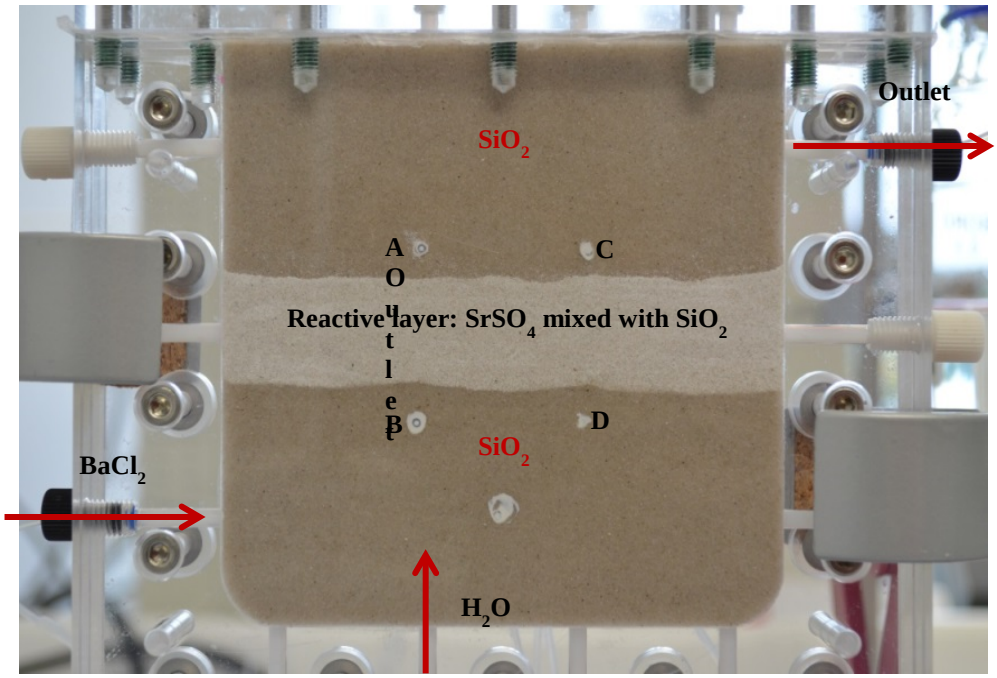

Fig. 3.14: *Experimental setup for a reactive transport benchmarking experiment with one outlet, and 2 inlets where $BaCl_2$ and H_2O are pumped in at different flow rates to generate a non-uniform flow field. A, B, C and D are ports at which the pressure is monitored.*

3.5 References

BRADBURY M.H., BAEYENS B. (2000)
A generalised sorption model for the concentration dependent uptake of caesium by argillaceous rocks. J. Contam. Hydrol 42, 141-163.

BRADBURY M.H., BAEYENS B. (2005)
Modelling the sorption of Mn(II), Co(II), Ni(II), Zn(II), Cd(II), Eu(III), Am(III), Sn(IV), Th(IV), Np(V) and U(VI) on montmorillonite: linear free energy relationships and estimates of surface binding constants for some selected heavy metals and actinides, Geochim. Cosmochim. Acta 69, 875-892.

COCHEPIN B.L., TROTIGNON O., BILDSTEIN C.I., STEEFEL V., LAGNEAU J., VAN DER LEE J. (2008)
Approaches to modelling coupled flow and reaction in a 2D cementation experiment. Adv. Water Resources 31, 1540–1551.

DAUZERES A.P., LE BESCOP P., SARDINI P., CAU DIT COUMES C.(2010)
Physico-chemical Investigation of Clayey/cement-based Materials Interaction in the Context of Geological Waste Disposal: Experimental Approach and Results." Cem. Concr. Res. 40, 1327–1340.

DE WINDT L. (2004)
Coupled modelling of cement/claystone interactions and radionuclide migration. J. Contam. Hydrol. 68, 165–182.

DE WINDT L., BADREDDINE R., LAGNEAU V. (2007)
Long-term reactive transport modelling of stabilized/solidified waste: From dynamic leaching tests to disposal scenarios. J. Hazard. Mater. 139, 529–36.

JAKOB A., PFINGSTEN W., VAN LOON L. (2009)
Effects of sorption competition on caesium diffusion through compacted argillaceous rock. Geochim. Cosmochim. Acta 73, 2441-2456.

KOSAKOWSKI G., WATANABE N. (2013)
OpenGeoSys-GEM: A numerical tool for calculating geochemical and porosity changes in saturated and partially saturated media. J. Phys. Chem. Earth, Parts A/B/C submitted. doi:10.1016/J.pce.2013.11.008.

LABBEZ C., JONSSON B., POCHARD I., NONAT A., CABANE B. (2006)
Surface charge density and electrokinetic potential of highly charged minerals: Experiments and Monte Carlo simulations on calcium silicate hydrate. J. Phys. Chem. B 110, 9219-9230.

MARTY N.C.M., TOURNASSAT C.,. BURNOL A., GIFFAUT E., GAUCHER E.C. (2009)
Influence of reaction kinetics and mesh refinement on the numerical modelling of concrete/clay interactions. J. Hydrol. 364, 58–72.

NAGRA (2002)
Project Opalinus Clay – Safety Report – Demonstration of disposal feasibility for spent fuel, vitrified high-level waste and long-lived intermediate-level waste (Entsorgungsnachweis), Nagra, Wettingen, Switzerland.

PERKO J.J., GOVAERTS D., JACQUES K.U., MAYER D.S.U, KOSAKOWSKI G., DE WINDT L., MEEUSSEN J.C.L. (2013)
Decalcification of cracked cement structures. Phys. Chem. Earth, Parts A/B/C in preparation.

PFINGSTEN W., BRADBURY M.H., BAEYENS B. (2011)
The influence of Fe(II) competition on the sorption and migration of Ni(II) in MX-80 bentonite. Appl. Geochem. 26, 1414-1422

SAVOYE S., BEAUCAIRE C., FAYETTE A., HERBETTE M., COELHO D. (2012)
Mobility of cesium through the Callovo-Oxfordian claystones under partially saturated conditions. Environ. Sci. Technol., 46, 2633−2641.

SENGER R.K, EWING J. (2009)
Gas-L/ILW: gas pressure buildup and transport in a deep geologic L/ILW repository in Opalinus Clay using large-scale and local-scale models. Wettingen, Switzerland: Nagra.

SULPIZI M., GAIGEOT M.P., SPRIK M. (2012)
The silica−water interface: How the silanols determine the surface acidity and modulate the water properties. J. Chem. Theory Comput. 8, 1037−1047.

TROTIGNON L., ADIDOT A., BILDSTEIN O., LAGNEAU V., MARGERIT Y. (2005)
Design of a 2-D cementation experiment in porous medium using numerical simulation. Oil Gas Sci Technol. 60, 307–318.

4 CLAY SORPTION MECHANISMS

B. Baeyens, M.H. Bradbury, R. Dähn, M. Marques Fernandes, A. Schaible, E. Eltayeb, D. Soltermann (PhD)

4.1 Overview

The activities in the framework of Stage 2 of the Sectoral Plan for Deep Geological Disposal (SGT-E2) continued in 2013. This work comprised of the following topics.

- Finalisation of the sorption data bases (SDBs) for the different host rocks (Opalinus Clay, "Brauner Dogger", Effinger Member, Helvetic Marl), for the underlying confining units, and for MX-80 bentonite, as input for the provision safety analyses for SGT-E2 (BAEYENS et al., 2013a).
- Sorption measurements on the potential host rocks (BAEYENS et al., 2013b) were extended to include Helvetic Marl. The experimental results were compared to blind predictions calculated using the same methodology developed to derive the sorption values given in the SDBs.

Mechanistic sorption studies on clay minerals are an on-going activity and involved the following:

- The influence of inorganic carbon on the sorption of U(VI) on montmorillonite was experimentally investigated and modelled using the 2 Site Protolysis Non Electrostatic Surface Complexation and Cation Exchange (2SPNE SC/CE) sorption model.
- Activities related to the Swiss-Hungarian co-operation project focussed on the application of the "bottom up" approach to the uptake of divalent metals on Boda Claystone Formation and Opalinus Clay combined with Extended X-Ray Absorption Fine Structure (EXAFS) spectroscopy.
- Sorption competition between Fe(II) and Zn(II) on a synthetic iron free montmorillonite was investigated in the framework of a PhD project. The Swiss National Foundation (SNF) granted an extension of the project by one year.

A new technician, Elmotaz Eltayeb joined the group on the 1st May 2013.

4.2 Activities in support of the Sectoral Plan

4.2.1 Sorption data bases for SGT-E2

In Stage 2 of the Sectoral Plan for Deep Geological Disposal (SGT-E2), four host rock types have been identified as being potentially suitable for constructing radioactive waste repositories, namely, Opalinus Clay (HLW, L/ILW), and 'Brauner Dogger', Effingen Member and Helvetic Marl (L/ILW) (NAGRA, 2008). Sorption data bases for all of these host rocks have been developed for the planned preliminary safety analyses, including all of the bounding porewater and mineralogical composition combinations. The data bases have been compiled and documented in NTB 12-04. This report was reviewed by the Swiss Federal Nuclear Safety Inspectorate (ENSI) and the methodology was presented to regulatory authorities (ENSI, Federal Commission for Nuclear waste (KNS), Expert Group Geological Disposal (EGT), Cantons) in the framework of an intermediate geochemistry (geosphere) expert meeting for SGT-E2.

4.2.2 Sorption measurements on Helvetic Marl

Sorption isotherm measurements of Cs(I), Co(II), Ni(II), Eu(III), Th(IV) and U(VI) were carried out on an Helvetic Marl sample from the Wellenberg SB4 borehole (WLB-334 m). The mineralogical composition of this sample is described by TRABER & BLASER (2013) and is given in Table 4.1. The isotherms were measured in a synthetic porewater which was equilibrated with air (pH = 8.4) and is based on the reference porewater defined for SGT-E2 (MÄDER, 2010). The composition of the marl sample equilibrated porewater is given in Table 4.2.

The sorption values were calculated using conversion factors derived following the methodology given in BRADBURY & BAEYENS (2013a). From Table 4.1 a mineralogical conversion factor (CF_{MIN}) of 0.26 was obtained. The speciation factors for Cs(I), Co(II), Ni(II), Eu(III), Th(IV) and U(VI) in the 0.1 M $NaClO_4$ and for the equilibrated marl porewaters are given in Table 4.3 together with the measured pH in the sorption experiments. Fig. 4.1 shows the sorption measurements for the six elements on Helvetic Marl and the predicted sorption values.

Table 4.1: *Mineralogical composition of Wellenberg Marl (TRABER & BLASER, 2013).*

Mineral	WLB-334 (wt.-%)
Calcite	51
Dolomite/ankerite	4
Quartz	11
K-feldspar	1
Pyrite	1.1
Illite	13
Illite/smectite mixed layers	13
Chlorite	6

Table 4.2: *Composition of the porewater equilibrated with the WLB-334 marl sample.*

pH	8.3 – 8.6
log pCO_2 (bar)	-3.50
Ionic strength	0.206
Cl (M)	2.02×10^{-1}
$C_{inorg.}$ (M)	1.54×10^{-3}
ICP-OES analyses of dissolved constituents (M)	
Na	1.97×10^{-1}
K	2.34×10^{-3}
Mg	8.05×10^{-4}
Ca	1.20×10^{-3}
Sr	1.90×10^{-4}
SO_4	2.25×10^{-4}
Si	3.6×10^{-5}
Al	1.0×10^{-5}

For Cs(I), Co(II), Ni(II), Eu(III) and Th(IV) the uncertainty limits estimated for the predicted sorption values overlap with those of the measured values. However, in the case of U(VI) the predicted value is below the measured data. As can be seen from Table 4.3 the speciation factor of U(VI) in the porewater is extremely small due to the formation of $UO_2Ca(CO_3)_3^{2-}$ and $UO_2(CO_3)_3^{4-}$ aqueous complexes at the high inorganic carbon concentrations associated with the marl porewater. The former complex is not contained in the PSI/Nagra TDB 12/07 (selected data) (THOENEN, 2012) but was included here since this species was required to describe previous uranyl sorption measurements on Opalinus Clay and MX-80 bentonite (BRADBURY & BAEYENS, 2011). The reason(s) behind this discrepancy is not currently understood.

4.3 Mechanistic sorption investigations

4.3.1 U(VI) sorption on montmorillonite: influence of inorganic carbon

Under the redox conditions calculated in the repository, part of the uranium exists in its hexavalent form as the uranyl ion UO_2^{2+}, and can form highly soluble aqueous complexes with many ligands existing in porewaters e.g., OH^-, SO_4^{2-} and CO_3^{2-}. Dissolved carbonate is ubiquitous in surface and deep groundwaters and forms strong aqueous complexes with U(VI) (GUILLAUMONT et al., 2003). The formation of such complexes can potentially lead to a decrease in sorption and thereby an increase in the migration rates of U(VI). A detailed understanding of the sorption processes over a wide range of conditions is essential for the development of predictive transport models.

U(VI) sorption measurements were performed on Na-SWy-1 montmorillonite in the absence of carbonate at a fixed ionic strength (0.1 M $NaClO_4$) as a function of pH (sorption edge) and as a function of U(VI) concentration (sorption isotherms) at pH 5, 6.8 and 8. Experiments were carried out in the presence of carbonate in equilibrium with atmospheric pCO_2 and in solutions containing 1, 3 and 5 mM $NaHCO_3$.

U(VI) sorption in the absence of carbonate. The results of the sorption measurements are shown in Fig. 4.2. Previously measured sorption data from BRADBURY & BAEYENS (2005) are included in Fig. 4.2 and indicate that the data are very consistent. The sorption edge and isotherms were modelled using the 2SPNE SC/CE sorption model. The aqueous uranyl hydrolysis constants were selected from the NEA TDB (GUILLAUMONT et al., 2003), which are different from the hydrolysis data used in BRADBURY & BAEYENS (2005).

A stepwise modelling procedure was carried out in which the edge data were modelled first, followed by the isotherm data sets. The pH dependent sorption data were modelled in terms of cation exchange (CE) on the planar sites at low pH and in terms of surface complexation at the amphoteric surface hydroxyl groups (≡SOH sites) with a series of four surface complexation reactions on the strong sites ($\equiv S^SOH$) of montmorillonite. Two additional surface complexation reactions on the weak sites ($\equiv S^{W1}OH$) were required to model the sorption isotherms at pH 5, 6.8 and 8 shown in Figs. 4.2b, c and d, respectively.

***Table 4.3**: Summary of the conversion factors used for the sorption predictions on the Helvetic Marl sample WLB-334 from the Wellenberg SB4 borehole.*

Metal	**pH**	**log $R_{d,ILLITE}$ [L kg^{-1}]**	**SF_{ILLITE}**	**SF_{MARL}**	**CF_{MIN}**	**CF_{SPEC}**	**log $R_{d,MARL}$ [L kg^{-1}]**
Cs(I)	8.3	3.1	1	1	0.26	1	**2.5**
Co(II)	8.4	4.6	1	0.76	0.26	0.76	**3.9**
Ni(II)	8.4	4.0	1	0.83	0.26	0.83	**3.3**
Eu(III)	8.5	5.7	0.22	0.052	0.26	0.24	**4.5**
Th(IV)	8.4	5.7	1	0.48	0.26	0.48	**4.8**
U(VI)	8.6	4.8	1	1.3×10^{-4}	0.26	1.3×10^{-4}	**0.3**

CF_{MIN} = (MIN_{MARL} / MIN_{ILLITE}) where MIN_{MARL} = illite + illite/smectite mixed layer weight fraction in the marl and MIN_{ILLITE} = 1 (100% illite).

CF_{SPEC} = SF_{MARL} / SF_{ILLITE} where SF_{MARL} is the fraction of sorbing radionuclide species calculated to be present in the aqueous phase in the marl porewater and SF_{ILLITE} is the fraction of sorbing radionuclide species calculated to be present in the aqueous phase in the illite system.

$R_{d,\,MARL} = R_{d\,ILLITE} \cdot CF_{MIN} \cdot CF_{SPEC}$

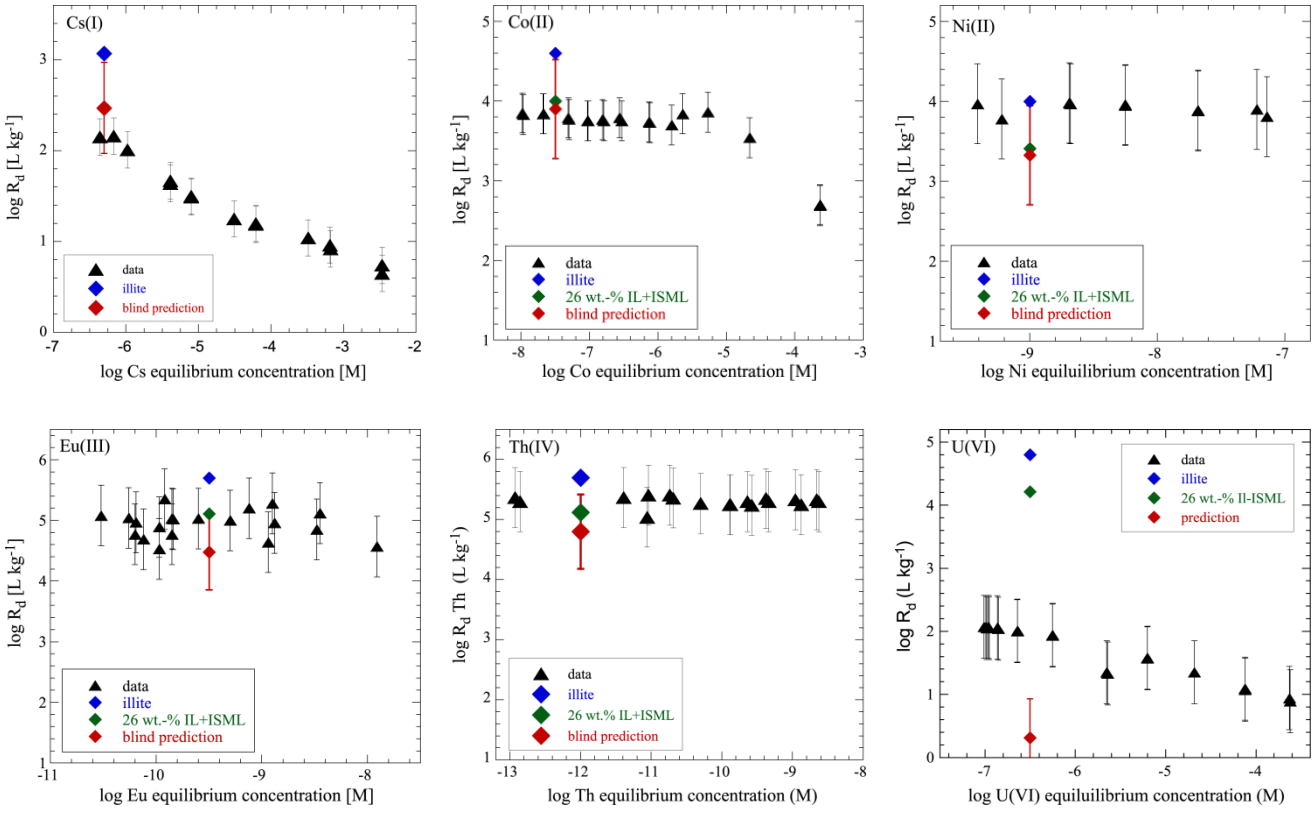

***Fig. 4.1:** Summary of the sorption measurements and the predicted sorption values for Cs(I), Co(II), Ni(II), Eu(III), Th(IV) and U(VI) on Helvetic Marl from the SB4 borehole (WLB-334).*

With the surface complexation constants obtained on the weak sites, the sorption edge at trace concentration (Fig. 4.2a) was refitted. This procedure was repeated until all data sets were successfully modelled with the same set of parameters. The results for all surface complexation reactions and associated constants on strong and weak sites are summarized in Table 4.4.

U(VI) sorption in the presence of carbonate. Sorption edges of U(VI) on Na-SWy-1 in equilibrium with atmospheric pCO_2, and in the presence of 1, 3 and 5 mM $NaHCO_3$, are shown in Figs. 4.3a and b, respectively. At pH values above 7 a decrease in the U(VI) sorption is observed which becomes more pronounced with increasing pH and carbonate concentration. In a first modelling approach the sorption parameters obtained for the carbonate free system were applied to the data under the assumption that no additional U(VI) surface complexation reactions were taking place *i.e.* aqueous U(VI) carbonate complexes were treated as being non sorbing. However, under this assumption the model predictions failed to reproduce the experimental data sets above pH ~7, and largely underestimated the experimental data at high carbonate concentrations (not shown). An iterative procedure similar to the one described above was applied to derive the surface complexation constants in which the aqueous speciation for U(VI) under the different experimental conditions was used to guide the choice of the potential surface complexes. The sorption reactions involving ternary surface complexes are summarized in Table 4.4, and the modelling results are shown in Fig. 4.3. The results show that for the four independent experimental data sets available (atmospheric pCO_2, in 1, 3 and 5 mM $NaHCO_3$) a consistent picture is obtained, and only slight deviations from the experimental data are observed.

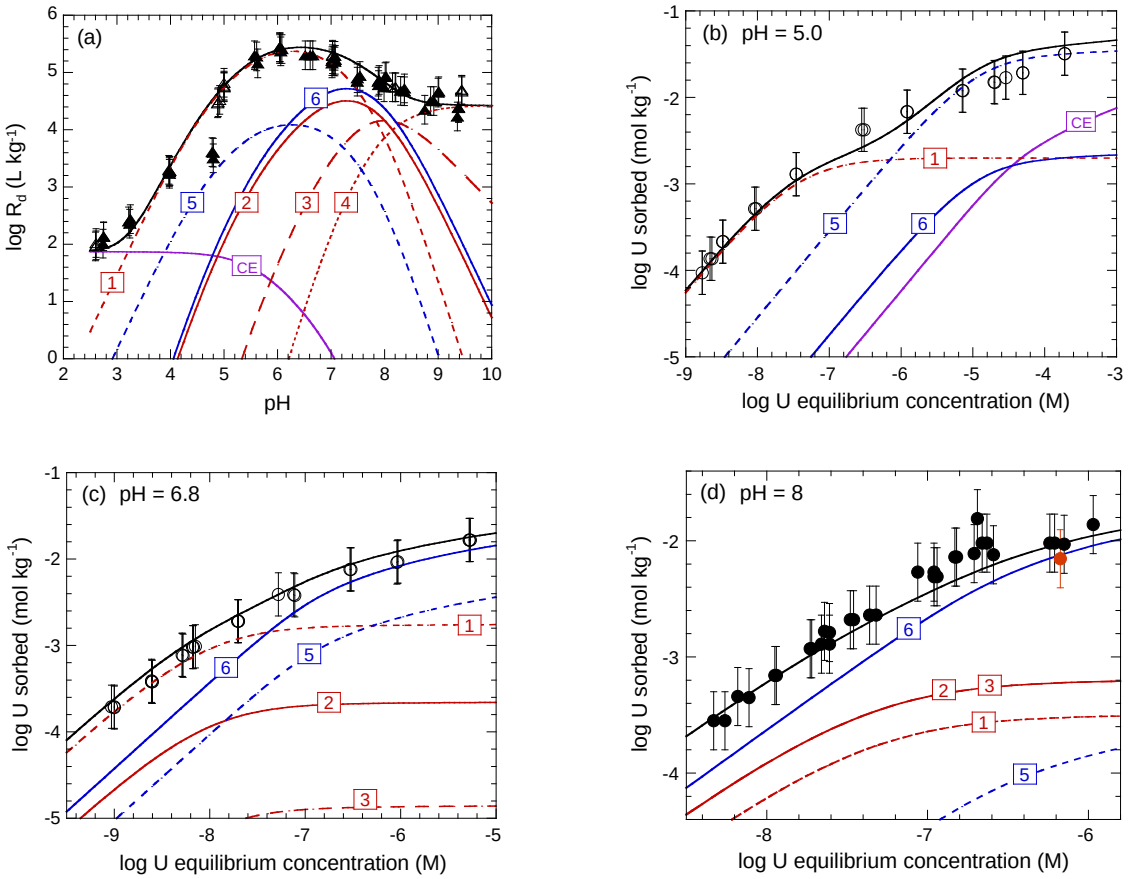

Fig. 4.2: *U(VI) sorption on Na-SWy-1 montmorillonite in 0.1 M $NaClO_4$. Sorption edge (a) and sorption isotherms (b) pH = 5, (c) pH = 6.8 and (d) pH = 8. The continuous black curves are the best fits obtained with the 2SPNE SC/CE sorption model (see text for details). Curves labelled (1-6) and CE represent the contribution to the overall sorption of the major individual U(VI) surface species in the absence of carbonate (see Table 4.4).*

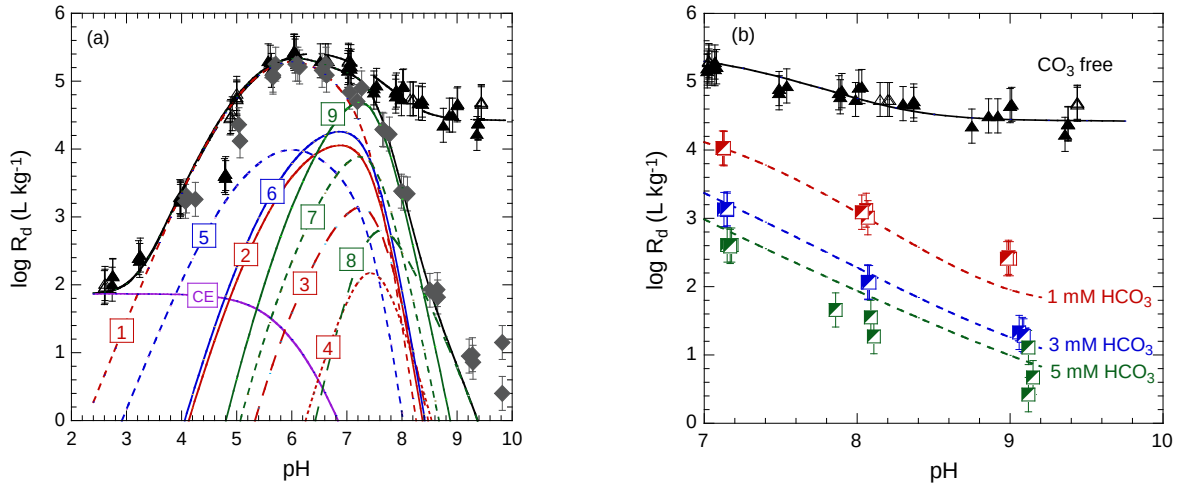

Fig. 4.3: *U(VI) sorption edge measurements on Na-SWy-1 montmorillonite in the absence of carbonate (◢, ◿) and (a) in equilibrium with atmospheric pCO_2 (♦); (b) in the presence of 1, 3 and 5 mM $NaHCO_3$. The curves are model calculations with the 2SPNE SC/CE model and the parameters given in Table 4.4.*

Finally, Fig. 4.4 shows the U(VI) sorption isotherm measured on conditioned Na-SWy-1 at pH ~ 8 in equilibrium with atmospheric pCO_2. In a first attempt to model the sorption isotherm data the SC constants on the strong sites and the weak sites derived in the absence of carbonate (Table 4.4), and the SC constants of the ternary carbonate surface complexes on strong sites ($\equiv S^SOUO_2CO_3^-$ and $\equiv S^SOUO_2(CO_3)_2^{3-}$) (Table 4.4) were used. Just using these constants was not sufficient and the best fit to the experimental data was obtained by including an additional ternary uranyl-carbonate surface complex ($\equiv S^{W1}OUO_2CO_3^-$) on the weak sites (Table 4.4). The inclusion of ternary uranyl-carbonate complexes on the strong and weak sites in the sorption modelling allowed the uptake of U(VI) on Na-SWy-1 to be quantitatively described over a wide range of conditions (U(VI) concentration, pH, pCO_2).

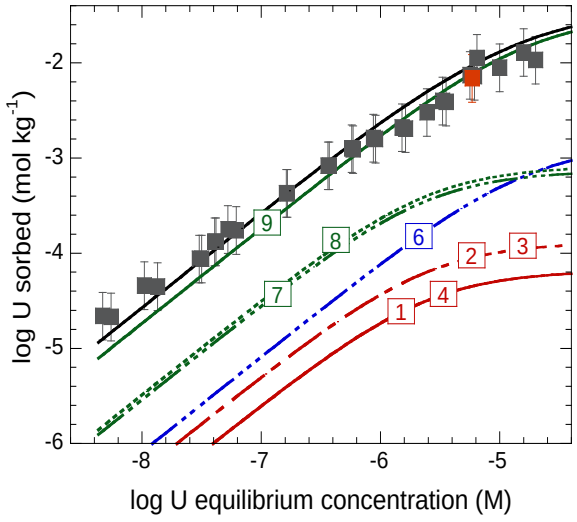

Fig. 4.4: *U(VI) sorption isotherm on Na-SWy-1 montmorillonite measured in equilibrium with atmospheric pCO_2 at pH 8 (■) and modelling (curves).*

Table 4.4: *Summary of the surface complexation constants and selectivity coefficients characterizing the sorption of U(VI) on Na-SWy-1 a) in the absence and b) presence of carbonate.*

Cation exchange reaction	$\log K_c$
CE: $2Na^+$-clay + $UO_2^{2+} \Leftrightarrow UO_2^{2+}$-clay + $2Na^+$	0.45
Surface complexation reactions in the absence of carbonate	$\log {}^{S,W1}K$
1) $\equiv S^SOH + UO_2^{2+} \Leftrightarrow \equiv S^SOUO_2^+ + H^+$	3.1
2) $\equiv S^SOH + UO_2^{2+} + H_2O \Leftrightarrow \equiv S^SOUO_2OH^0 + 2H^+$	-4.6
3) $\equiv S^SOH + UO_2^{2+} + 2H_2O \Leftrightarrow \equiv S^SOUO_2(OH)_2^- + 3H^+$	-12.6
4) $\equiv S^SOH + UO_2^{2+} + 3H_2O \Leftrightarrow \equiv S^SOUO_2(OH)_3^{2-} + 4H^+$	-20.9
5) $\equiv S^{W1}OH + UO_2^{2+} \Leftrightarrow \equiv S^{W1}OUO_2^+ + H^+$	0.5
6) $\equiv S^{W1}OH + UO_2^{2+} + H_2O \Leftrightarrow \equiv S^{W1}OUO_2OH^0 + 2H^+$	-5.7
Surface complexation reaction in the presence of carbonate	$\log {}^{S,W1}K$
7) $\equiv S^SOH + UO_2^{2+} + CO_3^{2-} \Leftrightarrow \equiv S^SOUO_2CO_3^- + H^+$	9.8
8) $\equiv S^SOH + UO_2^{2+} + 2CO_3^{2-} \Leftrightarrow \equiv S^SOUO_2(CO_3)_2^{3-} + H^+$	15.5
9) $\equiv S^{W1}OH + UO_2^{2+} + CO_3^{2-} \Leftrightarrow \equiv S^{W1}OUO_2CO_3^- + H^+$	9.3

4.3.2 Testing of the "Bottom up" approach: Me^{2+} metal sorption on Opalinus Clay and Boda Claystone

The aim of the joint research project between the Hungarian Academy of Sciences (Centre for Energy Research) and the Paul Scherrer Institut (LES) was to investigate the uptake of metals on the Boda Claystone Formation (BCF) and Opalinus Clay using a combined wet chemistry, geo-chemical modelling and spectroscopic approach and to test the validity of the "bottom-up" modelling methodology on both rock types.

The "bottom-up" approach is based on the premise that radionuclide uptake in complex mineral/ groundwater systems can be quantitatively predicted from the knowledge and understanding of the mechanistic sorption processes on single minerals, in particular clay minerals, and the models developed to describe them. The 2SPNE SC/CE sorption model (BRADBURY & BAEYENS, 2009) and the generalised sorption model for Cs (BRADBURY & BAEYENS, 2000) were used to make blind predictions of the sorption isotherms on both rock types.

Sorption isotherms for Cs(I), Ni(II), Co(II), Eu(III), Th(IV) and U(VI) were measured on BCF and Opalinus Clay in their respective synthetic porewaters (see LES annual report 2012). The sorption predictions on these argillaceous rocks was then carried out using the two mechanistic sorption models developed for illite and the results were scaled over the illite and illite/smectite weight content in the sample. Generally a good agreement between the measured data and the predicted values was found for most of the metals. However, as shown in Fig. 4.5 the blind predictions clearly under predict Ni(II) sorption on BCF and Opalinus Clay at higher Ni(II) equilibrium concentrations. The same trend was observed for the sorption of Co(II) on these clay rocks.

EXAFS was used to provide additional information on the sorption processes occurring along the isotherm at the molecular level. The uptake of Ni(II) and Zn(II) on BCF and Opalinus Clay was investigated at different metal loading in their respective porewaters. The EXAFS measurements focused on Zn, rather than Ni or Co, because of the lower detection limits and a better signal to noise ratio in the Fe-rich rock matrix.

The EXAFS measurements were performed at the Beamline 11-2 at the Stanford Linear Accelerator Center (SLAC, USA) in fluorescence mode using a one hundred-element solid-state detector. The k^3-weighted K-edge of Zn-EXAFS spectra for both argillaceous rocks and the corresponding radial structure functions (RSFs) are shown in Figs. 4.6 and 4.7. Additionally, the EXAFS spectra of the "intrinsic" Zn of ~2 mmol kg^{-1} (no externally added Zn) in these rocks was measured (see Figs. 4.6 and 4.7). The spectral features of this intrinsic Zn are typical for structurally incorporated Zn in 2:1 phyllosilicates (DÄHN et al., 2011, CHURAKOV & DÄHN, 2012).

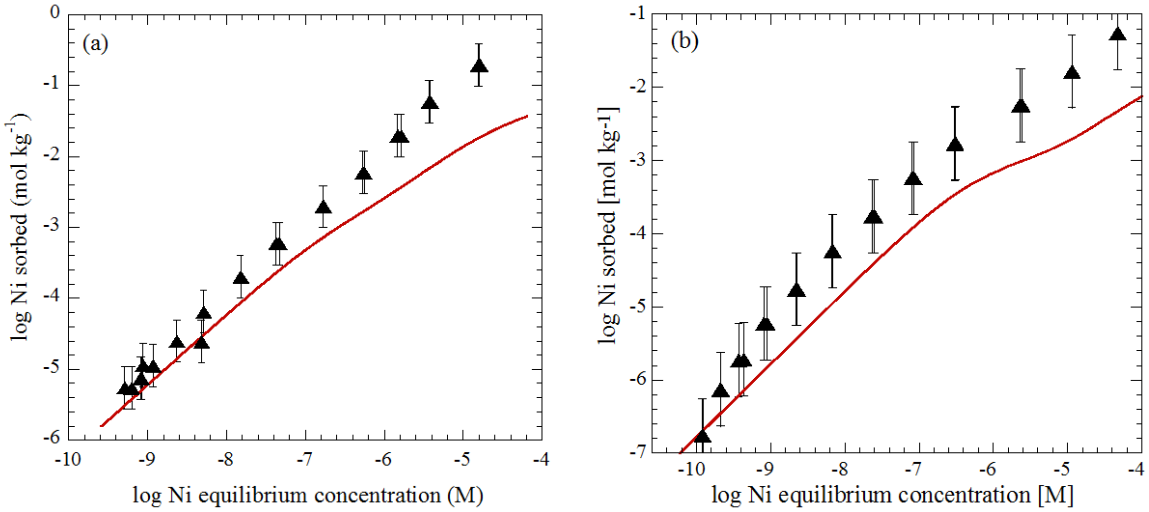

Fig. 4.5: *Ni(II) sorption isotherms on a) BCF and b) Opalinus Clay: Experimental results (symbols) and modelling (continuous line).*

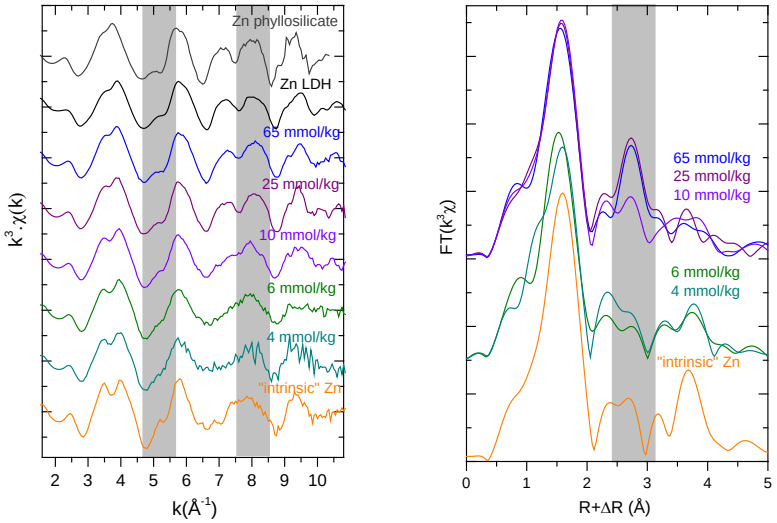

Fig. 4.6: *k^3-weighted K-edge Zn-EXAFS spectra and the corresponding radial structure functions for Boda at different Zn loadings and 2 reference spectra (Zn-phyllosilicate and Zn-LDH).*

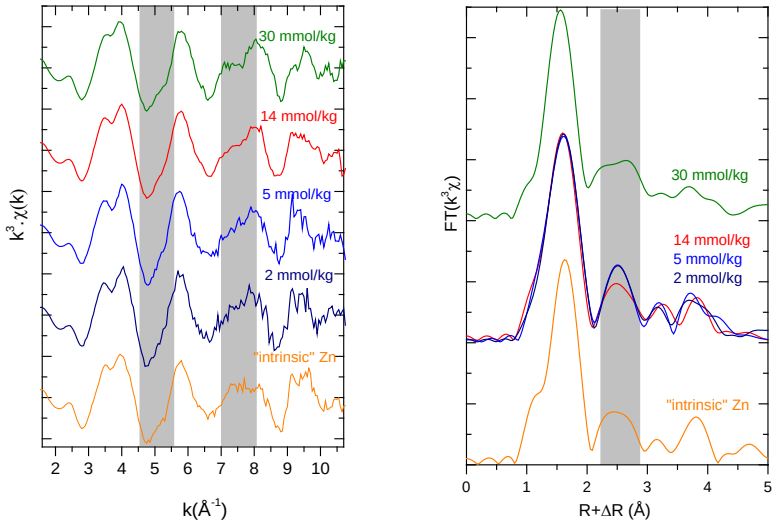

Fig. 4.7: *k3-weighted K-edge Zn-EXAFS spectra and the corresponding radial structure functions for OPA at different Zn loadings.*

EXAFS spectra of the low loaded Zn BCF and Opalinus Clay samples exhibit mixed spectral features of incorporated and/or sorbed species (Figs. 4.6 and 4.7). Thus, based on this similarity, and the absence of any characteristic features of Zn precipitation, it can be concluded that at these low metal loadings inner-sphere complexation is the predominant uptake mode. Consequently, in the isotherm region where prediction and measurement coincide, sorption through inner sphere complexation seems to be the only uptake mechanism. However, further data processing requires the subtraction of the spectral contribution of the intrinsic Zn and the comparison of the resulting spectra to Zn on illite to verify whether illite is the main mineral phase responsible for the uptake.

The higher loaded Zn BCF and Opalinus Clay samples show a splitting of the oscillation between 7-8 $Å^{-1}$ in the EXAFS spectra and the presence of Zn-Zn backscattering pairs at ~2.7 Å (R+ΔR) in the RSF, indicating the precipitation of Zn solid phases, even though the initial Zn concentrations were below the solubility limits of Zn-hydroxide. The EXAFS analysis for Ni treated samples indicated similar uptake behaviour to Zn, though the quality of the spectra were noisy.

These EXAFS results clearly show precipitation as an additional process in the isotherm region where prediction and measurement deviate, and is probably the reason for the mismatch between the modelling and the experimental data (Fig. 4.5). These findings suggest that there could be solubility limiting phases in these argillaceous rock-groundwater systems which are not currently included in the thermodynamic data bases. The similarity of the spectra with those of Zn layered double hydroxides (LDH) and Zn phyllosilicates supports this hypothesis (see Fig. 4.6). However, the exact nature of the precipitate has not yet been clarified.

4.3.3 Competitive Fe(II)-Zn(II) uptake on synthetic montmorillonite (PhD project)

Within the framework of the PhD thesis entitled "*The influence of Fe(II) on clay properties, the sorption of Fe(II) on clays, and competitive sorption investigations*" EXAFS and Mössbauer spectroscopy measurements, combined with batch sorption experiments and modelling, were carried out to investigate the competition between Fe(II) and Zn(II) on a synthetic iron-free montmorillonite (IFM). In these experiments the sorption of one element was measured at "trace metal" concentrations in the presence of a "competing metal" whose concentration varied from trace to relatively high concentrations (10^{-7} to 10^{-3} M).

The results of the batch experiments are illustrated in Fig. 4.8. Fig. 4.8a shows that the sorption of trace ^{65}Zn(II) (< 10^{-7} M) (blue circles)) on Na-IFM in 0.1 M $NaClO_4$ at pH = 6.2 does not remain constant in the presence of varying concentrations of Fe(II) but rather follows the non-linear sorption isotherm of Fe(II) (red circles) within an experimental error of ±0.3 log units on the R_d values. The decreasing log R_d values of Zn(II) with increasing competing metal concentration suggest that under the given experimental conditions the two metals compete with one another for the uptake on the strong sites. The Fe(II) sorption isotherm was modelled using the 2SPNE SC/CE model with the parameters given in SOLTERMANN et al. (2013).

Fig. 4.8b shows the sorption of trace Fe(II) in the presence of Zn(II) at concentrations ranging from 10^{-6} M to 10^{-3} M. In contrast to the trace Zn(II) sorption behaviour described above, the sorption of trace Fe(II) remains high (log R_d = 4.8 ±0.4 $L \cdot kg^{-1}$) and constant and independent of the Zn equilibrium concentration. Thus, Fe(II) is not competing with Zn(II) under the experimental conditions chosen. A plausible explanation for this behaviour could be the oxidation of a part of Fe(II) to Fe(III) on the edge sites of Na-IFM. This possible oxidation process was confirmed by Mössbauer measurements (GEHIN et al. 2007, SOLTERMANN et al. 2013). The non-competitiveness between the surface-bound Fe(III) with competing Zn(II) suggests that within the octahedral sites there might be a subset of strong sites where a surface-induced oxidation of sorbed Fe(II) occurs and which are not accessible for Zn(II).

For both combinations, i.e. trace Zn(II)/competing Fe(II) and trace Fe(II)/competing Zn(II), EXAFS measurements were performed.

Under the experimental conditions chosen (trace Zn(II)/competing Fe(II)), and assuming competitive sorption, the model predictions indicate that Zn surface complexes are predominantly formed on the weak sites in the EXAFS sample. The splitting of the oscillation at ~ 4 Å in the k^3-weighted Zn EXAFS spectra (Fig. 4.9a) of the Zn-IFM sample is characteristic for Zn situated in octahedral positions of the montmorillonite structure.

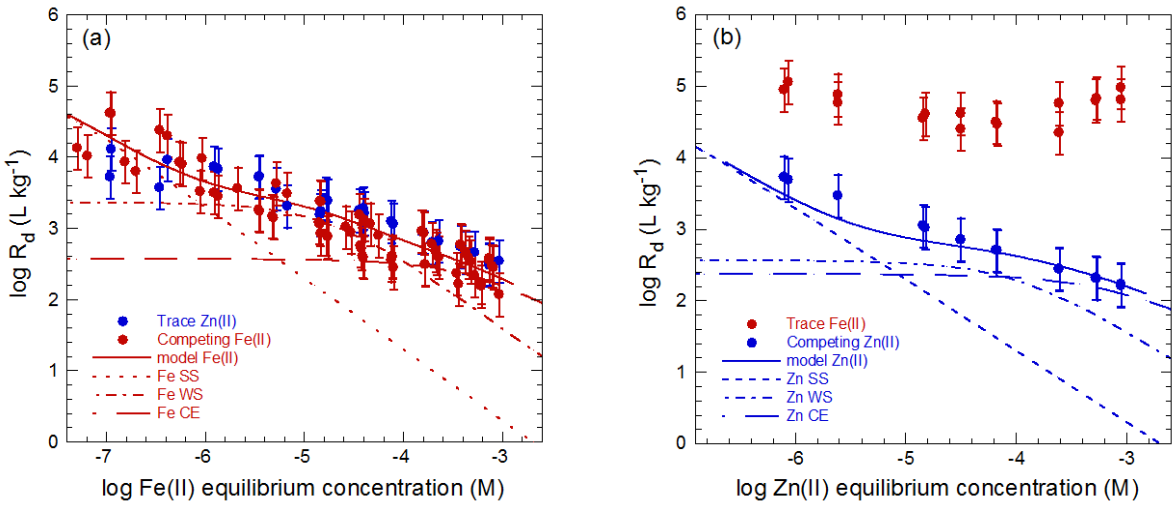

Fig. 4.8: *(a) The sorption of trace Zn (●) in the presence of increasing Fe(II) concentrations (●)on Na-IFM in 0.1 M $NaClO_4$ at pH 6.2. (b) the sorption of trace Fe (●) in the presence of Zn(II) (●) at concentrations ranging from 10^{-6} M to 10^{-3} M on Na-IFM in 0.1 M $NaClO_4$ at pH 6.2. The curves are the model calculations using the 2SPNE SC/CE sorption model.*

The weakening of this feature in the Zn/Fe IFM sample indicates that Zn complexes are located in less well defined crystallographic positions, e.g. that a variety of Zn complexes are forming at the montmorillonite surface. This observation supports the assumption that predominantly Zn weak-site complexes are prevailing in the presence of Fe(II), which is in agreement with competitive uptake (Fig. 4.8a).

The Fe K-edge EXAFS spectra at low and medium Fe loading without any competing Zn were used as a basis for the interpretation of the Fe data in the presence of competing Zn. The EXAFS spectra of the low Fe loaded Na-IFM samples (~1.8 mmol·kg^{-1}) in the absence or presence of Zn(II) are similar, Fig. 4.10a. This finding indicates that Fe in the EXAFS samples sorbs on the strong sites and the presence of Zn(II) is not having any influence on the Fe(II) uptake mechanism at low Fe(II) equilibrium concentrations (< 10^{-5} M). Once again, this observation is consistent with the absence of any competitive effects in the Fe/Zn montmorillonite system where Zn(II) is the competing metal.

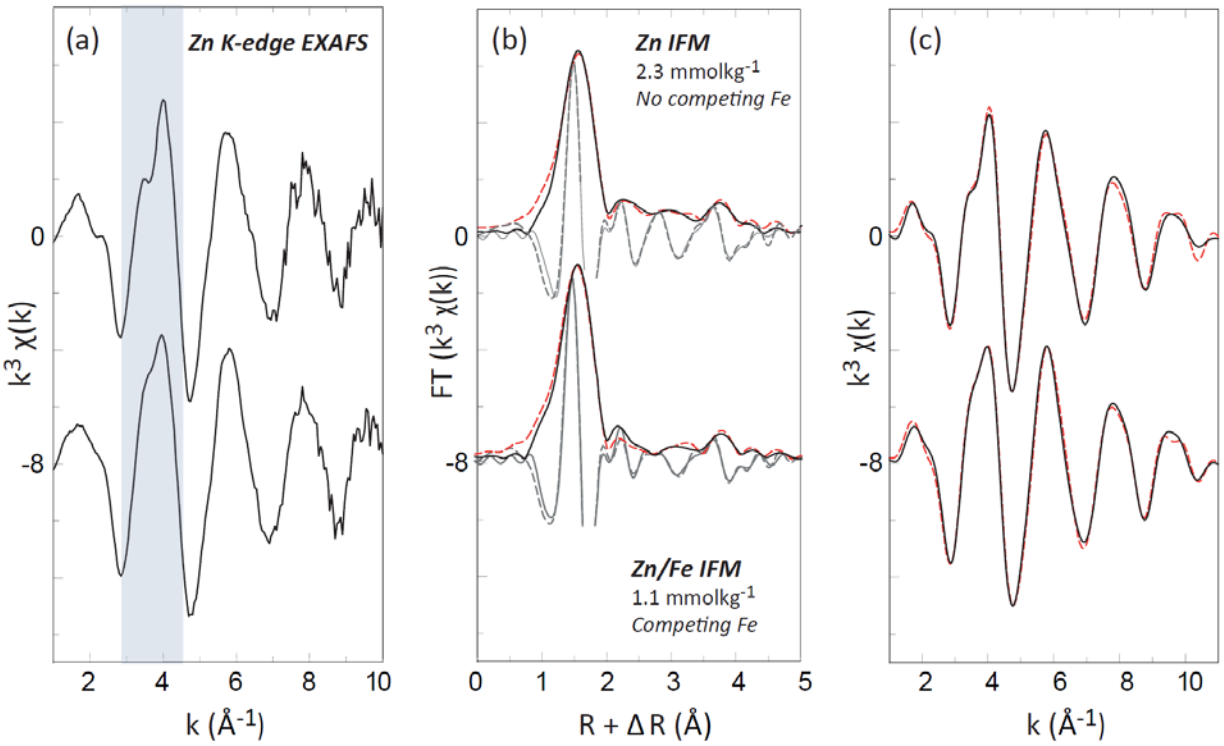

Fig. 4.9: *(a) k^3-weighted Zn K-edge EXAFS spectra obtained for Zn sorbed on synthetic Na-IFM in absence (Zn IFM) or presence of ~ 50 mmol kg^{-1} competing Fe (Zn/Fe IFM), (b) FT for Zn sorbed on Na-IFM. Dashed lines represent the simulation of the amplitude and imaginary parts and, (c) FT^{-1} EXAFS data and the least-squares fit (dashed line).*

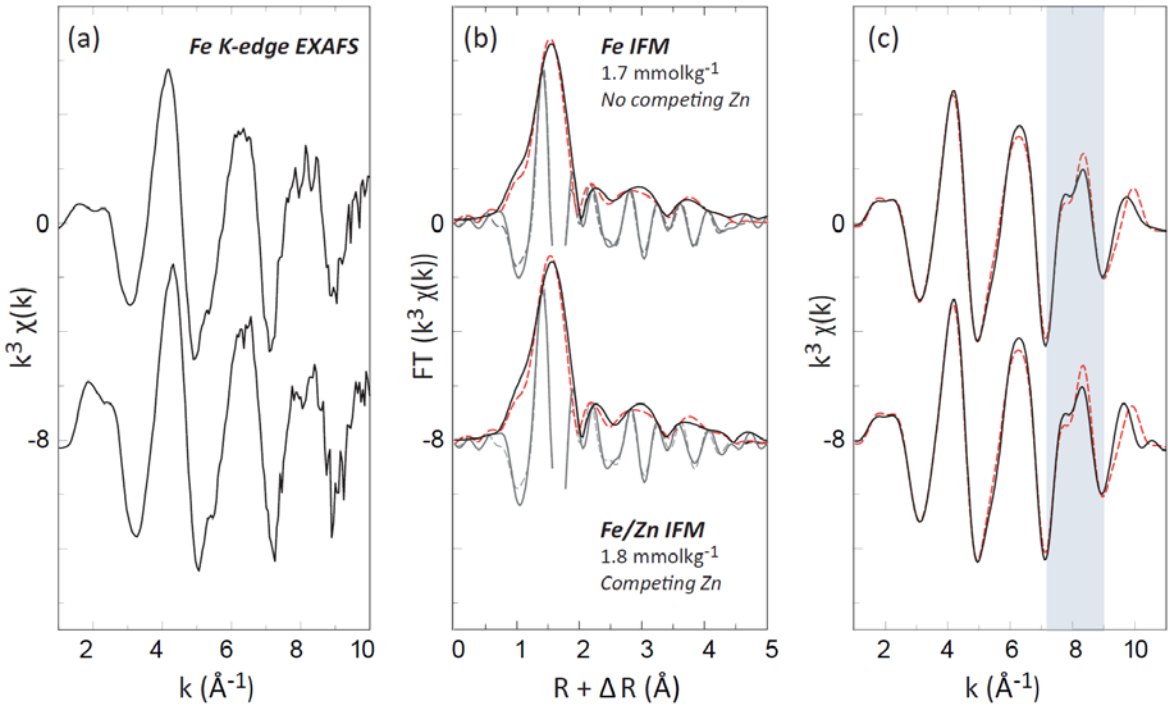

Fig. 4.10: *(a) k^3-weighted Fe K-edge EXAFS spectra obtained for Fe sorbed on synthetic Na-IFM in absence (Fe IFM low) or presence of ~ 68 mmol kg^{-1} competing Zn (Fe/Zn IFM low), (b) FT for Fe sorbed on Na-IFM. Dashed lines represent the simulation of the amplitude and imaginary parts and, (c) FT^{-1} EXAFS data and the least-squares fit (dashed line).*

4.4 References

BAEYENS B., THOENEN T., BRADBURY M.H., MARQUES FERNANDES M. (2013a)
Sorption data bases for the host rocks and lower confining units and bentonite for provisional safety analyses for SGT-E2. Nagra Technical Report NTB 12-04 (in press) Nagra, Wettingen, Switzerland.

BAEYENS B., MARQUES FERNANDES M., BRADBURY M.H. (2013b)
Comparison between host rock and bentonite sorption measurements and predictions using the SDB approach applied in the provisional safety analyses for SGT-E2. Nagra Technical Report NTB 12-05 (in press) Nagra, Wettingen, Switzerland.

BRADBURY M.H., BAEYENS B. (1997)
A mechanistic description of Ni and Zn sorption on Na- montmorillonite. 2. Modelling, J. Contam. Hydrol. 27, 3-4, 223-248.

BRADBURY M.H., BAEYENS B. (2000)
A generalised sorption model for the concentration dependent uptake of Cs by argillaceous rock. J. Contam. Hydrol. 42, 141-163.

BRADBURY M.H., BAEYENS B. (2005)
Modelling the sorption of Mn(II), Co(II), Ni(II), Zn(II), Cd(II), Eu(III), Am(III), Sn(IV), Th(IV), Np(V) and U(VI) on montmorillonite: Linear free energy relationships and estimates of surface binding constants for some selected heavy metals and actinides Geochim. Cosmochim. Acta 69, 22, 875-892.

BRADBURY M.H., BAEYENS B. (2009)
Sorption modelling on illite. Part I: Titration measurements and the sorption of Ni, Co, Eu and Sn. Geochim. Cosmochim. Acta 73, 990-1003.

BRADBURY M.H., BAEYENS B. (2011)
Predictive sorption modelling of Ni(II), Co(II), Eu(III), Th(IV) and U(VI) on MX-80 bentonite and Opalinus Clay: A “bottom-up” approach. Appl. Clay Sci. 52, 27-33.

CHURAKOV S.V., DÄHN R. (2012)
Zn adsorption on clays inferred from atomistic simulations and EXAFS spectroscopy. Envir. Sci. &Tech. 46, 5713-5719.

DÄHN R., BAEYENS B., BRADBURY M.H. (2011)
Investigation of the different binding edge sites for Zn on montmorillonite using P-EXAFS - The strong/weak site concept in the 2SPNE SC/CE sorption model. Geochim. Cosmochim. Acta *75*, 5154-5168.

GÉHIN A., GRENECHE J.M., TOURNASSAT C., BRENDLE J., RANCOURT D.G., CHARLET L. (2007)
Reversible surface-sorption-induced electron-transfer oxdiation of Fe(II) at reactive sites on a synthetic clay mineral. Geochim. Cosmochim. Acta 71, 863-876.

GUILLAUMONT R., FANGHÄNEL T., FUGER J., GRENTHE I., NECK V., PALMER D.A., RAND M. H. (2003)
Update on the chemical thermodynamics of Uranium, Neptunium, Plutonium, Americium and Technetium, Amsterdam, Elsevier.

MÄDER U. (2010)
Reference porewater for the Helvetic marls for the provisional safety analysis in the framework of the sectoral plan – interim results (SGT-ZE). Nagra Arbeitsbericht. Nagra, Wettingen Switzerland.

NAGRA (2008)
Begründung der Abfallzuteilung, der Barrieren-systeme und der Anforderungen an die Geologie. Bericht zur Sicherheit und technischen Machbarkeit. Nagra Technical Report NTB 08-05. Nagra, Wettingen, Switzerland.

SOLTERMANN D., MARQUES FERNANDES M., BAEYENS B., DÄHN R., MIEHE-BRENDLÉ J., WEHRLI B., BRADBURY M.H. (2013)
Fe(II) sorption on a synthetic montmorillonite. A combined macroscopic and spectroscopic study. Environ. Sci. Technol. 47, 6978-6986.

THOENEN T. (2012)
The PSI/Nagra Chemical Thermodynamic Data base 12/07: Compilation of updated and new data with respect to the Nagra/PSI Chemical Thermodynamic Data Base 01/01. PSI Internal Report TM-44-12-06.

TRABER D., BLASER P. (2013)
Gesteinsparameter der Wirtgesteine Opalinuston, 'Brauner Dogger', Effinger Schichten und Helvetische Mergel als Grundlage für die Sorptionsdatenbank. Nagra Arbeitsbericht NAB 12-39. Nagra, Wettingen, Switzerland.

5 CEMENT SYSTEMS

E. Wieland, J. Tits, A. Laube, D. Kunz, Ph. Schaub (post doc), J. Schenzel (post doc), H. Rojo Sanz (guest scientist)

5.1 Overview

Cementitious materials are foreseen to be used in the deep geological repositories for low-level and short-lived intermediate-level (L/ILW) as well as long-lived intermediate-level (ILW) radioactive waste in Switzerland. The research programme carried out by the group "Cement Systems" aims at strengthening the credibility of the sorption values used in performance assessment (PA) for predicting radionuclide release from the cementitious near field into the host rock, and improving the knowledge on the chemical processes occurring in cement-based repositories.

In 2013 the group was involved in the preparation of a cement sorption data base and a report on the evolution of heterogeneities in the cementitious near field in connection with the the Sectoral Plan for Deep Geological Disposal (SGT-E2). The SGT related experimental research data baseme comprised of: i) activities aimed at the characterization of activated steel samples to be used in a long-term corrosion experiment, ii) investigations into the formation of low molecular weight (LMW) organics during the anoxic corrosion of steel, iii) measurements of the chemical stability of selected LMW organics under hyper-alkaline conditions, and iv) mechanistic sorption studies with redox-sensitive actinides (Np(IV/V)) and dose-determining anions (Se(IV/-II)) on hardened cement paste (HCP) and cement phases.

The studies on the formation of LMW organics during anoxic steel corrosion are partially financed by Swissnuclear in the framework of a long-term study on the formation of ^{14}C-containing organic compounds released during the anoxic corrosion of activated steel. Specific tasks within the Swissnuclear project are being developed in co-operation with PSI internal partners (Dr. I. Günther-Leopold - Hot Laboratory; Dr. D. Schumann - Laboratory for Radiochemistry & Environmental Chemistry), and external partners in Switzerland (Prof. Dr. G. Schlotterbeck - Institute of Chemistry & Bioanalytics (ICB), Fachhochschule Nordwest-schweiz (FHNW), Muttenz; PD Dr. S. Szidat - Department of Chemistry & Biochemistry, University of Bern).

Investigations into Se uptake mechanisms on cementitious materials under reducing conditions are partially financed by the German Federal Ministry of Education and Research in the framework of the Verbundprojekt "Immorad" (Grundlegende Untersuchungen zur Immobilisierung langlebiger Radionuklide durch die Wechselwirkung mit endlagerrelevanten Sekundärphasen; coordinator: Dr. Th. Schäfer (KIT-INE)).

Dr. Ph. Schaub (post doc) left the group on April 30th, 2013, to accept a position at the Swiss Federal Office of Energy. Dr. J. Schenzel (post doc) left the group on October 31st, 2013, to accept a position at Eawag (Switzerland).

Dr. B. Cvetković joined LES on November 1st, 2013. His research activities will focus on the development of the analytical techniques required for identifying and quantifying ^{14}C-containing organic compounds in the framework of the Swissnuclear financed project.

5.2 Activities in support of the Sectoral Plan: Report on the evolution of heterogeneities in the cementitious near field

A multi-barrier concept is foreseen to ensure the safe disposal of L/ILW and ILW in cement-based deep geological repositories (NAGRA, 2002). Barriers comprise the waste matrix, the waste-containing steel drums, the emplacement containers for the steel drums, the cavern backfill used to fill vaults within and between the emplacement containers, liners and eventually the host rock. In PA it is currently considered that all materials (waste, backfill, container etc.) inside the cavern are homogeneously distributed, i.e. homogenized in accordance with a "mixing-tank" approach. On the basis of this approach it is further assumed that the containments (drums and waste packages) are not effective as barriers. This leads to the assumption that about 50 years after closure of the cavern all the radionuclides are distributed homogeneously in the cementitious near field (Nagra pers. comm.), which determines the source term of radionuclide release into the host rock.

A report is currently being prepared with the aim of assessing the barrier function of the waste drums by considering the heterogeneity of the waste matrices. In particular, preliminary kinetic and mass balance calculations for relevant chemical processes were carried out with the aim of predicting the temporal evolution of the chemical conditions in selected waste packages, e.g. a resin-containing bitumised waste package, a cemented waste package, and resin-containing waste embedded in polystyrene. These waste packages were selected as being representative of important waste forms to be emplaced in the L/ILW caverns. The temporal evolution of the waste matrix in these packages was described on the basis of the most important chemical reactions: i) metal corrosion, ii) degradation of organics, and iii) dissolution of silicate aggregates. In the report, the effect of these chemical processes on the lifetime of the steel drums and on the time scale for the homogenization of the near field will be estimated by scoping calculations.

5.3 Speciation and fate of organic compounds in the cementitious near field

5.3.1 ^{14}C project

Carbon-14 containing LMW organic compounds such as methane, ethane etc., or oxidized hydrocarbons, such as alcohols, aldehydes, carboxylic acids, can potentially form during the anoxic corrosion of steel in a cementitious near field. If such ^{14}C-containing organics are produced, they would be major contributors to the annual dose released from a L/ILW repository. Although the ^{14}C inventory in the repository is well known, the chemical speciation of the ^{14}C liberated from activated steel is only poorly known. The Swissnuclear financed ^{14}C project aims at filling this gap in our knowledge. To this end, a long-term corrosion experiment with activated steel is planned. In 2013, the first steps in connection with this experiment were completed.

5.3.1.1 Sample preparation and characterization of activated steel

Five stainless steel nuts were retrieved from the "Brennelement-Lagerbecken" of the Kernkraftwerk Gösgen (KKG) and transported to the PSI Hot Laboratory in February 2012. The nuts (Brennelement-Führungsrohrmuttern) were positioned at the top and bottom end of fuel rods. Each nut (Fig. 5.1a) had a weight of ~5 g (diameter: 1 cm; height: 1.1 cm) and a contact dose ratio of ~100 mSv/h. Two nuts were processed to prepare ~10 small specimens for laboratory experiments (Fig. 5.1b). Three of these small specimens were dissolved to determine the ^{14}C inventory. The method was based on a stepwise dissolution process using a mixture of concentrated HCl and HNO_3 heated to boiling point in the first step, and a mixture of boiling concentrated sulfuric, perchloric and nitric acids in the second dissolution step. The carbon contained in the activated steel was released as CO_2 and collected in two traps containing 1 M NaOH solution. Aliquots taken from the NaOH solutions and the ^{14}C activity determined by liquid scintillation counting (LSC). A standard steel sample with certified carbon content (0.864%) was used to test and check the method. The results showed that in the activated steel the larger portion of ^{14}C was released in the first dissolution step (~90 %) and only a small portion remained in the graphitic residue (~10 %) (Table 5.1). The total ^{14}C inventory from three replicates was determined to be 17841 ± 2524 Bq g^{-1}, showing that the ^{14}C inventory in the activated steel is very low.

Sample preparation was carried out in collaboration with the PSI Hot Laboratory (Dr. I. Günther-Leopold and M. Martin), while the characterization of the activated steel was performed in collaboration with the Laboratory for Radio- and Environmental Chemistry (LCH) of PSI (Dr. D. Schumann, T. Stowasser).

Table 5.1: *^{14}C activities determined in the first (^{14}C - first) and the second (^{14}C - second) dissolution step and the total activities of ^{14}C.*

Sample No	Mass (g)	^{14}C - first (Bq/g steel)	^{14}C - second (Bq/g steel)	Total ^{14}C (Bq/g steel)
1	0.0956	17279	2120	19399
2	0.0849	15009	2318	17328
3	0.0693	14878	1919	16797

a **b**

***Fig. 5.1**: a) Activated steel nuts obtained from KKG; b) Segments prepared from a steel nut.*

5.3.1.2 Identification and quantification of organics released during iron corrosion

An analytical approach has been developed that allow volatile and dissolved LMW organics (number of carbon atoms C ≤ 5) to be identified and quantified (LES progress report 2012) using gas chromatography (GC) coupled with mass spectrometry (MS) for the volatile LMW organics, and high performance ion exclusion chromatography (HPIEC) coupled with mass spectrometry (MS) and conductivity detection (CD) for the dissolved LMW organics. The gas phase analysis was developed in the framework of a LES-ICB/FHNW collaboration.

In 2013 a series of corrosion experiments with iron powders in alkaline solution was carried out. The formation of dissolved and volatile small organic molecules was determined as a function of time (Fig. 5.2). The iron powders from two different manufacturers, i.e. Sigma Aldrich and BASF, were used. Prior to use, the powders, produced by reducing $Fe(CO)_5$ with hydrogen, were pre-treated according to a procedure reported in the literature (DENG et al., 1997). For the batch-type corrosion experiments, the iron powders (1 g) were immersed in 20 mL of three different artificial cement pore fluids with different pH values (pH = 13.3, pH = 12.5, pH = 11.5) in zero-headspace, gas-tight vials and shaken end-over-end in a N_2 atmosphere glove box for a maximum of 35 days. Dissolved and volatile organics were determined in the supernatant solution. For HPIEC, aliquots of the solution were filtered using special cartridges to remove components which interfered with the analysis (e.g. Fe, Cl). Samples for subsequent headspace GC-MS analysis were generated using a method developed at ICB/FHNW for extracting volatile organics from the supernatant solution.

Fig. 5.2 shows the results of the time-dependent concentrations of methane and formate determined in the corrosion experiments with treated and untreated iron powders at pH = 11.5. The concentration of formate is constant within the experimental uncertainties, indicating that this compound is not generated during iron corrosion. Note that the same behaviour was observed for acetate, malonate and oxalate, which were the other carboxylates identified and quantified by HPIEC. Furthermore, the concentration of all carboxylates is significantly lower in iron- cement-type solution systems with untreated iron powder than with pre-treated iron powder, indicating that these compounds were most likely produced during the pre-treatment process. In contrast, the methane concentration increased with time, suggesting that this molecule was formed as a consequence of the corrosion process (Fig. 5.2). In addition, the methane concentrations are comparable in the untreated and pre-treated iron powder samples. Also, a similar behaviour was observed for ethane/ethene, propane and butane, which were the other volatile organics identified and quantified by GC-MS. The results thus show that carbon is released from the iron during corrosion mainly in the form of volatile organic compounds. The presence of carboxylates is most probably an artifact arising from the pre-treatment of the iron powders. Note further that the concentrations of all organics, dissolved and volatile, were found to be constant within experimental uncertainty in the solutions at pH = 12.5 and 13.3 due to the very low corrosion rate under these conditions.

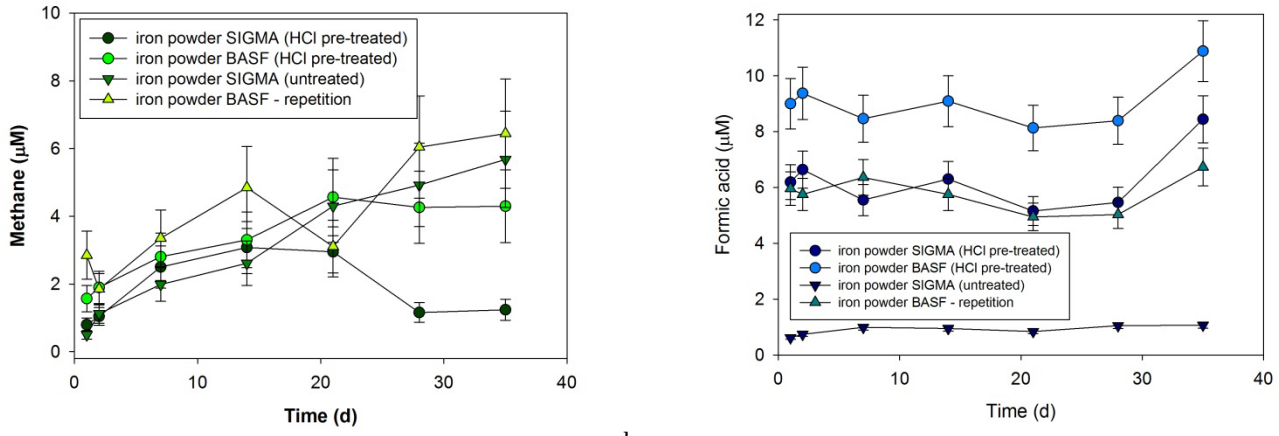

a b

Fig. 5.2: *Time dependence of the concentrations of a) methane and b) formic acid during the corrosion of un-treated Sigma-Aldrich and pre-treated Sigma-Aldrich and BASF iron powders in a cement-type solution (pH = 11.5). Note that the measurements at 28 and 35 days in figure a) are considered to be outliers.*

5.3.2 Chemical stability of organic compounds under hyper-alkaline conditions

The ^{14}C containing LMW organic molecules released during the corrosion of activated steel may not be chemically stable under the hyper-alkaline, reducing conditions of a cement-based repository. The chemical stability of LMW organic compounds under these conditions was examined on the basis of thermodynamic modelling (WIELAND & HUMMEL, 2010). The calculations revealed that the predominant, dissolved species in the case of complete thermodynamic equilibrium are $CO_{2(aq)}$, HCO_3^-, CO_3^{2-} and methane, $CH_{4(aq)}$. Note that organic compounds in the solid or gaseous state were not considered in the modelling. All other organic species were either present at trace levels or thermodynamically unstable. However, since complete stable redox equilibrium is rarely achieved in the C-H-O system, at least at moderate temperatures, it was considered that partial thermodynamic equilibria might prevail. For example, thermodynamic calculations were carried out under the assumption that the formation of $CH_{4(aq)}$ or alkanes/alkenes, respectively, is kinetically inhibited. In the case of partial thermodynamic equilibrium where methane is not formed, the predominant dissolved species were found to be ethane, $C_2H_{6(aq)}$, in addition to $CO_{2(aq)}$, HCO_3^- and CO_3^{2-}. Furthermore, the predominance of carboxylic acids was observed when it was assumed that the formation of dissolved alkanes, i.e. methane, ethane, propane, butane and pentane, was kinetically inhibited. Thus, it is presently unclear whether or not complete equilibrium in the C-H-O system can be assumed under the conditions existing in a cement-based repository. In order to try to improve the situation it was decided to study the chemical stability of formic and acetic acids in laboratory experiments simulating the conditions in a cementitious near field.

An experimental set-up for studying the chemical stability of LMW organic compounds under alkaline, reducing conditions and a H_2 overpressure was developed over the last few years. In 2013, the custom-made gas-tight overpressure reactor, sampling and analytical methods were tested using an oxygen-free, portlandite-saturated solution (pH = 12.5) containing $3 \cdot 10^{-3}$ M Na-acetate spiked with ^{14}C labelled acetic acid. This solution was aged under strict anoxic conditions for up to 60 days under an inert N_2 atmosphere at a pressure of 4 bar. Both the aqueous and the gas phases were sampled at regular intervals. The ^{14}C activity in the aqueous phase was determined by LSC and showed that the concentration of ^{14}C labelled acetate did not change over a period of 60 days. The gas samples were analysed at ICB/FHNW using GC-MS to check for the presence of volatile degradation products. GC-MS analysis revealed the presence of propane and butane at concentrations slightly above the detection limit of the GC-MS equipment (0.05 µM). The concentration of the volatile species (~0.34 µM) was much lower than that of acetate acid ($3 \cdot 10^{-3}$ M). The formation of the volatile compounds is presently not understood since the concentration of acetate (stable and ^{14}C labelled) remained constant within the uncertainty of the analytical methods (IC, LSC). Sampling will be repeated with the aim of checking this finding.

5.3.3 Sorption/diffusion of formic acid and acetic acid

Sorption measurements with formic acid and acetic acid were reported earlier (LES progress report, 2010). It has been speculated that these compounds might be present as ^{14}C containing species in the cementitious near field of a repository for radioactive waste (SASOH, 2004). The uptake of formic and acetic acids in compact samples of hydrating cement was found to be very weak (formic acid: $R_d \sim 10^{-3}$ $m^3 \cdot kg^{-1}$; acetic acid: $R_d \sim 10^{-4}$ $m^3 \cdot kg^{-1}$). In the past years, through- and out-diffusion experiments with ^{14}C labelled formic and acetic acids were carried out with the aim of checking the sorption values derived from the earlier sorption measurements on compact HCP samples. Modelling of the diffusion data is reported in the Transport Mechanisms group chapter.

5.4 Immobilization of redox-sensitive radionuclides by cementitious materials

5.4.1 Reversibility of Np(IV/V) uptake by HCP and C-S-H phases

Extended X-ray absorption fine structure (EXAFS) spectroscopy studies and batch sorption experiments on the uptake of Np(IV) and Np(V) by calcium silicate hydrates (C-S-H phases) and HCP have shown that these cations are incorporated into the interlayer of C-S-H phases rather than bound to the surface (GAONA et al., 2011; GAONA et al., 2013). Incorporation may result in irreversible, or partially reversible, immobilization over the time scale of a repository. In 2013, desorption studies were carried out on C-S-H phases and HCP loaded with $^{237}Np(IV)$ and $^{237}Np(V)$ with the aim of testing the reversibility of Np(IV/V) uptake (Fig. 5.3). ^{237}Np was sorbed onto C-S-H phases (Ca:Si ratio (C:S) = 0.65, pH = 10.1, solid:liquid ratio (S:L) = 10^{-4} $kg \cdot L^{-1}$, [^{237}Np] = 10^{-5} M) and HCP (pH = 13.3, S:L = 10^{-4} $kg \cdot L^{-1}$) for 1 and 60 days and subsequently desorbed by replacing the supernatant solution with a fresh, ^{237}Np-free solution in equilibrium with the respective solid phases. The activity of ^{237}Np released from the solid was determined as a function of increasing desorption time. At pH = 10.1, a high total ^{237}Np concentration (10^{-5} M) was used which was, however, below the solubility of Ca-neptunate (solubility limit ~$5 \cdot 10^{-5}$ M at pH = 10). High ^{237}Np concentrations were required in order to determine the ^{237}Np activity in the supernatant solution with an acceptable uncertainty. In the case of the reversibility tests with Np(IV) on HCP (pH = 13.3), the solubility limits with respect to Ca-neptunate and $Np(OH)_4$ were exceeded shortly after addition of the Np tracer. Thus, Np precipitation could occur, although earlier EXAFS measurements showed that at similar total Np concentrations and higher S:L ratios, fast sorption prevented Np precipitation (GAONA et al., 2011; GAONA et al., 2013). For the Np(IV) experiments, the tetravalent redox state was stabilized by the addition of $5 \cdot 10^{-3}$ M hydrazine.

The reversibility tests showed that ^{237}Np desorption from C-S-H phases and HCP is a fast process (Fig. 5.3). Equilibrium was reached within a maximum of five days. The R_d values determined at desorption equilibrium agree, within the experimental uncertainty limits, with those obtained in the initial sorption tests (Fig. 5.3) indicating that Np(IV/V) uptake into the interlayer of C-S-H phases is a reversible process. The uptake process on HCP is also reversible, which is consistent with earlier observations that C-S-H phases are the uptake-controlling cement phase in HCP (GAONA et al., 2011; GAONA et al., 2013).

5.4.2 Retention of selenium by cement phases

^{79}Se (half-life $3.27 \cdot 10^5$ years) is an important redox-sensitive, dose-determining radionuclide in a L/ILW repository (NAGRA, 2002). The selenium speciation under oxidizing conditions is dominated by the oxyanions SeO_4^{2-} and SeO_3^{2-} (e.g. OLIN et al., 2005). In alkaline, reducing conditions, i.e. 10.0<pH<13.5 and -750mV<Eh<-230mV, Se(0), HSe^- and polyselenide species exist along with SeO_3^{2-}. Robust sorption data and, in particular, a detailed mechanistic understanding of the retention of Se(-II) in a cementitious environment are lacking (WIELAND & VAN LOON, 2002).

The influence of the transition from oxidizing to reducing conditions on the immobilization of Se in cementitious materials will be investigated in the framework of our contribution to the "Immorad" project. During solidification of the waste, and during the operational phase of the repository, i.e. under oxidizing conditions, Se is expected to exist predominantly as SeO_3^{2-}, which sorbs on the different cement phases (C-S-H, AFm, AFt,…) of HCP. After the closure of the repository, however, conditions will slowly become reducing, which might eventually result in a transformation of SeO_4^{2-} and SeO_3^{2-} into Se(-II).

Kinetic studies of Se(IV) uptake by different cement phases were carried out and an experimental procedure to reduce Se(IV) to Se(-II) under alkaline conditions was tested.

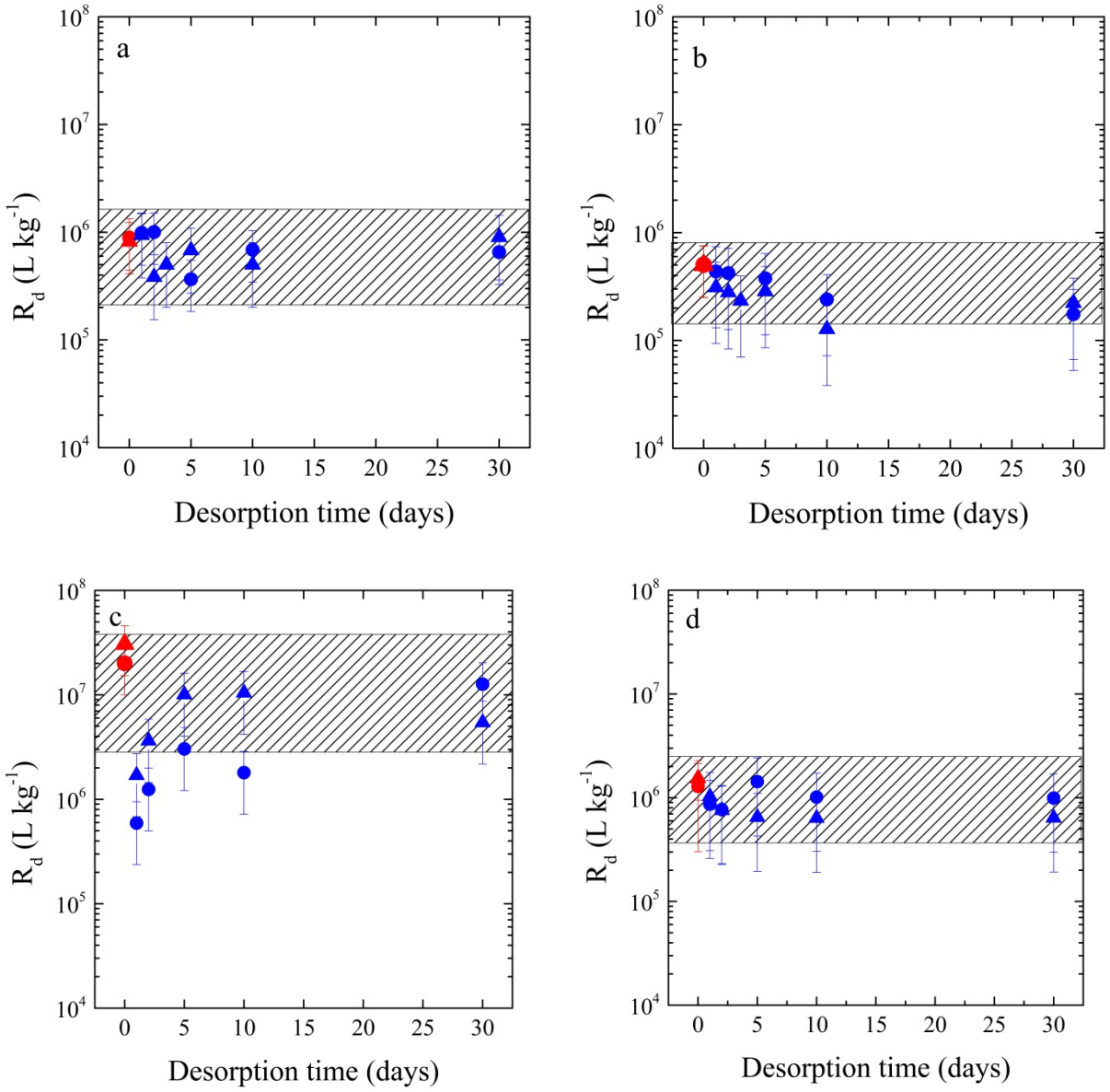

Fig. 5.3: *Neptunium desorption experiments on C-S-H phases (C:S = 0.65, pH = 10.1) and on HCP in ACW (pH = 13.3). a) Np(V) on C-S-H phases; b) Np(V) on HCP; c) Np(IV) on C-S-H phases; d) Np(IV) on HCP. The shaded areas represent the 95% confidence interval on the desorption data. (●) R_d (sorption for 1 day), (●) R_d desorption as a function of time after 1 day sorption, (▲) R_d sorption for 60 days, (▲) R_d desorption as a function of time after 60 days sorption.*

Se(IV) sorption kinetic studies were carried out on different synthetic cement phases with the aim of identifying the uptake-controlling phase for Se(IV) in HCP: C-S-H phases (tobermorite and amorphous C-S-H phases) with different C:S ratios, ettringite and different layered double hydroxides (LDH's) phases with important anion exchange properties: AFm-Cl_2 (monochloride), AFm-SO_4 (monosulphate), AFm-CO_3 (mono-carbonate), and AFm-OH-CO_3 (hemicarbonate). In addition, Se(IV) sorption was studied at pH = 10 on the "reference solid" TiO_2 (Degussa P25, Evonik AG) in the presence of 10^{-3} M Ca. TiO_2 is stable under hyper-alkaline conditions and Se(IV) is bound as surface complex on this solid.

The experiments showed that Se(IV) uptake by AFm phases is higher than by ettringite (Fig. 5.4). Furthermore, the sorption of Se(IV) is strong. R_d values on C-S-H phases were approximately two orders of magnitude higher than those determined on TiO_2 and tobermorite, a crystalline C-S-H phase. The high affinity of C-S-H phases for Se(IV) may be partially explained by their very high specific surface area (~200 $m^2\ g^{-1}$ - 1000 $m^2\ g^{-1}$; JENNINGS et al., 2008). Note that the TiO_2 and tobermorite used in this study had much lower surface areas (56.4 $m^2 \cdot g^{-1}$ and 7 $m^2 \cdot g^{-1}$, respectively; COMARMOND et al., 2011; MANDALIEV et al., 2010).

It is expected that C-S-H phases are the uptake-controlling phase for Se(IV) in HCP due to the large quantities of C-S-H phases in HCP (~50 wt%) and the high affinity of these phases for Se(IV).

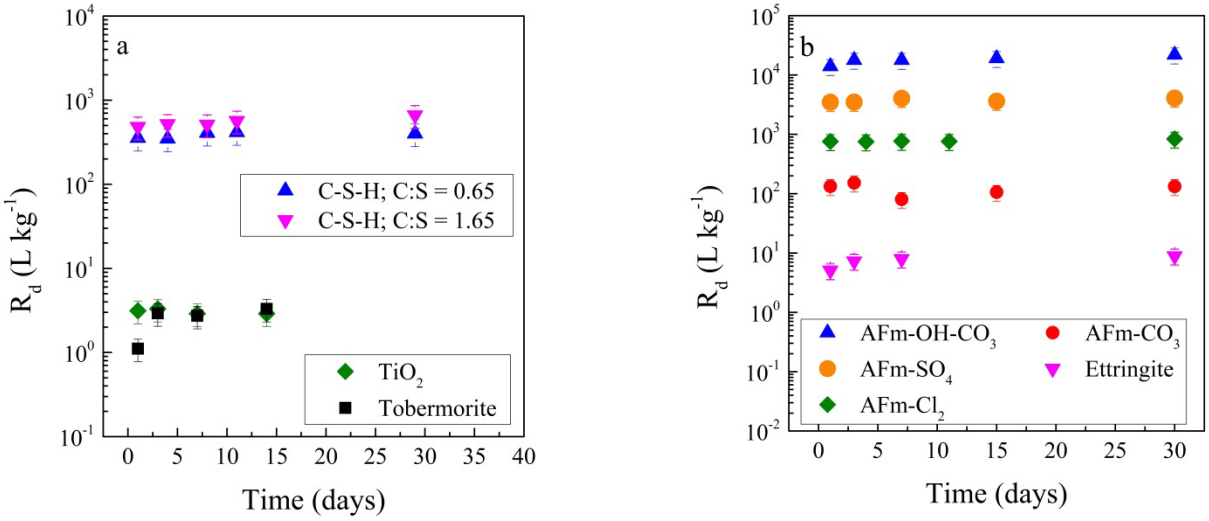

***Fig. 5.4**: Se(IV) sorption kinetics on different cement components: a) C-S-H phases and TiO_2. b) AFm phases and ettringite.*

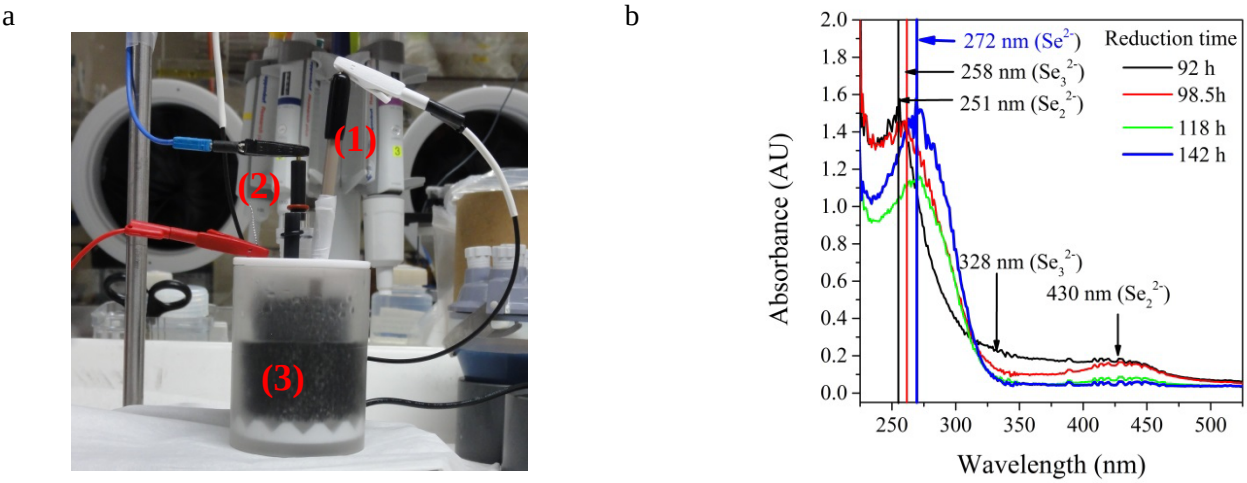

***Fig. 5.5**: a) Electrochemical cell with (1) leak-free reference electrode, (2) auxiliary electrode and (3) reticulated vitreous carbon electrode (dark material in container). b) UV-Vis spectra of a 0.08 M Se solution in 2 M NaOH during electrochemical reduction.*

The electrochemical reduction of Se(IV) to Se(-II) in solution is a challenging task. It has to be carried out in an inert atmosphere under hyper-alkaline conditions to avoid the precipitation of Se(0) which retards the reduction. The aqueous reduction of Se(IV) to Se(-II) ([Se] = 0.08 M, in 2 M NaOH) was carried out in a glove box ($[O_2]< 0.1$ ppm) using an electrochemical cell with three electrodes (Fig. 5.5a). The cell consisted of a polyacryl container, a high surface area reticulated vitreous carbon (RVC) working electrode, a platinum (Pt) wire as counter electrode and a leak-free Ag/AgCl reference electrode embedded in peek. The counter electrode was kept isolated from the cell solution in a separate compartment within the electro-chemical cell. Electrical contact was made through an alkali-resistant ion-exchange membrane (Nafion®, DuPont, USA). The initially applied redox potential of -0.25V (SHE) was slowly reduced to the required value of -1.28 V (SHE). UV-V is spectra recorded during the reduction showed that the appearance of different polyselenides (Se_3^{2-} and Se_2^{2-}) precedes the formation of Se^{2-} (peak max. at 272 nm) (Fig. 5.5b). The reduction process was completed after 250 h, which was indicated coulometrically (current between working electrode and counterelectrode < ~1% of the initial value) and spectroscopically (peak max. at 251 nm and absence of polyselenide peaks). The Se(-II) solution will be used in future sorption experiments on cement phases.

5.5 References

COMARMOND M.J., PAYNE T.E., HARRISON J.J., THIRUVOTH S., WONG H., AUGTERSON R.D., LUMPKIN G.R., MÜLLER K., FOERSTENDORF H. (2011)
Uranium sorption on various forms of titanium dioxide - influence of surface area, surface charge, and impurities. Environ. Sci. Technol. 45, 5536-5542.

DENG B.L., CAMPBELL T.J., BURRIS D.R. (1997)
Hydrocarbon formation in metallic iron/water systems. Environ. Sci. Technol. 31, 1185-1190.

GAONA X., DÄHN R., TITS J., SCHEINOST A., WIELAND E. (2011)
Uptake of Np(IV) by C-S-H phases and cement paste: an EXAFS study. Environ. Sci. Technol. 45, 8765-8771.

GAONA X., WIELAND E., TITS J., SCHEINOST A., DÄHN R. (2013)
Np(V/VI) redox chemistry in cementitious systems: XAFS investigations on the speciation under anoxic and oxidizing conditions. Appl. Geochem. 28, 109-118.

JENNINGS H.M., BULLARD J.W., THOMAS J.J., ANDRADE J.E., CHEN J.J., SCHERER G.W. (2008)
Characterization and modelling of pores and surfaces in cement paste: Correlations to processing and properties. J. Adv. Concr. Technol. 6, 5-29.

MANDALIEV P., WIELAND E., DÄHN R., TITS J., CHURAKOV S.V., ZAHARKO O. (2010)
Mechanisms of Nd(III) uptake by 11Å tobermorite and xonotlite. Appl. Geochem. 25, 763-777.

NAGRA (2002)
Project Opalinus Clay: Safety report. Demonstration of disposal feasibility for spent fuel, vitrified high-level waste and long-lived intermediate-level waste (Entsorgungsnachweis), Nagra Technical Report NTB 02-05. Nagra, Wettingen, Switzerland.

OLIN Å., NOLÄNG B., OSADCHII E.G., ÖHMAN L.-O., ROSÉN E. (2005)
Chemical thermodynamics of Selenium. Elsevier, Amsterdam.

SASOH M. (2004)
The study for the chemical forms of C-14 released from activated metals. In: L.H. Johnson and B. Schwyn (eds), Proceedings of a workshop on the release and transport of C-14 in repository environments. Nagra unpublished internal report, Nagra, Wettingen, Switzerland, 2004.

WIELAND E., VAN LOON L.R. (2002)
Cementitious near field sorption data base for performance assessment of an ILW repository in Opalinus Clay, PSI Bericht 03-06, Paul Scherrer Institut, Villigen, Switzerland and Nagra Technical Report NTB 02-20, Nagra, Wettingen, Switzerland.

WIELAND E., HUMMEL W. (2010)
The speciation of ^{14}C in the cementitious near field of a repository for radioactive waste, TM 44-10-01, Paul Scherrer Institut, Switzerland.

6 COLLOID CHEMISTRY

C. Degueldre, S. Frick

6.1 Overview

The aim of the colloid sub-programme is to understand the role of colloids in the migration of radionuclides in the geosphere. The colloid properties studied are: concentration, size distribution and nature, all of which influence their behavior under safety relevant conditions. The main activities over the past year were carried out within the framework of the Grimsel colloid project: "Colloid Formation and Migration" (CFM), and focused on colloid generation using single particle counting (SPC) as a characterisation technique. The colloid generation approach followed is novel in this area and has the possibility of evaluating clay colloid size distributions, not only in batch systems, but also under the quasi-stagnant conditions in the CFM system. The knowledge and understanding in groundwater colloid science gained over the last decade allows well founded estimates to be made concerning the potential role played by colloids in the transport of radionuclides in the argillaceous rock formations proposed by Nagra in the frame of the Sectoral Plan for Deep Geological Disposal (SGT).

6.2 Activities in the colloid formation and migration project

The CFM project is conducted at the Grimsel Test Site (GTS), Switzerland in the framework of Phase VI of the research programme which runs from 2004 to 2013 and is dedicated to repository-relevant (i.e. large-scale, long-term) in-situ experiments. The research programme has been extended until at least 2016.

In July 2013, a radionuclide-colloid cocktail was injected into the MI shear zone at the GTS. The colloids were FEBEX bentonite doped with selected radionuclides (see Table 6.1). This tracer test (test 13-05) involved injection into the borehole CRR 99.002-i2 CFM -i2 and extraction downstream 2.23 m away at BOMI 87.010 CFM -i2 as depicted in Fig. 6.1.

The tracer cocktail was made up of three different types of tracer, AGA or amino-G acid (7 amino-1,3-naphtalene disulfonic acid, injected mass 3706 µg, concentration 1140 µg L^{-1}), radionuclide tracers, and bentonite colloids (injection mass 228.150 ± 5600 µg, injection concentration 70.200 ± 1700 µg L^{-1}). Table 6.1 gives an overview of the composition of the radionuclide tracer cocktail and the initial activity for each radionuclide.

The tracer cocktail was injected at a flow rate of approximately 0.3 mL min^{-1} (in BoMi 99.002) and water was continuously extracted at a flow rate of 5 mL min^{-1} from BoMi 87.010, while a flow rate of 25 mL min^{-1} was maintained at the instrumented surface spring on the tunnel wall (Fig. 6.1). The test was initiated by introducing the tracer cocktail into a flow loop circulating through the injection interval at a relatively high rate to keep the interval well mixed while maintaining a near constant net injection flow rate into the shear zone. The volume of the vessel containing the tracer cocktail was 2.25 L, and the volume of the injection flow loop was 1.0 L, so that the entire injection circuit volume was 3.25 L. This arrangement resulted in an exponentially decaying source term in the shear zone as the tracers were slowly blend out of the injection circuit.

Table 6.1: *Composition of radionuclide tracer cocktail (in 3.25 L) in CFM Tracer Test 13-05.*

Nuclide	Activity at t(0)* (Bq)	Colloidal Fraction		Nuclide	Activity at t(0)* (Bq)	Colloidal Fraction
^{22}Na	$1.50 \cdot 10^{+06}$	0-0.03		^{237}Np	$1.21 \cdot 10^{+02}$	1.0
^{133}Ba	$9.60 \cdot 10^{+06}$	0.24-0.34		^{243}Am	$1.74 \cdot 10^{+03}$	1.0
^{137}Cs	$9.00 \cdot 10^{+05}$	0.97		^{242}Pu	$1.67 \cdot 10^{+02}$	1.0

**t(0): time 0, the time of cocktail preparation*

The identity and activities of the tracers in the injection cocktail, as well as the fractions of each radionuclide that were initially partitioned to the bentonite colloids in the cocktail, are listed in Table 6.1. The tracer concentrations in the extracted water as a function of time are shown in Fig. 6.2. All the data shown in Fig. 6.2 should be considered preliminary. The actinide concentrations were also measured by ICP-MS at the Karlsruher Institute of Technology, KIT. The ^{22}Na, ^{137}Cs and ^{133}Ba activities were measured by gamma spectrometry at both PSI and KIT, and were found to be in excellent agreement. The Amino-G acid concentrations were measured in the field using an inline fluorimeter and were found to be in good agreement with offline measurements.

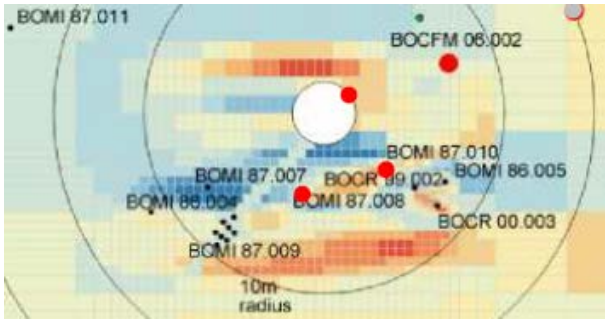

Fig. 6.1: *Schematic illustration of the CFM field test zone. Injection in BoMi 99.002 and breakthrough downstream at BoMi 87.010, within the flow oriented toward the surface spring in the access tunnel wall.*

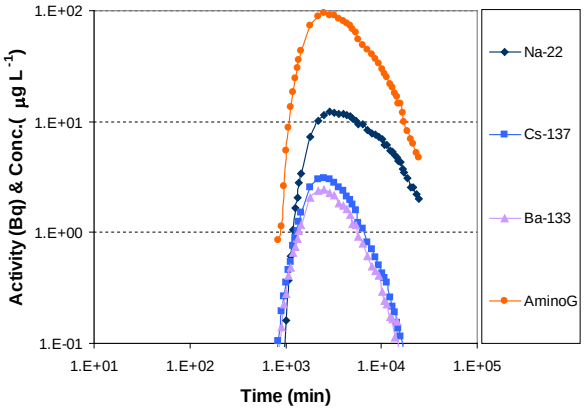

Fig. 6.2: *Comparison of ^{22}Na, ^{137}Cs and ^{133}Ba (Bq) and AGA (µg L^{-1}) breakthrough curves in the CFM tracer test 13-02 at the Grimsel Test Site.*

Offsite colloid measurements were conducted by PSI using a single-particle counter (SPC) and the data are shown in Fig. 6.3. The colloid concentrations were also measured in the field using a mobile laser-induced breakdown detection (LIBD) system operated by KIT personnel. The general trends in the LIBD and SPC data were in good agreement. The SPC data are size normalized. They show that the colloid size ranges relevant for the breakthrough are between 50-100 and 100-150 nm, and that sizes above 200 nm have little effect on the transport in the test.

The activity and concentration maxima were observed between 2160 and 2520 mins for the colloids (independent of size), for AGA, and for Cs and Ba; and between 2880 and 2940 mins for Na. The maximum for Na appears a little later because of its weaker sorption on the colloids (see Table 6.1) and also because it sorbs weakly on the host rock within which it may diffuse deeper than the colloids. The analysis of the data is in progress in close cooperation with the CFM modelling group.

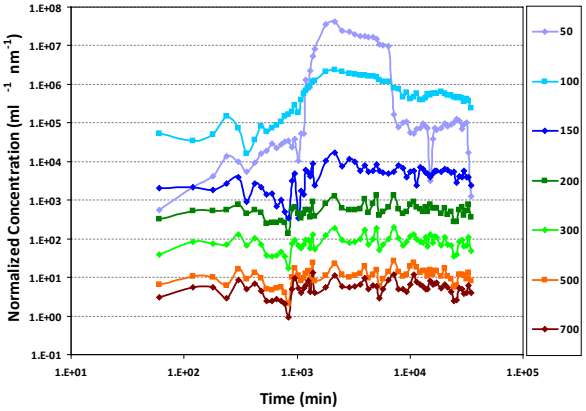

Fig. 6.3: *Comparison of colloid breakthrough curves in the CFM tracer test 13-02 at the Grimsel Test Site. Conditions: single particle counting (SPC) data recorded for the 50-100, 100-150, 150-200, 200-300, 300-500, 500-700 and 700-1000 nm size range channels.*

6.3 Other colloid activities

The co-operation with CIEMAT continues in a very productive manner. The main aim is to optimise the radio-analytical effort required to measure colloid breakthrough curves in the CFM experiment at the GTS.

The application of the advances made in groundwater colloid sciences over the last decade have allowed colloid data to be derived for the hydro-geochemical systems in the argillaceous rock formations proposed by Nagra in the frame of the SGT. A publication has been prepared which includes:

- groundwater colloid concentration results from field experiments ranging from dilute systems to saline groundwaters,

- a comparison of colloid concentration results with laboratory batch experiments, and
- the results of colloid adhesion tests (attachment factor values).

The study will be completed by calculations of colloid concentrations in the relevant systems using the suspension pseudo-equilibrium model (DEGUELDRE et al., 2009). This field/lab and model study will provide the required colloid data for the rock formations being investigated by Nagra.

The new model of colloid generation (batch stagnant & transient) has also been applied to upgrade the Bangombe (fossil reactor in Gabon) colloid data produced in 1996.

6.4 Future work

At Grimsel, the clay source foreseen for the long term CFM experiment will be installed early in 2014, and intensive sample analysis campaigns are anticipated in 2014-2015. A PhD student from CIEMAT will be involved in the analytical effort required (mainly) at the beginning of the new CFM experiment. The colloid project leader has been asked to participate at the CFM Modellers & Lab meeting early in February 2014 at the NDA, Oxford and at the CFM meeting in Asia the autumn of 2014. Participation at the BelVar meeting in Meringen (16-18 June 2014) is also anticipated.

6.5 References

DEGUELDRE C., AEBERHARD PH., KUNZE P., BESSHO K. (2009)
Colloid generation/elimination dynamic processes: Toward a pseudo-equilibrium? Colloids Surf. A, 337, 117-126.

7 DIFFUSION PROCESSES

L.R. Van Loon, M.A. Glaus, S. Frick, S. Dale, P. Bunic, Y. Chen (PhD)

7.1 Overview

The foci of the activities in the "Diffusion Processes" group are i) to understand the diffusion mechanism(s) of radionuclides in compacted argillaceous materials and ii) to measure diffusion parameters (effective diffusion coefficients and rock capacity values) which can be used in performance assessment studies.

Within the framework of the Sectoral Plan for Deep Geological Disposal (SGT) diffusion measurements with HTO and $^{36}Cl^-$ on fresh samples of Opalinus Clay and "Brauner Dogger" from the deep borehole at Schlattingen were performed. The measurements were used to confirm/check the validity of the extended Archie's relation over a wide range of porosities for estimating effective diffusion coefficients to be used in performance assessment studies. Due to some measurement difficulties, a second set of measurement was started on the same samples. The results of these measurements, and a compilation of effective diffusion coefficients for the different Swiss host rocks currently under investigation, were summarised in a Nagra NTB (VAN LOON, 2013). This diffusion data base will be used in the provisional safety analyses for SGT-E2.

Within the framework of the EU CatClay project, sorption measurements with $^{60}Co(II)$ and $^{65}Zn(II)$ on Opalinus Clay were performed. The results were compared with sorption values derived from in-diffusion measurements using a filter-free in-diffusion technique (VAN LOON & MÜLLER, 2014). The latter values were smaller than those measured on crushed material. Similar conclusions could also be drawn from diffusion measurements of the same tracers on purified compacted illite. For these experiments a new type of diffusion cell in which the clay samples are separated from the contacting solution by a thin membrane were used.

Additional in-diffusion measurements of caesium in Opalinus Clay and purified illite were performed to check whether sorption-enhanced diffusion phenomena observed for caesium depend on the mobility of the predominant sorption type, as suggested by GIMMI & KOSAKOWSKI (2011).

The TRAPHICS programme on pure clay minerals was continued. Experiments with $^{85}Sr^{2+}$ tracer were carried out under salt-gradient conditions. In contrast to the previous tests with $^{22}Na^+$ (GLAUS et al., 2013) a much more extended time range could be covered during which significant changes in the concentrations of the electrolytes in the reservoirs could be observed. The excellent consistency obtained for both tracer and electrolyte concentrations confirmed the working hypothesis that the local concentration gradient of tracer cations bound to the cation exchange sites is the dominant driving force for diffusion of these species in compacted smectites.

Two PhD projects on reactive transport are on-going in close co-operation with the Transport Mechanisms Group.

A new PhD on the fate of organic molecules in compacted clay systems was started. The first results with lactate, acetate and gluconate showed that these small organic molecules are unstable unless precautions are taken against the presence of microbes.

A new PhD proposal concerning the anion accessible porosity in clay rocks was accepted by the PSI research committee. The project will start in 2014.

A project to develop a QM-system based on the ISO 9001 norm was started in close cooperation with the Hot Laboratory. The aim is to have a functional QM system for LES by the end of 2014. The QM system will be compatible with the QM systems of the Hot Laboratory (AHL) and the Laboratory for Nuclear Materials (LNM).

7.2 Activities in support of the SGT

Diffusion measurements with HTO and $^{36}Cl^-$ on fresh samples of Opalinus Clay and "Brauner Dogger" from the deep borehole at Schlattingen were performed. Due to some anomalies in the data, the measurements had to be repeated. So far, diffusion values for HTO and $^{36}Cl^-$ are available. Measurements with $^{22}Na^+$ will be finished early in 2014. The measurements on the new samples confirmed the applicability of the extended Archie's relation for estimating effective diffusion coefficients from accessible porosity values (VAN LOON, 2013). Although anion exclusion can be explained qualitatively, a quantitative explanation in the case of clay rocks is not yet available. This is especially so regarding the somewhat remarkable observation that the anion accessible porosity

measured with $^{36}Cl^-$ is ~50% of the total porosity in the case of Opalinus Clay, Effingen Members and "Brauner Dogger", but only ~ 12% in the case of Helvetic Marls. A new collaborative research project between LES, NWMO Canada and the University of Bern to study anion exclusion in more detail, and to relate diffusion to the mineral composition and the pore structure, will start at the beginning of 2014 (VAN LOON et al., 2013).

7.3 CatClay

The contribution of LES to WP3 in the CatClay project is to perform and interpret the diffusion and sorption results of strongly sorbing radionuclides in a complex rock matrix such as Opalinus Clay. In 2013 the results of $^{60}Co(II)$ and $^{65}Zn(II)$ diffusion into Opalinus Clay samples from the Mont Terri Rock Laboratory were modelled using PHREEQC. The modelling indicated that the sorption of $^{60}Co(II)$ and $^{65}Zn(II)$ on intact samples was lower than the sorption measured on crushed material. Fig. 7.1 shows the sorption isotherms for Co(II) and Zn(II) as measured in batch sorption experiments together with a sorption value derived from diffusion experiments. It can be seen that sorption on crushed Opalinus Clay is larger than the sorption on the intact material. The reason for this apparent discrepancy is currently not understood.

The scope of WP2 in the CatClay project was to assess whether strongly sorbing radionuclide species bound to the clay surface can contribute to the overall diffusive fluxes, or, in other words, whether they are mobile or not. From previous experiments with Sr^{2+}, which sorbs predominantly on the planar cation exchange sites, it was concluded that the surface species on these sites are mobile and contribute to the overall diffusive flux ("sorption-enhanced diffusion"). The situation is expected to be more complex in the case of cations from the transition metal or lanthanide series. According to current sorption models these cations sorb either on planar sites by cation exchange (independent of pH) or by specific sorption on sites where competition with protons may take place. In the original planning it was foreseen to carry out tracer diffusion experiments in Na-exchanged illite (Na-IdP-CC) with Sr^{2+}, Zn^{2+}, and Eu^{3+} as the test cations. These aims were redefined during a technical meeting at PSI on March 25/26, 2013. It was decided to cancel the experiments with Eu^{3+} and focus instead on the bivalent transition metals and to include Co^{2+}. The first scoping experiments with the membrane confined diffusion cells (MCDCs) were carried out using $^{60}Co(II)$ and $^{65}Zn(II)$ as tracers. Although the duration of the in-diffusion phase in these experiments was relatively short, useful information could be gained.

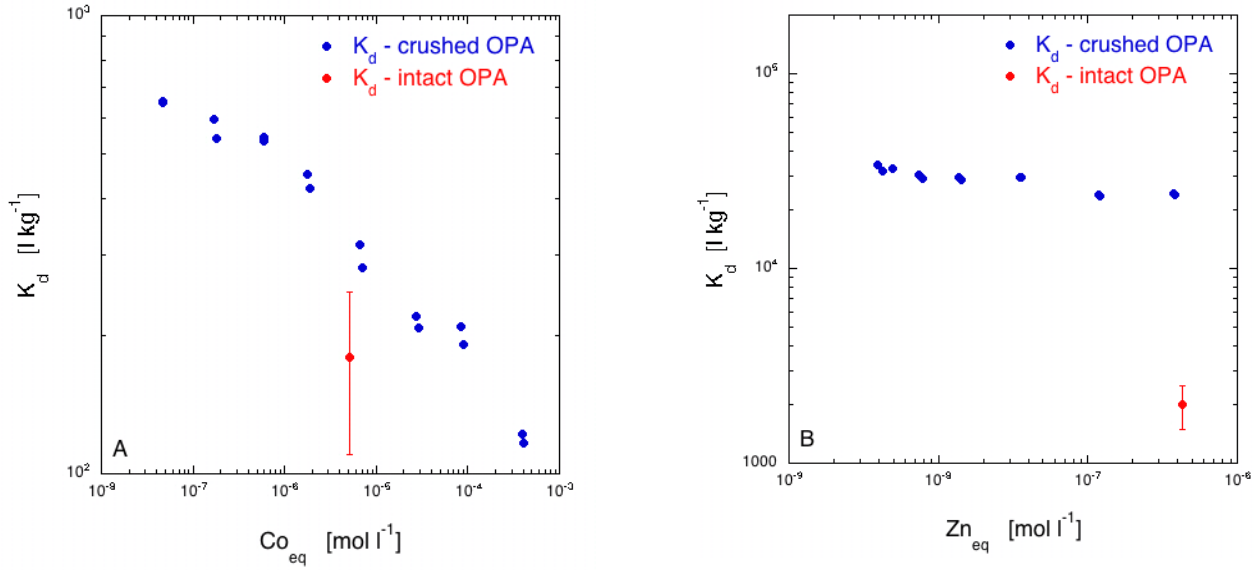

Fig. 7.1: *Sorption isotherms of Co(II) and Zn(II) on Opalinus Clay. Comparison between sorption measurements from batch sorption experiments and sorption values derived from in-diffusion measurements. A) Sorption of Co(II) on Opalinus Clay; B) sorption of Zn(II) on Opalinus Clay.*

The experiments were designed with relatively small reservoir volumes in order to ensure that a measurable decrease in tracer concentration occurred during the duration of the experiment. This, together with the tracer profiles measured after the phase of in-diffusion, helped to increase the reliability of the interpretation of the data. The layout of the MCDCs requires that the modelling be carried out in 3D. Thus PHREEQC cannot be used. A suitable 3D model was set up using Comsol Multiphysics in which the difference in the cross section of the clay and the cross section of the aperture could be adequately taken into account. Fig. 7.2 illustrates the resulting inhomogeneities with respect to concentration in the clay region near the membrane interface.

The Comsol model was subsequently further developed involving a 2D-rotational axisymmetric geometry which reduced the computing times to reasonable levels (e.g. for parameter optimisation routines, etc.). Further, an option for introducing basic sorption models (Freundlich, Langmuir, etc.), as well as other user-defined functions, was introduced so as to be able to take into account non-linear sorption behaviour.

Because of the low concentrations used, most of the results could be described using a constant K_d value. The interaction of Na-IdP-CC with Zn(II) was much stronger than with Co(II). As in the case of the in-diffusion experiments with Co(II) and Zn(II) in Opalinus Clay, the K_d values observed in the experiments with compacted Na-IdP-CC tended to be lower than those measured in dispersed clay suspensions in batch sorption tests. Further, the effective diffusion coefficients calculated on the basis of the tracer concentrations in the source reservoir were larger than expected from the analogy of diffusion in bulk water, and exhibit a trend of increasing values with decreasing ionic strength. This is a possible indication that sorption-enhanced diffusion is also a relevant transport process for these cations, although the contribution to the overall diffusion rate is less than for cations interacting predominantly by a cation exchange with Na-IdP-CC. It is however too early to give a definitive evaluation of the diffusion experiments because the ICP-MS analyses of the stable cations in the reservoir solutions and sorption measurements in dispersed Na-IdP-CC systems are still on-going. A detailed knowledge on the chemical composition of the contact solutions and a sorption model for the interaction of Co(II) and Zn(II) with Na-IdP-CC are important prerequisites for a consistent evaluation of the in-diffusion experiments carried out under different conditions. Sorption data are currently being measured by a guest scientist from the Karlsruhe Institute of Technology (Dr. T. Kupcik).

The in-diffusion experiments are currently being repeated using longer in-diffusion times in order to check the consistency of the measured data and obtain deeper tracer penetration profiles.

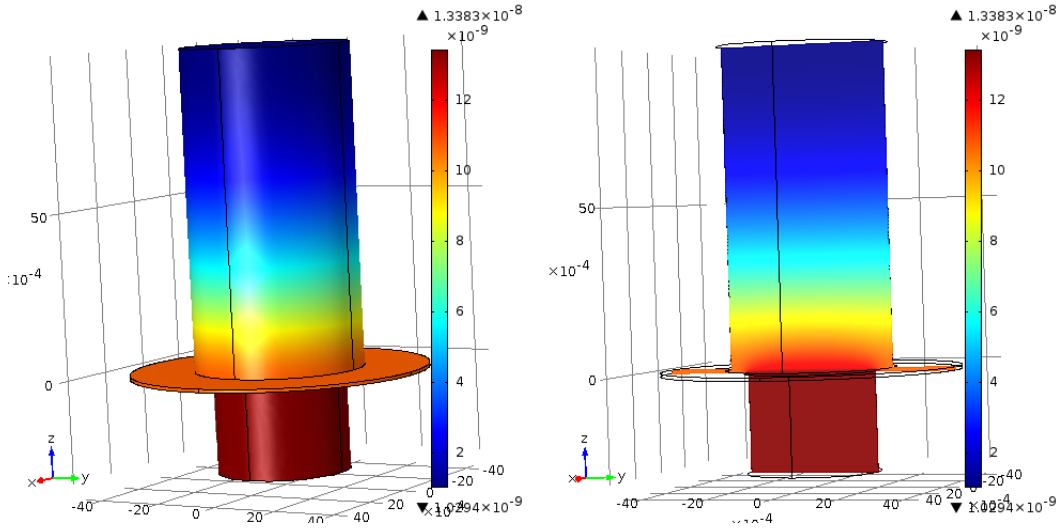

Fig. 7.2: *The modelled layout is given in the figure on the left and on the right a central cross section is shown of the distribution of the $^{85}Sr^{2+}$ tracer in the compacted Na-illite after an in-diffusion time of 11 d in the MCDC. The area above z=0 represents the clay, the orange plane at z~0 is the membrane and the red area below is the contacting solution. Inhomogeneities can be observed near the clay-membrane interface, but these disappear further into the sample. The tracer concentration in the reservoir solution is assumed to be homogeneous through mixing.*

7.4 Transport phenomena in compacted clay systems (TRAPHICCS)

The progress made in the experiments in which the influence of aqueous phase speciation on diffusion is being investigated is relatively slow. No results from experiments involving both radio-labelled ligand and cationic radionuclide species are available. In these experiments the intention was to investigate the role of anionic complexes (e.g Sr–EDTA or UO_2–carbonato complexes) in diffusion processes in compacted montmorillonite. However, the necessary preparatory work, such as the pre-treatment of the clay with EDTA and the investigation of the transport behaviour of the bicarbonate ion in such clays was completed and first experiments using radiolabelled ligands are currently underway.

Diffusion experiments in salt gradient using $^{85}Sr^{2+}$ in Na-montmorillonite compacted to bulk dry densities of ~1300 $kg \cdot m^{-3}$ were carried out as a follow-up to the previous tests with $^{22}Na^{+}$ (GLAUS et al., 2013). In such experiments the concept is that the tracer diffuses to the larger concentrations in the contacting reservoir solutions owing to oppositely directed gradients in concentrations of tracer species bound to the cation exchange sites. Such gradients are accomplished by using electrolyte solutions differing in concentration on the two sides of the diffusion cell. While these experiments start with equal tracer concentrations in both reservoir solutions, a concentration difference develops over time. The experiments serve the purpose of demonstrating that the concentration of surface species is the dominant driving force for diffusion. The direction of diffusion is thus only seemingly against the gradient. In contrast to the previous experiments in salt gradient with $^{22}Na^{+}$, the dynamics in the experiments with $^{85}Sr^{2+}$ are much faster owing to (i) the stronger sorption of $^{85}Sr^{2+}$ and to the lower bulk dry density of the Na-montmorillonite. The large tracer fluxes involved required the use of diffusion cells with flushed filters. In order to monitor the concentration evolution with time adequately, online γ-spectroscopy was applied in collaboration with J. Eikenberg (Division Radioprotection and Safety, Radioanalytics, PSI). Fig. 7.3 shows the evolution with time of the concentrations of tracer species and the background electrolyte in two experiments in which the reservoir volumes differed. Interestingly, the flux in the reservoir with the larger background electrolyte concentration changed direction at two time points. The complex behaviour of the system can be adequately described with a single-porosity model incorporated in Comsol Multiphysics in which the diffusive tracer fluxes are linked to the concentrations of the background electrolyte via a cation exchange mechanism. Note that the modelled curves in both experiments are described using a single set of parameter values. These were only slightly different from published values measured in experiments carried out under conditions of equal background electrolyte solutions on both sides of the diffusion cell (GLAUS et al., 2007). The good consistency between the results obtained under both iso-saline and salt gradient conditions, and for tracer and background electrolyte species with differing sorption properties, strongly increases the confidence in the simplified model which neglect electrochemical and osmotic effects.

The γ-online monitoring technique was also used to study in detail the effect of increasing tracer concentrations in the downstream reservoir in a classical through-diffusion experiment using $^{85}Sr^{2+}$ as the tracer cation. It was demonstrated that concentration levels in the downstream reservoir as low as ~2 % of the upstream reservoir concentration may have significant effects on the local gradients in the clay resulting in reduced tracer fluxes. In general, therefore, it is incorrect to model experiments on the assumption of a zero-concentration at downstream boundary when this has not been verified. The results indicate once more that although through-diffusion is a well-established technique used for many decades, its use still requires a careful handling of experimental and modelling issues. Literature data need to be scrutinised very carefully in this respects in order to obtain robust and reliable data sets.

Both the results of the experiments in salt gradient and the experiments dealing with boundary effects were presented as oral and poster contributions respectively at the Migration'13 conference in Brighton, UK.

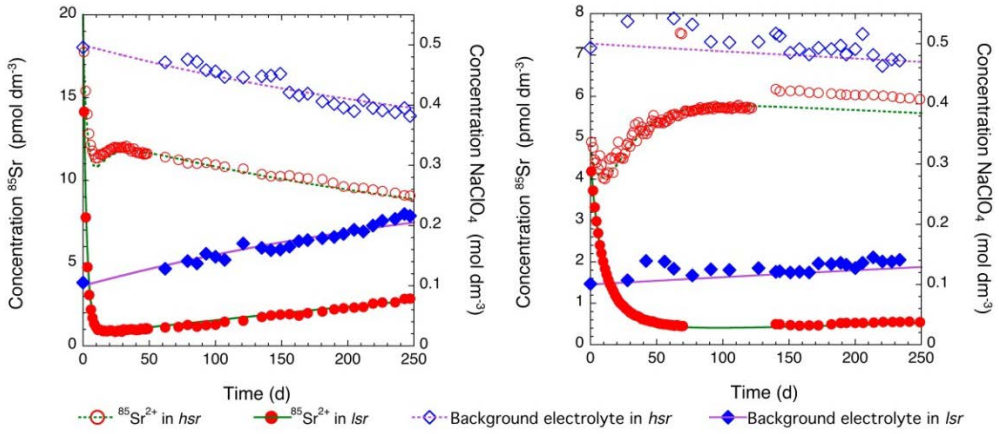

***Fig. 7.3**: The evolution with time of the concentrations of the tracer species and the background electrolyte in an experiment carried out under salt gradient conditions using 0.1 M $NaClO_4$ in the low-salinity reservoir (lsr) and 0.5 M $NaClO_4$ in the high-salinity reservoir (hsr). The left-hand plot shows the results from an experiment with 100 ml reservoirs, the right-hand plot from an experiment with 25 ml reservoirs. The clay thickness was 10 mm in both cases.*

7.5 Sorption-enhanced diffusion of Cs in Opalinus Clay and pure illite

In the case of "sorption-enhanced diffusion", the concentration gradient of surface species is the driving force for diffusion. It was postulated by GIMMI & KOSAKOWSKI (2011) that the higher the sorption, the stronger the sorption-enhanced diffusion effect. It is known that caesium shows a non-linear sorption behaviour because of the different sorption sites involved: at low Cs-concentrations, sorption is high and vice versa. From this sorption behaviour it would be expected that the diffusion of caesium should depend on the concentration of caesium in solution if a "sorption-enhanced diffusion" mechanism is operating. In-diffusion experiments on Opalinus Clay performed at different aqueous caesium concentrations showed that the effective diffusion coefficient indeed increased with decreasing caesium concentration (Table 7.1). Although this is in line with what might be expected, the results are somewhat remarkable because they seem to show that the caesium sorbed on so called frayed edge sites (FES) is mobile. The mobility of caesium adsorbed on FES sites, however, might be different from caesium sorbed on other site types e.g. planar sites.

These observations are in agreement with those made on the diffusion of Cs in pure illites preconditioned to various Cs loadings (see the LES annual report, 2012). Finally, a series of in-diffusion experiments using $^{134}Cs^{+}$ tracer in a background of 1 mM of stable Cs^{+} were finished in the present reporting period. A typical result is shown in Fig. 7.4. It was neither possible to fit these data using a constant-K_d approach, nor with a single-site Langmuir isotherm. A satisfying result was finally obtained using a 2-site Langmuir isotherm in which the site capacities were set to literature values measured in dispersed systems (POINSSOT et al., 1999). The resulting best-fit parameter values for the site affinities are in good agreement with those in the cited work. There is therefore a good consistency between Cs sorption data obtained from batch sorption experiments and those measured on compacted samples. The model could potentially be refined by introducing a site dependent mobility according to Table 7.1. Preliminary tests however showed that the variations thereby introduced lie within the range of the error bars.

7.6 Porosity changes in porous media

Repository systems have several interfaces where there are strong chemical gradients. The most striking example is the cement-clay interface. Due to dissolution-precipitation reactions occurring at these interfaces, porosity changes can result in changes in the transport properties of solutes and gases. In order to achieve a better understanding of dissolution-precipitation reactions and their effect on solute transport, two projects are on-going; one on the interface between cement and montmorillonite and the other on the effects of porosity changes on transport phenomena. The projects are a co-operation between the Transport Mechanisms Group, the Diffusion Processes Group and the University of Bern. More information on these projects is given in Transport Mechanisms group chapter.

Table 7.1: *Best-fit parameters (including upper and lower bounds) for the in-diffusion of $^{134}Cs(I)$ in Opalinus Clay at different background Cs(I) concentrations.*

$^{133}Cs(I)$ ($mol \cdot l^{-1}$)	K_d ($ml \cdot g^{-1}$)	D_e ($m^2 \cdot s^{-1}$)	Remark
$1 \cdot 10^{-2}$	4.5	$1.5 \cdot 10^{-10}$	best fit
	6.0	$2.0 \cdot 10^{-10}$	upper bound
	3.5	$1.1 \cdot 10^{-10}$	lower bound
$1 \cdot 10^{-4}$	18	$2.5 \cdot 10^{-10}$	best fit
	30	$4.0 \cdot 10^{-10}$	upper bound
	10	$1.5 \cdot 10^{-10}$	lower bound
$1 \cdot 10^{-6}$	120	$2.8 \cdot 10^{-10}$	best fit
	150	$3.7 \cdot 10^{-10}$	upper bound
	90	$2.0 \cdot 10^{-10}$	lower bound
$8.52 \cdot 10^{-8}$	380	$8.0 \cdot 10^{-10}$	best fit
	500	$1.2 \cdot 10^{-9}$	upper bound
	260	$5.0 \cdot 10^{-10}$	lower bound

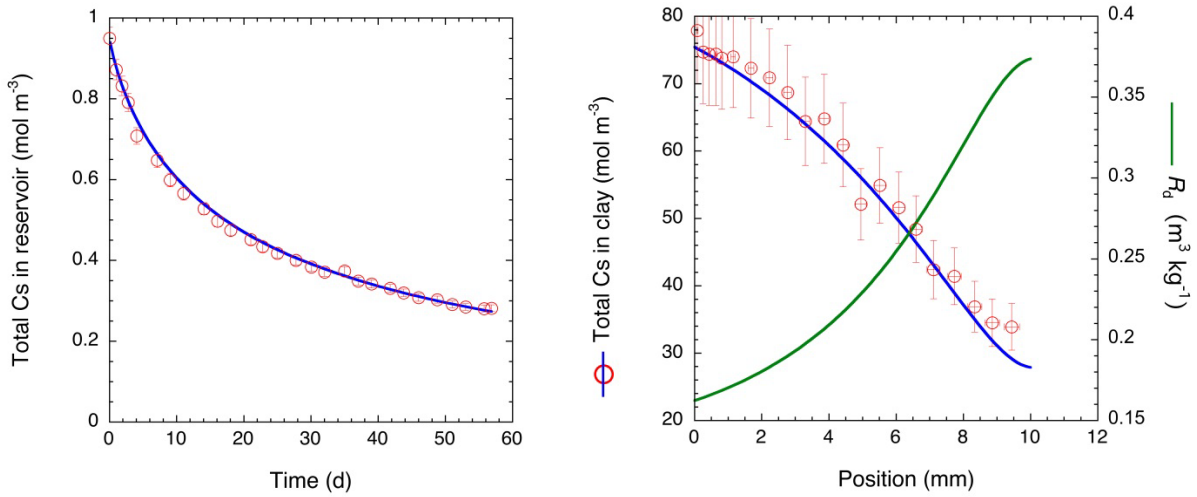

Fig. 7.4*: Evolution of the reservoir concentration (left) and profile measured after in-diffusion in an experiment in which a mixture of $^{134}Cs^+$ and stable Cs^+ in 0.1 M $NaClO_4$ was contacted with Na-illite compacted to a bulk dry density of 1900 kg m^{-3}. Fit curves were obtained from a Comsol Multiphysics model using a 2-site Langmuir isotherm.*

7.7 Transport of small organic molecules in dense clay systems

A PhD project on the structure-transport relationships for small molecular weight organic compounds in Opalinus Clay and compacted clay minerals was started. Basic preparatory experiments using acetate, lactate and gluconate as test compounds were carried out. It was shown that these are rapidly degraded, most probably by microbial processes, for a typical Opalinus Clay porewater composition. However, encouraging results were obtained if K_2CrO_4 was added to the porewater solutions. Whether this agent can be used as a microbial inhibitor in infiltration experiments using compacted clay minerals or clay rocks is currently being tested. A few sorption measurements on pure illite using the batch sorption technique were also carried out with these organic compounds. The results will be used as a comparison with the results from future infiltration experiments carried out under medium-pressure conditions on compacted clay minerals. The experimental equipment for such experiments and for the high-pressure infiltration experiments using intact cores of Opalinus Clay are currently being set up.

7.8 References

GIMMI T., KOSAKOWSKI G. (2011)
How mobile are sorbed cations in clays and clay rocks? Environ. Sci. Technol. 45, 1443-1449.

GLAUS M.A., BAEYENS B., BRADBURY M.H., JAKOB A., VAN LOON L.R., YAROSHCHUK A. (2007)
Diffusion of ^{22}Na and ^{85}Sr in montmorillonite: Evidence of interlayer diffusion being the dominant pathway at high compaction. Environ. Sci. Technol. 41, 478-485.

GLAUS M.A., BIRGERSSON M., KARNLAND O., VAN LOON L.R. (2013)
Seeming steady-state uphill diffusion of $^{22}Na^+$ in compacted montmorillonite. Environ. Sci. Technol. 47(20), 11522-11527.

POINSSOT C., BAEYENS B., BRADBURY M. (1999)
Experimental and modelling studies of caesium sorption on illite. Geochim. Cosmochim. Acta 63, 3217–3227.

VAN LOON L.R., EIKENBERG J. (2005)
A high-resolution abrasive method for determining diffusion profiles of sorbing radionuclides in dense argillaceous rocks. Appl. Radiat. Isotopes 63, 11-21.

VAN LOON L.R. (2013)
Effective diffusion coefficients and porosity values for argillaceous host rocks: measured and estimated values for provisional safety analyses for SGT-E2. Nagra Technical Report NTB 12-03, Nagra, Wettingen, Switzerland.

VAN LOON L.R., MÜLLER W. (2014)
A modified version of the combined in-diffusion/abrasive peeling technique for measuring diffusion of strongly sorbing radionuclides in argillaceous rocks: a test study on the diffusion of caesium in Opalinus Clay. Submitted to Applied Radiation and Isotopes.

VAN LOON L.R., HOBBS M., AL T., GIMMI T., MÄDER U. (2013)
Anion accessibility in low porosity argillaceous rocks (ANPOR). PhD proposal, Paul Scherrer Institut, Villigen, Switzerland.

8 Publications

8.1 Peer reviewed journals

BENEDICTO A.[1], MISSANA T.[1], DEGUELDRE C.,
Predictions of TiO_2-driven migration of Se(IV) based on an integrated study of TiO_2 colloid stability and Se(IV) surface adsorption. Sci. Total Environ. 449, 214-222 (2013).
[1] CIEMAT, Madrid, Spain

BERNER U., KULIK D.A., KOSAKOWSKI G.
Geochemical impact of a low-pH cement liner on the near field of a repository for spent fuel and high-level radioactive waste. Phys. Chem. Earth 64, 46–56 (2013).

CHURAKOV S.V.
Mobility of Na and Cs on montmorillonite surface under partially saturated conditions Environ. Sci. Technol. 47, 9816-9823 (2013).

CURTI E., AIMOZ L., KITAMURA A.[1]
Selenium uptake onto natural pyrite. J. Radioanal. Nucl. Chem. 295, 1655-1665 (2013).
[1] JAEA, Tokai-mura Ibaraki, Japan

DÄHN R., POPOV D., SCHAUB P., PATTISON P., GROLIMUND D., JENNI A., WIELAND E.
X-ray micro-diffraction studies of heterogeneous interfaces between cementitious materials and geological formations. Phys. Chem. Earth (2013). http://dx.doi.org/10.1016/j.pce.2013.10.010

DEGUELDRE C., BENEDICTO A.[1]
Colloid generation during water flow transients. Appl. Geochem. 27, 1220-1225 (2012).
[1] CIEMAT, Madrid, Spain

GAONA X., WIELAND E., TITS J., SCHEINOST A.C.[1], DÄHN R.
Np(V/VI) redox chemistry in cementitious systems: XAFS investigations on the speciation under anoxic and oxidizing conditions. Appl. Geochem. 28, 109-118 (2013).
[1] HZDR, Dresden, Germany; ROBL/ESRF, Grenoble, France

GIMMI TH, LEUPIN, O.X.[1], EIKENBERG J., GLAUS M., VAN LOON L.R., WABER H.N.[2], WERSIN P.[2], WANG H.A.O., GROLIMUND D, BORCA C.N., DEWONCK S.[3], WITTEBROODT C.[4]
Anisotropic diffusion at the field scale in a four-year multi-tracer diffusion and retention experiment - I: Insights from the experimental data. Geochim. Cosmochim. Acta 125, 373-393 (2014).
[1] Nagra, Wettingen, Switzerland
[2] University of Bern, Bern, Switzerland
[3] Andra, Chatenay Malabry, France
[4] IRSN, Fontenay-aux-Roses, France

GIN S.[1], FRUGIER P. [1], JOLLIVET P. [1], BRUGUIER F.[1], CURTI E.
New insight into the residual rate of borosilicate glasses: Int. J. Appl. Glass Sci. (2013).
http://dx.doi.org/10.1111/ijag.12048
[1] CEA, Saclay, France

GLAUS M.A., BIRGERSSON M.[1], KARNLAND O.[1], VAN LOON L.R.
Seeming steady-state uphill diffusion of $^{22}Na^{+}$ in compacted montmorillonite. Environ. Sci. Technol. 47(20), 11522-11527 (2013).
[1] Clay Technology AB, Lund, Schweden

JOSEPH C.[1], VAN LOON L.R., JAKOB A., STEUDTNER R.[1], SCHMEIDE K.[1], SACHS S.[1], BERHARD G.[1]
Diffusion of U(VI) in Opalinus Clay: Influence of temperature and humic acid. Geochim. Cosmochim. Acta 109, 74-89 (2013).
[1] HZDR, Dresden, Germany

KOSAKOWSKI G., BERNER U.
The evolution of clay rock/cement interfaces in a cementitious repository for low- and intermediate level radioactive waste. Phys. Chem. Earth 64, 65–86 (2013).

KULIK D.A., WAGNER T.[1],·DMYTRIEVA S.V.[2], KOSAKOWSKI G., HINGERL F.F.[3],·KONSTANTIN V.[4] CHUDNENKO K.V.[4], BERNER U.
GEM-Selektor geochemical modelling package: revised algorithm and GEMS3K numerical kernel for coupled simulation codes. Comput. Geosci. 17, 1-24 (2013).
[1] University of Helsinki, Helsinki, Finland
[2] SSE Technocentre, Kyiv, Ukraine
[3] Stanford University, Stanford, USA
[4] Vinogradov Institute of Geochemistry, Irkutsk, Russia

MACÉ N., WIELAND E., DÄHN R., TITS J., SCHEINOST A.C.[1]
EXAFS investigation on U(VI) immobilization in hardened cement paste: Influence of experimental conditions on speciation. Radiochim. Acta 101, 379-389 (2013)
[1] HZDR, Dresden, Germany; ROBL/ESRF, Grenoble, France

PAYNE T.E.[1], BRENDLER V.[2], OCHS M.[3], BAEYENS B., BROWN P.L.[4], DAVIS J.A.[5], EKBERG C.[6], KULIK D.A., LÜTZENKIRCHEN J.[7], MISSANA T.[8], TACHI Y.[9], VAN LOON L.R., ALTMANN S.[10]
Guidelines for thermodynamic sorption modelling in the context of radioactive waste disposal. Environ. Modell. Software 42, 143-156 (2013).
[1] Nuclear Science and Technology, Kirrawee, Auastralia
[2] HZDR, Dresden, Germany
[3] BMG Engineering, Schlieren, Switzerland
[4] Geochem Australia, Kiama, Australia
[5] Lawrence Berkeley National Laboratory, Berkeley CA, USA
[6] Chalmers University Göteborg, Sweden
[7] KIT-INE, Karlsruhe, Germany
[8] CIEMAT, Madrid, Spain
[9] JAEA, Tokai-mura Ibaraki, Japan
[10] ANDRA,Châtenay-Malabry, France

ROJO H., TITS J., GAONA X.[1], GARCIA-GUTIERREZ M.G.[2], MISSANA T.[2], WIELAND E.
Thermodynamics of Np(IV) complexes with gluconic acid under alkaline conditions: sorption studies. Radiochim. Acta 101, 1-6 (2013).
[1] KIT-INE, Karlsruhe, Germany
[2] CIEMAT, Madrid, Spain

SHAO H.[1], KOSAKOWSKI G., BERNER U., KULIK D.A., MÄDER U.[2], KOLDITZ O.[1]
Reactive transport modelling of the clogging process at Maqarin natural analogue site. Phys. Chem. Earth 64, 21–31. (2013).
[1] HZDR, Dresden, Germany
[2] University of Bern, Bern, Switzerland

SOLTERMANN D., MARQUES FERNANDES M., BRADBURY M.H., DÄHN R., BRENDLÉ J.[1], BAEYENS B.
Investigations of Fe(II) sorption on synthetic montmorillonite. A combined macroscopic and spectroscopic study. Environ. Sci. Technol. 47, 6978–6986 (2013).
[1] Université de Haute Alsace, Mulhouse, France

TYAGI M., GIMMI T., CHURAKOV S.
Multi-scale micro-structure generation strategy for up-scaling transport in clays. Advances Water Res. 59, 181–195 (2013).

WAGNER T.[1], KULIK D.A., HINGERL F.F., DMYTRIEVA S.V.[2]
GEM-Selektor geochemical modelling package: TSolMod library and data interface for multicomponent phase models. Can. Mineral., 50, 1173-1195 (2012).
[1] University of Helsinki, Helsinki, Finland
[2] SSE Technocentre, Kyiv, Ukraine

8.2 Publications in books

WIELAND E., DÄHN R., GAONA X., MACÉ N., TITS J.
Micro- and macroscopic investigations of actinide binding in cementitious materials, in: Bart F., Cau-di-Coumes C., Frizon F., Lorente S. (Eds.), Cement-Based Materials for Nuclear Waste Storage. Springer, pp. 93-103. (2013).
ISBN 978-1-4614-3444-3

8.3 Conference proceedings

THIEN B., KULIK D.A., CURTI E.
Modelling Trace Element Uptake Kinetics in Secondary Minerals. Proceedings of the Fourteenth International Symposium on Water-Rock Interaction, WRI 14. Proc. Earth Planet Sci. 7, 838–841. WRI 14, Avignon, France, June 14-19, 2013.

WERSIN P.[1], WABER H.N.[1], MAZUREK M.[1], MÄDER U.K.[1], GIMMI T., RUFER D.[1], TRABER D.[2].
Resolving Cl and SO_4 profiles in a clay-rich rock sequence. Proc. Earth Planet Sci. 7, 892–895.
[1] University of Bern, Bern, Switzerland
[2] Nagra, Wettingen, Switzerland

8.4 Conferences/workshops/presentations

BAEYENS B., MARQUES FERNANDES M., BRADBURY M.H.
Sorption values in sorption data bases for argillaceous rocks and bentonite: a comparison between derived and measured values. Migration 2013, 14th International Conference on Chemistry and Migration Behaviour of Actinides and Fission Products in the Geosphere, Brighton, UK, 8-13 September, 2013.

BESTEL M.F., JURÁNYI F., GIMMI T., GLAUS M.A., VAN LOON L.R., DIAMOND L.
Water distribution in Na- and Cs-montmorillonite. 5th Swiss Bentonite Meeting, Bern, Switzerland, 26 June, 2013.

CHURAKOV S.V. DÄHN R., BAEYENS B., BRADBURY M.H.
Mechanism of Zn adsorption on montmorillonite inferred from atomistic simulations, P-EXAFS-spectroscopy and sorption experiments. International Clay Conference, Rio de Janeiro, Brasil, 7-11 July, 2013.

CHURAKOV S.V., LABBEZ CH., PEGADO L., SULPIZI M.
Understanding ion adsorption by C-S-H: From ab initio simulations to thermodynamic equilibrium. 3rd International Workshop on "Mechanisms and modelling of waste/cement interactions", Ghent, Belgium, 6-8 May, 2013.

CURTI E.
Long-term dissolution kinetics, element redistribution and redox reactions during aqueous alteration of simulated nuclear waste glass. 2nd International Summer School of Nuclear Glass Wasteform, Pont du Gard, France, 23-27 September, 2013.

DÄHN R., SCHAUB P., POPOV D., PATTISON P., JENNI A., MÄDER U., WIELAND E.
Micro-X-ray-diffraction investigations of an altered cement-clay interface. 23rd Annual V. M. Goldschmidt Conference, Florence, Italy, 25-30 August, 2013.

DEGUELDRE C.
Colloid analysis for CFM, CFM (lab/modellers) meeting organised by USDOE, Sterling VA, USA, 8-10 May, 2013.

DEGUELDRE C.
Colloid generation modelling: from pseudo-equilibrium in quasi-stagnant aquifers to transients induced by flow variation or seismic features, CFM (lab/modellers) meeting organised by USDOE, Sterling VA, USA, 8-10 May, 2013.

GAONA X., MARQUES FERNANDES M., BAEYENS B., ALTMAIER M.
Solubility and hydrolysis of U(VI) at 80° under acidic to hyperalkaline pH conditions. Migration 2013, 14th International Conference on Chemistry and Migration Behaviour of Actinides and Fission Products in the Geosphere, Brighton, UK, 8-13 September, 2013.

GIMMI T., LEUPIN O.X., SOLER J.M., VAN LOON L.R.
Perturbing a field diffusion experiment: First results of the DR-A test in the Mont Terri Rock Laboratory (Switzerland). Goldschmidt Conference 2013, Florence, Italy, 25-30 August, 2013.

GLAUS M.A, EIKENBERG J., FRICK S., RÜTHI M., VAN LOON L.R.
Diffusion of $^{85}Sr^{2+}$ in compacted montmorillonite seemingly against its own concentration gradient. Migration 2013, 14th International Conference on Chemistry and Migration Behaviour of Actinides and Fission Products in the Geosphere, Brighton, UK, 8-13 September, 2013.

GLAUS M.A., VAN LOON L.R., VAN LAER L., AERTSENS M., BRUGGEMAN C., GOVAERTS J., MAES N.
Benchmark experiments for the investigation of the diffusive behaviour of $^{85}Sr^{2+}$ in compacted Na-illite. Migration 2013, 14th International Conference on Chemistry and Migration Behaviour of Actinides and Fission Products in the Geosphere, Brighton, UK, 8-13 September, 2013.

HUMMEL W.
Dissolved metals in redox-state zero: A gap in thermodynamic databases. 23rd Annual V.M. Goldschmidt Conference, Florence, Italy, 25-30 August, 2013, Min. Mag. 77(5), 1345.

KOSAKOWSKI G., BERNER U., KULIK D.A.
Reactive transport with OpenGeoSys-GEM: developments and applications related to the evolution of cement materials in radioactive waste repositories. 3rd International Workshop on "Mechanisms and modelling of waste/cement interactions", Ghent, Belgium, 6-8 May, 2013.

KULIK D.A., KOSAKOWSKI G., LOTHENBACH B.' WIELAND E., BERNER U.
Local- and partial equilibria in thermodynamic- and transport modelling of cement systems. 3rd International Workshop on "Mechanisms and modelling of waste/cement interactions", Ghent, Belgium, 6-8 May, 2013.

KULIK D.A., DMYTRIEVA S.V., WAGNER T., THOENEN T, BERNER U.
GEMS: Gibbs energy minimization software for geochemical modelling. 23rd Annual V.M. Goldschmidt Conference, Florence, Italy, 25-30 August 2013.

PEGADO L., LABBEZ CH., CHURAKOV S.V.
First principles investigations of Al substitution in novel cementitious systems. E-MRS Fall meeting Warsaw, University of Technology 16-20 September.

ROJO H., GAONA X., RABUNG TH., GARCÍA-GUTIÉRREZ M., MISSANA T., ALTMAIER M.
Complexation of Nd(III)/Cm(III) with gluconate in dilute NaCl and $CaCl_2$ alkaline solutions: solubility and TRLFS studies. 3rd International Workshop on "Mechanisms and modelling of waste/cement interactions", Ghent, Belgium, 6-8 May, 2013.

ROJO H., GAONA X., RABUNG TH., GARCÍA-GUTIÉRREZ M., MISSANA T., ALTMAIER M.
Complexation of Nd(III)/Cm(III) with gluconate in alkaline NaCl and $CaCl_2$ solutions: solubility and TRLFS studies. 23rd Annual V.M. Goldschmidt Conference, Florence, Italy, 25-30 August, 2013.

ROJO H., GAONA X., RABUNG TH., GARCÍA-GUTIÉRREZ M., MISSANA T., ALTMAIER M.
Complexation of Nd(III)/Cm(III) with gluconate in alkaline NaCl and $CaCl_2$ solutions: solubility and TRLFS studies. Migration 2013, 14th International Conference on Chemistry and Migration Behaviour of Actinides and Fission Products in the Geosphere, Brighton, UK, 8-13 September, 2013.

SCHAUB PH., DÄHN, R., POPOV D., LEEMANN A., MÄDER U., JENNI A., PATTISON P., WIELAND E.
In-situ X-ray micro-diffraction analysis of heterogeneous cementitious materials, 3rd International Workshop on "Mechanisms and modelling of waste/cement interactions", Ghent, Belgium, 6-8 May, 2013.

SCHENZEL J., WIELAND E., SCHLOTTERBECK G., GÜNTHER-LEOPOLD I., SZIDAT S.
Speciation of C-14 during the anoxic corrosion of activated steel: Set-up of a long-term corrosion experiment. 3rd International Workshop on "Mechanisms and modelling of waste/cement interactions", Ghent, Belgium, 6-8 May, 2013.

SCHENZEL J., WIELAND E., SCHLOTTERBECK G.
Speciation of carbon-14 in a cementitious repository for radioactive waste: Results from anoxic corrosion experiments, 37th Materials Research Society (MRS) Meeting, Barcelona, Spain, 29 September–3 October, 2013.

SOLTERMANN D., MARQUES FERNANDES M, BRADBURY M.H., DÄHN R., BAEYENS B.
Fe(II) uptake mechanisms on montmorillonite clay minerals. 6th IBP PhD Congress, Zurich ETH, Switzerland, 5 April 2013.

SOLTERMANN D., MARQUES FERNANDES M, BAEYENS B., BRADBURY M.H., DÄHN R.
Fe(II) uptake mechanism on montmorillonite clay minerals. A multidisciplinary approach. 23rd Annual V.M. Goldschmidt Conference, Florence, Italy, 25-30 August, 2013.

THIEN B., HEBERLING F., KULIK D.A.
Modelling non-equilibrium uptake of Se(IV) upon calcite precipitation. 23rd Annual V.M. Goldschmidt Conference, Florence, Italy, 25-30 August 2013.

THOENEN T., HUMMEL W., BERNER U.
The PSI/Nagra Chemical Thermodynamic Data base 12/07: Present status and future developments. 23rd Annual V.M. Goldschmidt Conference, Florence, Italy, 25-30 August, 2013.

TITS J., STUMPF T., WALTHER C., WIELAND E.
Wet chemistry and site-selective luminescence spectroscopy studies on the uptake of hexavalent actinides by cementitious materials. Migration 2013, 14th International Conference on Chemistry and Migration Behaviour of Actinides and Fission Products in the Geosphere, Brighton, UK, 8-13 September, 2013.

VESPA M., DÄHN R., KUNZ D., WIELAND E.
Competition behaviour of metal uptake in cementitious systems. 3rd International Workshop on "Mechanisms and modelling of waste/cement interactions", Ghent, Belgium, 6-8 May, 2013.

WANG H.A.O., GROLIMUND D., VAN LOON L.R., GÜNTHER D.
Imaging using LA-ICP-MS Workshop on "Laser Ablation-ICP-MS: Instruments, Basics, Operation, Evaluation and Application", 9 April 2013, Zürich, Switzerland.

WIELAND E., SCHENZEL J., SCHLOTTERBECK G.
Source and speciation of carbon-14 in a cement-based repository for radioactive waste, 23rd Annual V.M. Goldschmidt Conference, Florence, Italy, 25-30 August, 2013.

WIELAND E.
Chemical form of ^{14}C released from ILW: Status of PSI research, TRU-6 Workshop, Lenzburg, Switzerland, 16-18 September, 2013.

WIELAND E., TITS J., ROJO H., DÄHN R., KULIK D.A.
Mechanisms of iodine and selenium uptake by hardened cement paste. 37th Materials Research Society (MRS) Meeting, Barcelona, Spain, 29 September–3 October, 2013.

WIELAND E., DÄHN R., DILNESA B.Z., LOTHENBACH B.
Determination of the Fe speciation in cementitious materials using synchrotron-based micro-spectroscopic techniques. 3rd International Workshop on "Mechanisms and modelling of waste/cement interactions", Ghent, Belgium, 6-8 May, 2013.

8.5 Invited talks

CHURAKOV S.V., GIMMI TH. JURÁNYI F., VAN LOON L.R., BESTEL M.
Experimental and modelling studies of water mobility in compacted clay systems. International Clay Conference, Rio de Janeiro, Brasil, 7-11 July, 2013.

DÄHN R.
Uptake and alteration processes in Opalinus clay: An X-ray absorption and micro-X-ray-diffraction study. 50th Annual Meeting of the Clay Minerals Society, Urbana, USA, 6-10 October, 2013.

DÄHN R.
Validation of uptake processes of radionuclides such as Cs on clay minerals by EXAFS.
Fukushima recovery – understanding, modelling and managing radiocaesium decontamination. Fukushima/Japan, 30 September–3 October, 2013.

KULIK D., KOSAKOWSKI G., LOTHENBACH B., WIELAND E., BERNER U.
Local- and partial equilibria in thermodynamic and transport modelling of cement systems. 3rd International Workshop on "Mechanisms and modelling of waste/cement interactions", Ghent, Belgium, 6-8 May, 2013.

MARQUES FERNANDES M., VER N., DÄHN R., BAEYENS B.
Bottom up approach for the predictive modelling of sorption isotherms on argillaceous rocks. 23rd Annual V.M. Goldschmidt Conference, Florence, Italy, 25-30 August, 2013.

MARQUES FERNANDES M.
The fate of trivalent actinides in clay-based radioactive waste repositories. ACTINIDES 2013, Karlsruhe, Germany.

8.6 Teaching

CURTI E.
University of Bern in the framework of the block course entitled "Geological disposal of radioactive waste" (shared with PD Dr. Martin Mazurek and Dr. P. Wersin), an integral part of the master curriculum in Geological Sciences.

GIMMI TH., ALT-EPPING P.
Lecture and examinations 'Geochemical Modelling II: Reactive Transport', University of Bern, Master Course in Environmental and Resource Geo-chemistry, April 2013.

GIMMI TH.
Lecture 'Ausbreitung von Schadstoffen in Böden und Grundwasser: Von der Realität zum Modell – und zurück', Weiterbildungskurs Altlasten, University of Bern, 21/22 June, 2013.

HUMMEL W.
The teaching duties of W. Hummel as Privatdozent (PD) for "Nuclear Environmental Chemistry" at ETH Zurich included lectures and exercises on nuclear waste management within the scope of the courses "Nuclear Energy Systems" (Spring Semester 2013) and "Landfilling, nuclear repositories and contaminated sites" (Spring Semester 2013).

KOSAKOWSKI G.
Statistics in Earth Sciences. University of Tübingen, Germany, Summer Semester, 2013.

PFINGSTEN W.
Modelling of processes in soils and aquifers: 701-1334-00L, Department for Environmental Sciences, ETH, Zurich, Spring Semester, 2013.

PFINGSTEN W.
Seminar für Bachelorstudierende: Biogeochemie: 701-0419-01L, Department for Environmental Sciences, ETH, Zurich, Fall Semester 2013.

8.7 Other

KOSAKOWSKI G.
Guest-Editor for the journal "Physics and Chemistry of the Earth" for a special issue, 64 (2013), on: "Coupled Physical and Chemical Transformations Affecting the Performance of GeoSystems".

KULIK D.A.
GEM-Selektor tutorial at 3rd Workshop "From atomistic to thermodynamic modelling, Goethe Universität, Frankfurt-am-Main, 18-22 Februar, 2013.

KULIK D.A.
GEM-Selektor short course for PhD students and Postdocs from ETH domain institutes, PSI, 28 February-1 March, 2013.

Paul Scherrer Institut :: 5232 Villigen PSI :: Switzerland :: Tel. +41 56 310 21 11 :: Fax +41 56 310 21 99 :: www.psi.ch